LITHOFACIES, GEOCHEMICAL TRENDS, AND RESERVOIR POTENTAL, THIRTEEN FINGER LIMESTONE, HUGOTON EMBAYMENT, KANSAS

By

MICHAEL EVAN BAGLEY

Bachelor of Science in Geology

Brigham Young University - Idaho

Rexburg, Idaho

2007

Submitted to the Faculty of the
Graduate College of the
Oklahoma State University
in partial fulfillment of
the requirements for
the Degree of
MASTER OF SCIENCE
May, 2012

LITHOFACIES, GEOCHEMICAL, TRENDS,

AND RESERVOIR POTENTAL,

THIRTEEN FINGER LIMESTONE,

HUGOTON EMBAYMENT, KANSAS

Thesis Approved:

Dr. Jim Puckette

Thesis Adviser

Dr. Darwin Boardman

Dr. Mary Hileman

Dr. Sheryl A. Tucker

Dean of the Graduate College

TABLE OF CONTENTS

LIST OF FIGURES

Figure Page

Figure Page

Figure Page

Figure Page

LIST OF PHOTOGRAPHS

Photograph Page

Photograph Page

Photograph Page

Photograph Page

CHAPTER I

INTRODUCTION

Statement of Problem and Purpose of Study

Rocks of the Atokan stage (Kansas Geological Survey Stratigraphic Nomenclature) have been under studied across much of the Midcontinent, but debate exists where to place the boundary between the Morrowan and Atokan, as well as the Atokan and Desmoinesian. Some geologists believe that parts of the lower Pennsylvanian upper Morrowan are, in reality, Atokan in age (Curtis and Ostergard, 1982). Clay mineralogy shows a dominance of illite in Morrowan shales and that uplift during Atokan time triggered a dominance of montmorillonite in Atokan shales in areas near the Wichita Mountains and Criner Hills (Weaver, 1958).

The boundary between the Atoka and Desmoinesian is also debated and has not been satisfactorily identified in northwestern Oklahoma (Boler, 1959). Rough estimates put it ten (10) to thirty (30) feet below the Inola limestone (Mannhard and Busch, 1974), but the Inola Limestone is not a widespread, continuous bed across the Midcontinent Region (Midcontinent). Atokan strata have been found to contain Mississippian and Pennsylvanian foraminifera in the Arkoma Basin (Galloway and Ryniker, 1930). The key to delineating the Atokan is through biostratigraphy by using various microfossils including conodont assemblages and the foraminifera *Fusulinella* (Moore, 1948).

The middle Pennsylvanian (Atokan) Thirteen Finger Limestone in west-central Kansas doesn't outcrop and must be studied through core analysis. The core from the Amoco Production

Company, Rebecca K. Bounds #1 well has a nearly complete section of the Atoka stage that has not been extensively studied. The core was studied in both hand sample and thin section to determine lithology and sampled for various geochemical analyses including X-ray fluorescence (XRF), X-ray diffraction (XRD), and Total Organic Carbon (TOC) to gather compositional data used to interpret the depositional setting. Microfossil abundances and vertical distributions were determined to aid in the interpretation of the depositional setting and biostratigraphic ages of the core. In addition, shales have in recent years proven their ability to trap recoverable hydrocarbons (Nelson, 2009) and the Thirteen Finger Limestone shows potential as a hydrocarbon resource (Davis, 1964). Lastly, work by Loucks (2009) found that nanoporosity in shale commonly occurs in grains of organic matter. Spectral gamma-ray values of uranium will be compared to metal concentrations from XRF and TOC values to see if wireline measurements can be a predictor of TOC and thus nanoporosity in shale. This work lays the groundwork for future studies of the Atokan in Kansas and the remaining areas that make up the Hugoton Embayment and Anadarko Basin.

Location of Area of Study

The Thirteen Finger Limestone described in this study is core from the Amoco Production, Rebecca K. Bounds #1 well located in Section 17, T.18S., R.42W., Greeley County, Kansas (Fig. 1). The well is located in western Kansas approximately 16 miles (19.3 km) west of Tribune, KS and 4 miles (6.3 km) east of the Colorado border. This well was drilled March 6, 1988 and reached a total depth (TD) of 5,956 feet (1,815 m) on April 6. The well was continuously cored from a depth of 900 feet (274 m) to TD starting in the upper Cretaceous Greenhorn Limestone and stopping in the Arbuckle Group (Dean et al, 1995; Kansas Geological Survey, 2011).

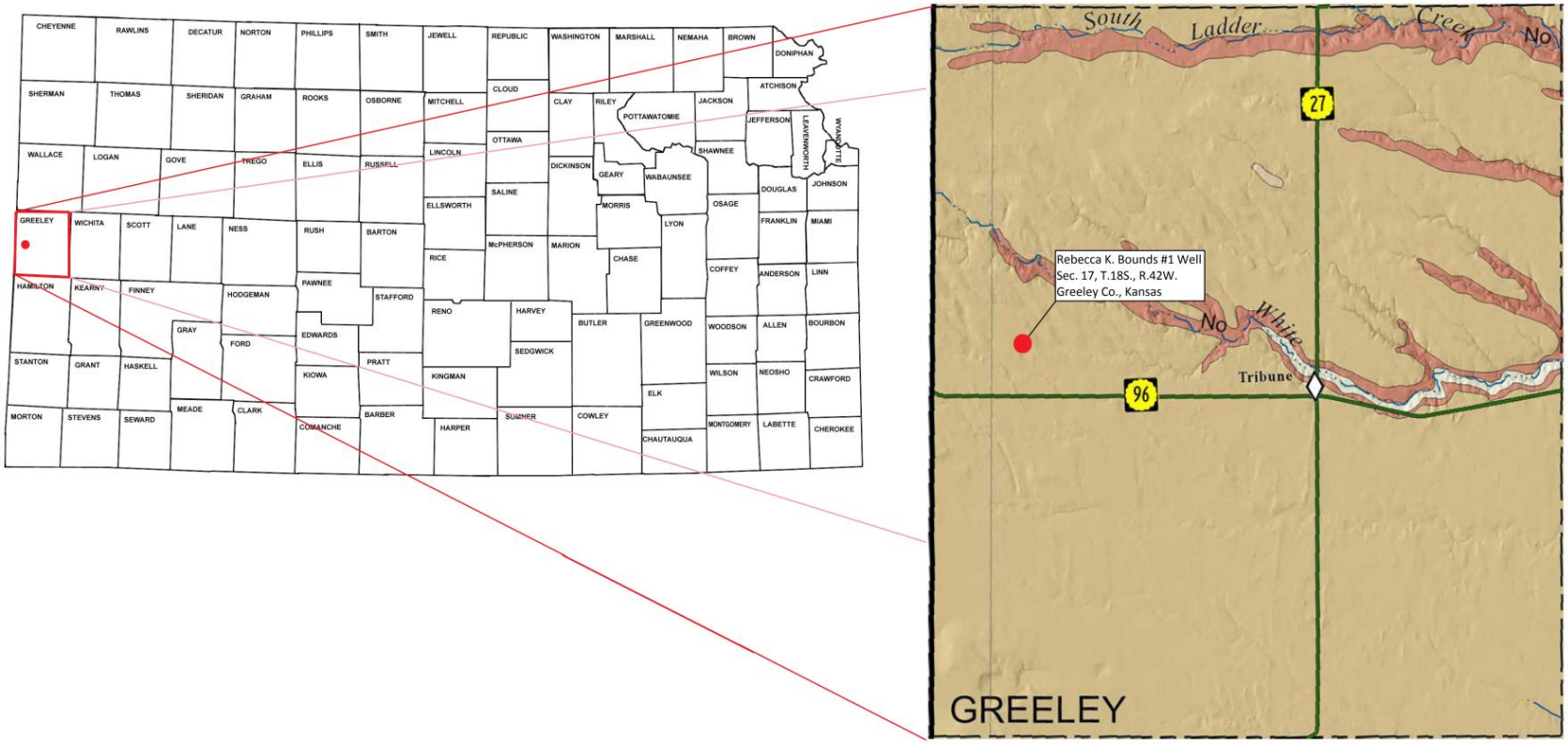

Figure 1: Location of the Rebecca K. Bounds #1 well drilled in Section 17, T.18S., R.42W., Greeley County, Kansas (Modified from Prescott et al., 1954).

In the Rebecca K. Bounds #1 well, the top of the Pennsylvanian is at a depth of 3525 feet, the base at 5222'. The Atokan stage spans the interval from approximately 4900'-5021'. This core is in the care of the Kansas Geological Survey, who provided photographs and well log data, and allowed sampling and analysis of the interval of interest.

Geologic Setting

The Anadarko Basin stretches from south-central Oklahoma, into the Texas Panhandle, and northward into the Oklahoma Panhandle and western Kansas as the Hugoton Embayment (Fig. 2). Flooding from the southeast during the early Mississippian created stable shelf conditions through the late Mississippian forming thick, continuous carbonates across the Midcontinent (Eddleman, 1961)(Fig. 3).

During the later stages of the Mississippian, the area containing northwest Oklahoma, northeast Texas Panhandle, southeast Colorado, and southwest Kansas underwent epeirogenic upwarp while the Amarillo-Wichita and Cimarron arches became positive along a line of Precambrian folds to the southwest of the Anadarko Basin (Huffman, 1959). At the end of the Mississippian the Central Kansas Uplift, Las Animas Arch, and Sierra Grande Highland experienced a slight uplift that triggered the exposure of much of the Anadarko Shelf and Hugoton Embayment (Curtis and Ostergard, 1982)(Fig. 4). This exposure (Fig. 4) triggered aggressive stream incision followed by a regional subsidence which led to the formation of the early Pennsylvanian Morrow channel sandstones of the Stateline Trend in east-central Colorado and west-central Kansas (Bowen and Weimer, 2003)(Fig. 2). At the close of the Morrowan, continued subsidence and transgression inundated the Anadarko shelf and Hugoton Embayment and the sediments that became the Atokan Thirteen Finger Limestone were deposited (Curtis and Ostergard, 1982)(Fig. 5).

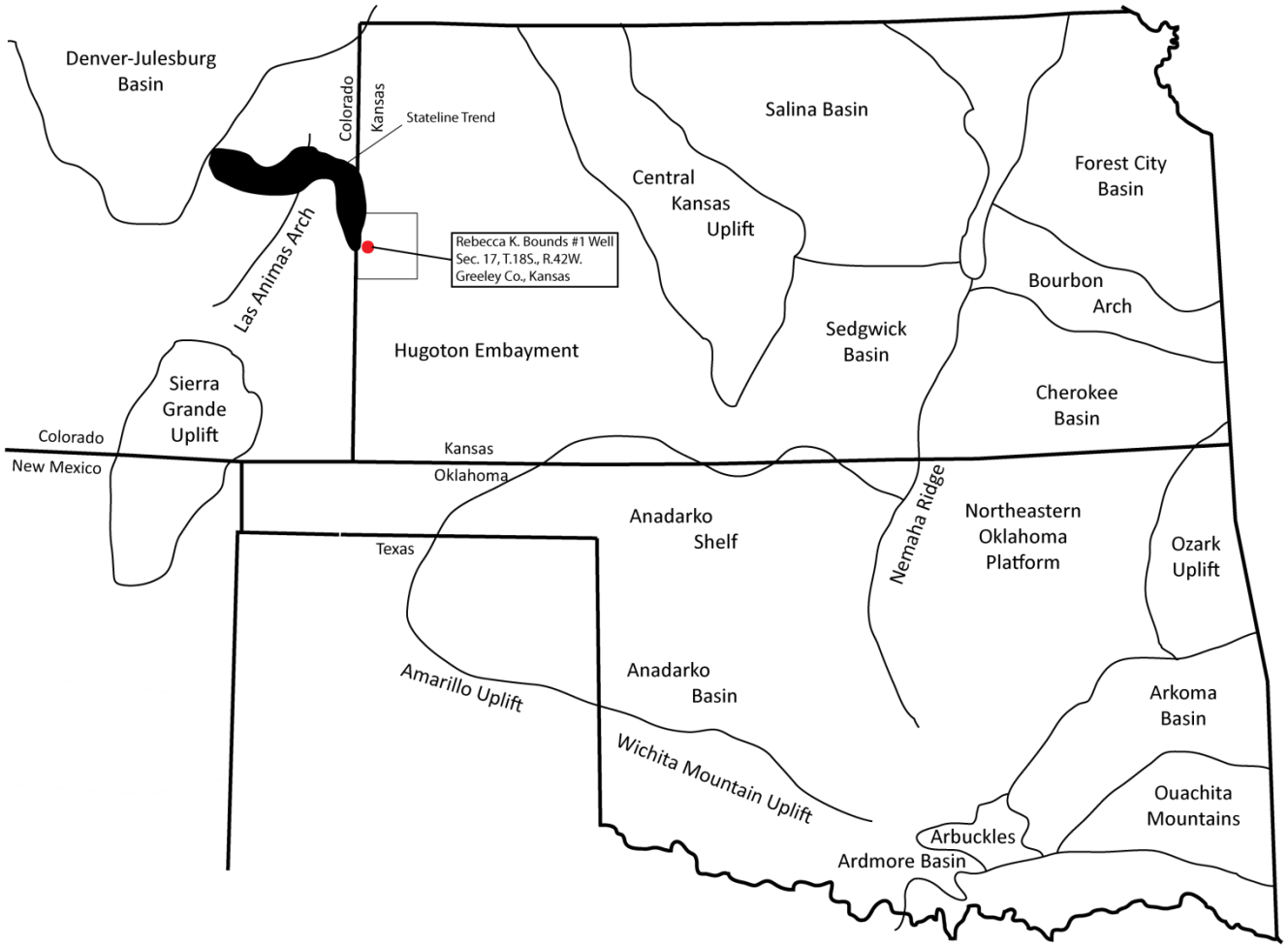

Figure 2: Map of the southern Midcontinent showing major tectonic features during the middle Pennsylvanian. The Stateline Trend of Colorado and Kansas is located approximately 4 miles west of the Rebecca K. Bounds #1 well. The location of the Rebecca K. Bounds #1 well is shown in red (Modified from Huffman, 1959).

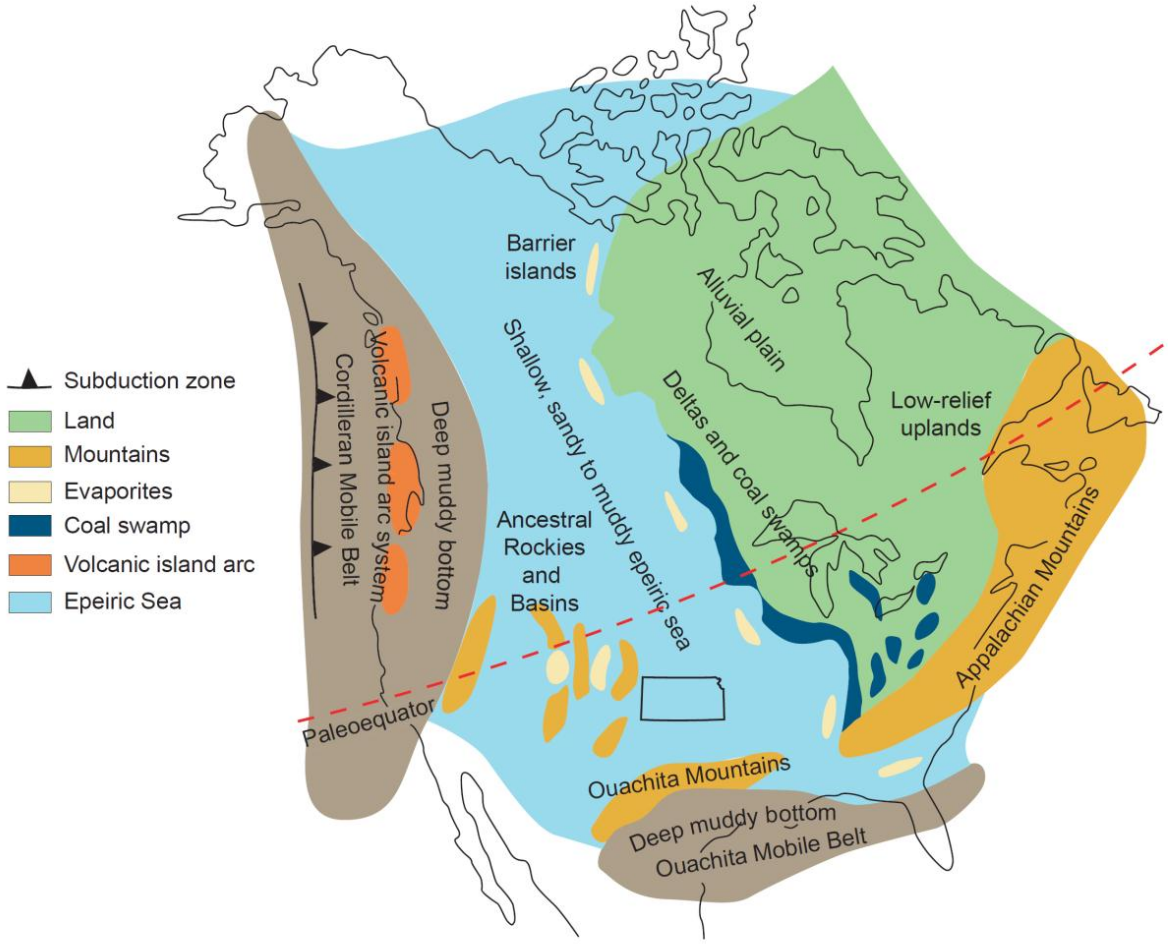

Figure 3: Paleogeographic map of North America during the Pennsylvanian (Modified from Wicander and Monroe, 1989)

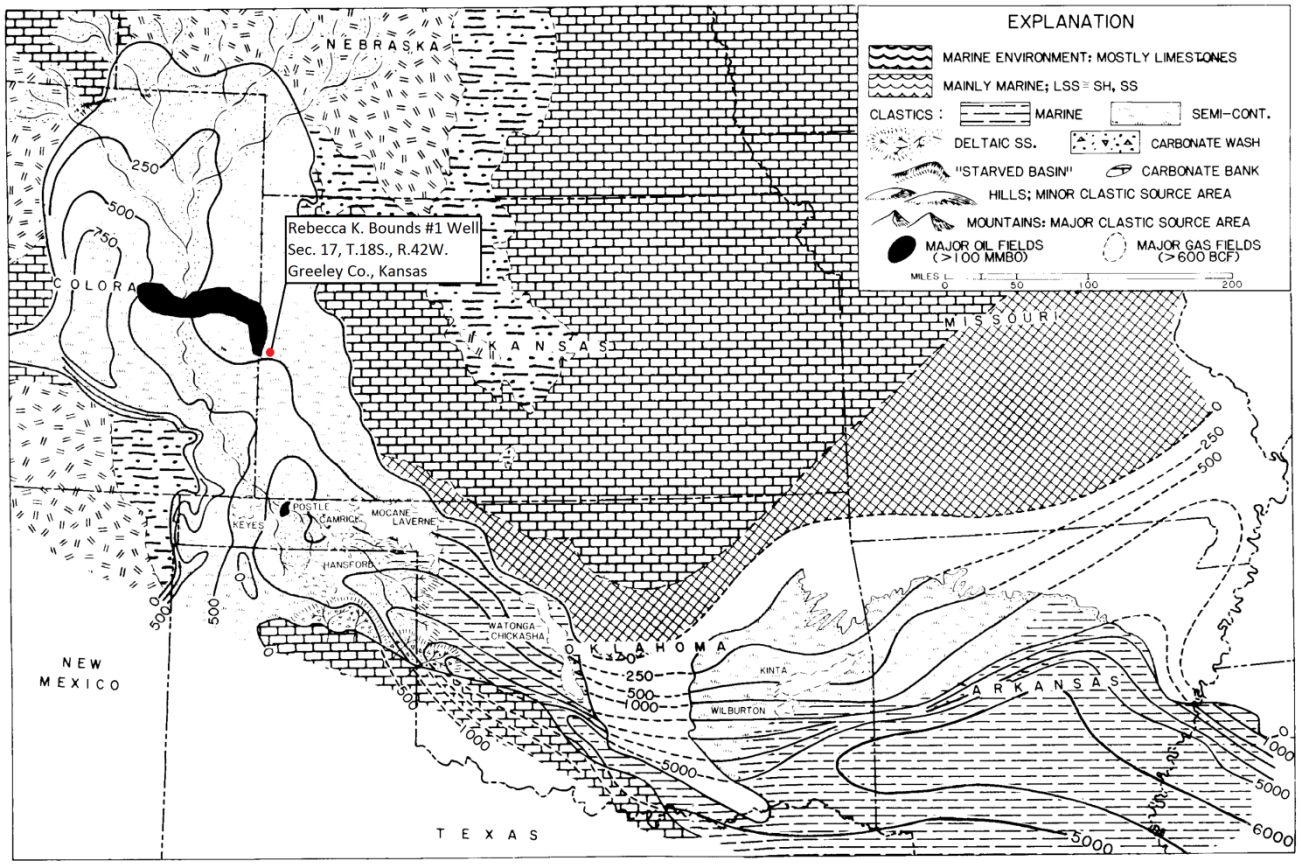

Figure 4: Depositional setting at the end of the Morrowan stage and thickness of Morrowan rocks. The Stateline Trend in black produces oil out of Morrowan channel sandstones and will have ultimate recoverable reserves of about 110 MMBO (Jones and LeBlanc, 2004) Rebecca K. Bounds #1 well in red (Modified from Rascoe and Adler, 1983).

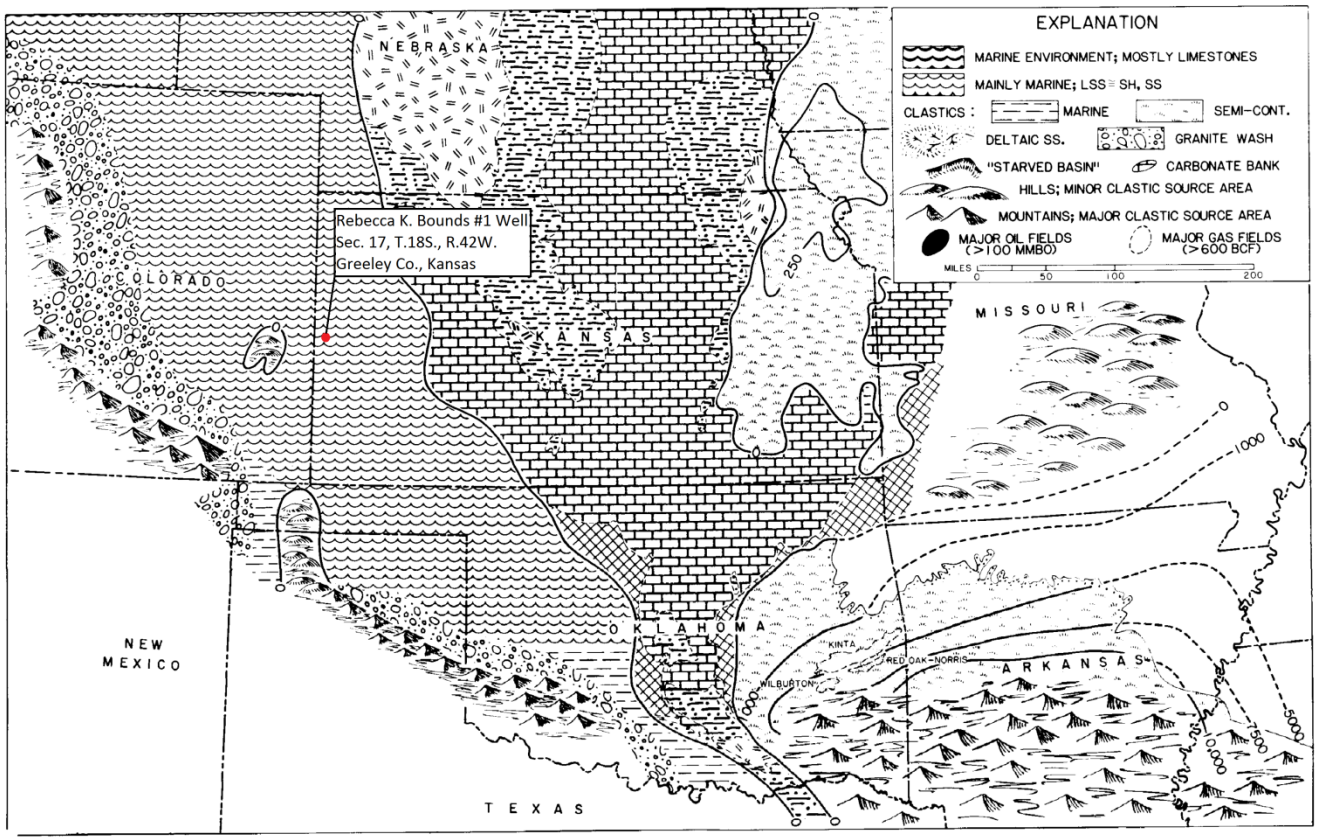

Figure 5: Depositional setting at the end of the Atokan stage and thickness of Atokan rocks in the Arkoma Basin. Rebecca K. Bounds #1 well in red (Modified from Rascoe and Adler, 1983).

The Rebecca K. Bounds #1 well is located in the Hugoton Embayment (Bowen and Weimer, 2003)(Fig. 2). The Hugoton Embayment, formally part of the "Dodge City Basin" until renamed by Maher and Collins (1949), existed as a broad shallow equatorial sea (Wicander and Monroe, 1989) that connected the early Anadarko Basin to the early Denver Basin. In the Carboniferous, uplift of the Las Animas Arch separated the Hugoton Embayment from the Denver Basin to the west. The Central Kansas Uplift separated the Hugoton Embayment from the Salina and Sedgwick Basins to the east (Huffman, 1959). The Hugoton Embayment remained open to the Anadarko Shelf to the south.

During the Pennsylvanian the Midcontinent of North America was dominated by epeiric seas (Fig. 3) that periodically inundated the craton developing cyclothems in response to eustasy (Heckel, 1986) and tectonism (Klein and Willard, 1989). Metal-rich marine black shales developed across the region. Fifteen of these marine black shales are found in a broad area of the Midcontinent USA covering 20,000 – 1,000,000 square kilometers (Coveney et al., 1991). Middle to upper Pennsylvanian strata of Kansas contain typical cyclothemic sequences composed of limestone, black core shale, gray shale, and coal (Heckel, 1986). Variance among cyclothemic deposits reflect decreased tectonic influence in the Midcontinent (Klein and Willard, 1989) although climate change may have affected cyclothem development as well (Cecil, 1990).

Brief Description of the Thirteen Finger Limestone

The Atokan is a middle Pennsylvanian stage below the Desmoinesian and above the Morrowan (Fig. 6). The Atoka Formation extends across western Oklahoma and into the Hugoton Embayment of southwestern Kansas and southeastern Colorado (Huffman, 1959). "Atokan" is the general subsurface name replacing the older term "Lampasas" (Cheney, 1940). The name comes

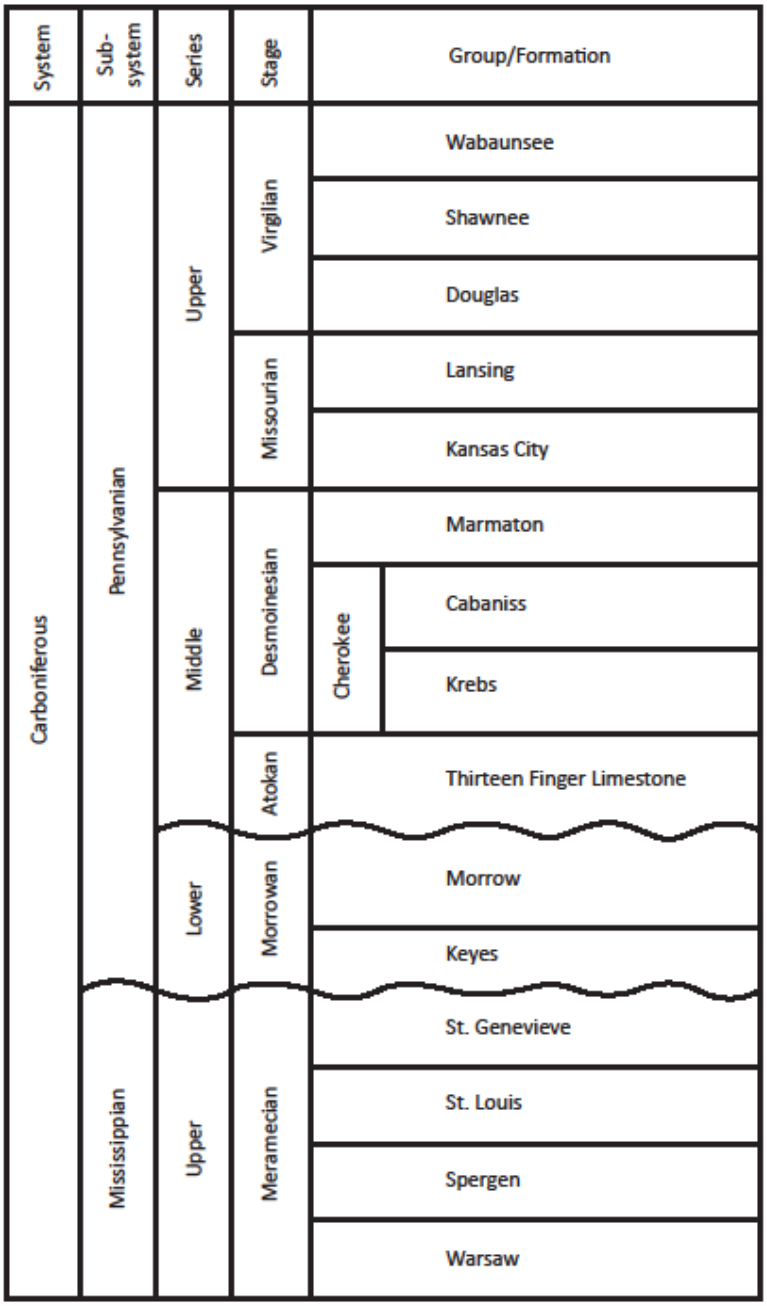

Figure 6: Geological time scale for the Carboniferous and generalized stratigraphy of the Stateline Trend of Colorado and Kansas. Nomenclature is that currently used by the Kansas Geological Survey (Modified from Moriarty, 1990)

from the type area near Atoka, Oklahoma (Branson, 1962) and was named in 1900 by J. A. Taff (Curtis and Ostergard, 1982). The type section for the Atoka Formation consists of 7,000 feet of dark shale with several sandstone tongues and lenses (Branson, 1962; Huffman, 1959). The thickest measured section of Atokan strata in the Anadarko Basin is in northern Beckham County (Huffman, 1959). In Colorado, Atokan lithologies become arkosic near the Sierra Grande Uplift. Atokan age sandstones transition to carbonates moving north from the Oklahoma Panhandle into Kansas. Near the southern margins of the Anadarko Basin, the Atokan is represented as a dolomite "wash" (Lyday, 1985). In the Arkoma Basin, thirteen gas-bearing sandstones are identified within the thick Atokan shale. In Arkansas, Atokan strata locally contain thin coal beds and carbonaceous streaks (Fort Smith Geological Society, 1960).

G. L. Meholin is credited for naming the Thirteen Finger Limestone because it has up to thirteen "fingers" on wireline resistivity logs (Jordan, 1957). This name is commonly used in the Texas and Oklahoma Panhandle portions of the Anadarko Basin. In Kansas, the Thirteen Finger Limestone consists of eleven (11) to thirteen (13) thin limestones interbedded with shale (Clark, 1987). In southwestern Clark County, Kansas, the limestone beds are light brown to gray, fossiliferous, finely crystalline to microcrystalline, and variably dolomitic, pyritic, or argillaceous. Shale units are gray to black, greasy in luster, micaceous, and fossiliferous (Mannhard and Busch, 1974). A hard coal with a greasy luster and underclay are found at the base (Curtis and Ostergard, 1982; Gibbons, 1964).

Because the Thirteen Finger Limestone is notable for its abundance of continuous interfingering shale and carbonate and widespread distribution, it is an excellent local time-stratigraphic datum (Swanson, 1979). It directly overlies the upper Morrowan shale and in turn is overlain by the Desmoinesian Cherokee Group. The Thirteen Finger Limestone is fourty-six (46) to seventy-four (74) feet thick in Texas County, Oklahoma and thickens into the Anadarko basin

(Curtis and Ostergard, 1982). The Thirteen Finger Limestone measures sixty (60) feet thick in southwestern Clark County, Kansas (Clark, 1987).

CHAPTER II

REVIEW OF LITERATURE

Most of the Pennsylvanian carbonates of the Rebecca K. Bounds #1 core were deposited in a shallow tropical sea with diverse marine biota including crinoids, bryozoans, brachiopods, bivalves, gastropods, corals, phylloid algae, borings and micritic rims and envelopes (Buijs et al., 2004). The Atokan Stage is extensively studied in the Arkoma Basin of Arkansas and Oklahoma and the Anadarko Basin of Oklahoma and Texas Panhandle where hydrocarbon production is economical. Atokan lithologies in these two basins are vastly different.

In the Anadarko Basin, the Morrowan contact with the Thirteen Finger Limestone ranges from disconformable to gradational. The Thirteen Finger Limestone is generally seventy-five (75) to one-hundred (100) feet thick and consists of a cyclic sequence of thin marine limestone and shale similar to the conformably overlying lower Desmoinesian section (Rascoe and Adler, 1983).

Worden (1961) examined pre-Desmoinesian rocks of the Amarillo-Hugoton area, a 38,000 square mile area of southwestern Kansas, southeastern Colorado, northeastern New Mexico, and the panhandles of Oklahoma and Texas. In this region, the lower contact of the Atokan consists of thin basal glauconitic sandstones to conglomerates that are interpreted to be evidence of a post-Morrowan unconformity. Above, is dark gray to brown, siliceous, “tight” Thirteen Finger

Limestone that is interbedded with dark gray to black, carbonaceous, micaceous, silty shale (Barby, 1956). Maher (1946) described the Thirteen Finger Limestone as a cream-colored, glauconitic limestone and black, dense limestones interbedded with green and black shale.

The Atokan becomes more sandy and shaly moving westward from southwestern Kansas into southeastern Colorado and becomes arkosic near the flanks of the Sierra Grande Uplift (Barby, 1956). It developes into an arkosic limestone-conglomerate interbedded with green, brown, and gray shales with lesser amounts of pink to brown "granite wash" near the top of the section along the north flank of the Amarillo Uplift (Worden, 1961).

In the deep Anadarko Basin, the Atokan consist of recycled detrital dolomites (Lyday, 1985). In the Berlin Field of Beckham County, Oklahoma, the Atoka is a 15,000' deep, overpressured reservoir encompassing 41 square miles. The source of the sediment is from erosion of the Cambro-Ordovician Arbuckle Dolomite during the Amarillo-Wichita uplift.

The Atokan has not been studied in detail in the vicinity of the study area. It is often indistinguishable from Desmoinesian strata (Rascoe and Adler, 1983) and can only be separated using fossil data, such as the predominant Atokan fusulinid *Fusulinella* (Worden, 1961). The focus of most research an Pennsylvanian rocks in west-central Kansas, eastern Colorado, and the Oklahoma Panhandle has been on oil and gas producing Morrowan channel sandstones (Bowen and Weimer, 2003).

CHAPTER III

METHODOLOGY

Research on the Atokan Series in the Rebecca K. Bounds #1 core consisted of 8 components: core description and sampling, x-ray fluorescence analysis, thin-section analysis, porosity and permeability measurements, organic carbon analysis, x-ray diffraction analysis, core digestion for biostratigraphy, and interpretation of all results.

X-ray fluorescence measurements were taken on forty-eight (48) samples with an emphasis on the shales of the Thirteen Finger Limestone. Core pieces were placed in a Thermo Scientific Portable Test Stand and tested using a Thermo Scientific Niton XL3t XRF analyzer. The XRF analyzer was set to bulk mineral mode and set to an aperture of 8mm. Three standards, including the USGS SCo-1, NIST 2780, and Iron Post Coal, were reanalyzed every seven samples. These values were compared to determine instrument reliability and accuracy of the readings over time.

Fourteen (14) carbonates and one (1) shale of the Thirteen Finger Limestone were sampled for thin sections. Samples were cut from core using a Target wet saw and polished with Buehler 600 grit silicon carbide powder on a 10" diameter Highland Park Manufacturing Co. polish wheel, followed by Buehler 1000 grit silicon carbide powder on a 1 ft^3 glass plate. These samples were attached onto Ward's 27 x 46 mm, 1.2 mm thickness petrographic microscope

slides using Loctite 0151 Hysol epoxy-patch adhesive and allowed to cure for 24 hours. Further trimming was completed using a water-cooled model 137 Ingram thin section cut-off saw and a water-cooled model 400U Ingram thin-section grinder. Final polishing was completed with Buehler 1000 grit silicon carbide powder on a glass plate. Thin sections were analyzed using a Nikon OPTIPHOT-POL thin-section petrascope with a Nikon CFW 10x point-count eyepiece.

Four plugs from unfractured carbonates were taken from the core using a water-cooled model A5816 Wilton 15" variable speed drill press. A 1" Scorpion Engineering coring bit was used. Core Labs Instruments PORG-200 using nitrogen was calibrated and used to measure porosity of the plug samples. Core Labs Instruments PERG-200 using nitrogen was calibrated and used to measure permeability of the plugs.

The core was sampled for total organic carbon (TOC) at each visibly noticeable change in lithofacies. Samples were prepared for TOC analysis by hand crushing using a porcelain mortar and pestle and by powdering in a Spex ball mill using porcelain bearings in a Spex SampleProp 8003 alumina vial.

Powdered samples weighing between 37.9 and 63.8 mg were measured using a Mettler Toledo XS205 DualRange scale, placed in Teflon blanks and run through a UIC Inc Coulometrics CM5130 Acidification Module using 2N perchloric acid to obtain the Total Inorganic Carbon (TIC) concentration. Duplicate samples were placed in ceramic blanks and run through a UIC TF55030A-1 Tube Furnace set at 950° C to measure the Total Carbon (TC) concentrations. Standards of pure calcite with 12% TC and TIC were used for calibration. CO_2 liberated through both methods was quantified by coulometric titration. Organic Carbon concentrations were calculated from the difference between the TC and TIC concentrations.

Six powdered samples that were left over from the TOC process were run through a Phillips PW 3200 X-ray Diffraction analyzer in a Phillips PW 3710 mpd control to measure the

bulk mineral composition of the Thirteen Finger limestone. These depths include 4877', 4947.5', 4952', 4953', 4973', and 5023'. Lithologies sampled included gray shale, black shale, carbonaceous black shale, and limestone.

Conodont biostratigraphy was used to date the core. Core pieces were broken into <1 in^3 pieces using a rock hammer and anvil. Crushed core was divided roughly into 500 gram sample batches and placed in 5 gallon buckets along with 6 liters of water and 550 mL of formic acid. Clay rich samples were further digested in 5 gallon buckets using hydrogen peroxide at 32% concentration. These processes were repeated until the core had been sufficiently broken down for analysis. Samples of unique core with recrystalized fractures and black shale were set aside and preserved for further analysis.

Digested samples were sifted using a Tyler Standard 0.0165 in^3 (425 μm) and U.S.A. Standard 0.0059 in^3 (50 μm) sieve. Residues in the 425 μm and 50 μm sieves were kept separate and wrapped in paper towels, labeled, and placed in a 100 series model 116G Fisher Isotemp oven to dry for 24 hours. Large residues were stored in labeled plastic bags. Fine grained residues were left to soak in kerosene for 24 hours to separate the clay from the rest of the sample. After a final sift, the remaining samples were dried and placed in small manila envelopes, labeled, and picked for microfossils. Conodonts were identified using a Nikon paleoscope. Types and abundances were calculated to aid in the interpretation of the age and depositional environments.

CHAPTER IV

CORE DESCRIPTION

The Rebecca K. Bounds #1 well drilled by Amoco Production Company was cored from 900’ to 5956 ‘. It was determined that there is a discrepancy between core depth and logged depth. Core depths, with the exception of 5005 feet and lower, are approximately five (5) feet lower than logging depths. All core descriptions, core photographs, thin section photographs, and other depths specified are in core depth. All lithologic columns, gamma-ray logs, and plotted XRF data are in log depth.

Analysis of the Rebecca K. Bounds #1 core (Fig. 7) began at 4825’ in a gray shale from the Desmoinesian Marmaton group. The Marmaton consists of gray shale, a burrowed fine-grained sandstone, the Little Osage core shale, a light gray dolomitic micrite, and a gray shale with a structureless zone (exposure surface) at the base at 4850.24’. The Little Osage Shale at 4842’ is the dominant marker bed of the Marmaton as it contains more than 22 ppm uranium (Fig. 7).

The Desmoinesian Cherokee Group stretches from an unconformity at 4850.25’ to an exposure surface at 4939.7’. Two major markers of the Cherokee include the Excello Shale at 4876’ and the Oakley Shale at 4884’. These two shales are black, organic rich, and contain more than 20 ppm uranium. The Cherokee is composed of mostly dolomitized clay-rich mud- to wackestone. Shaly fossil hash zones (2” to 6” thick) occur in the carbonates. Examples include

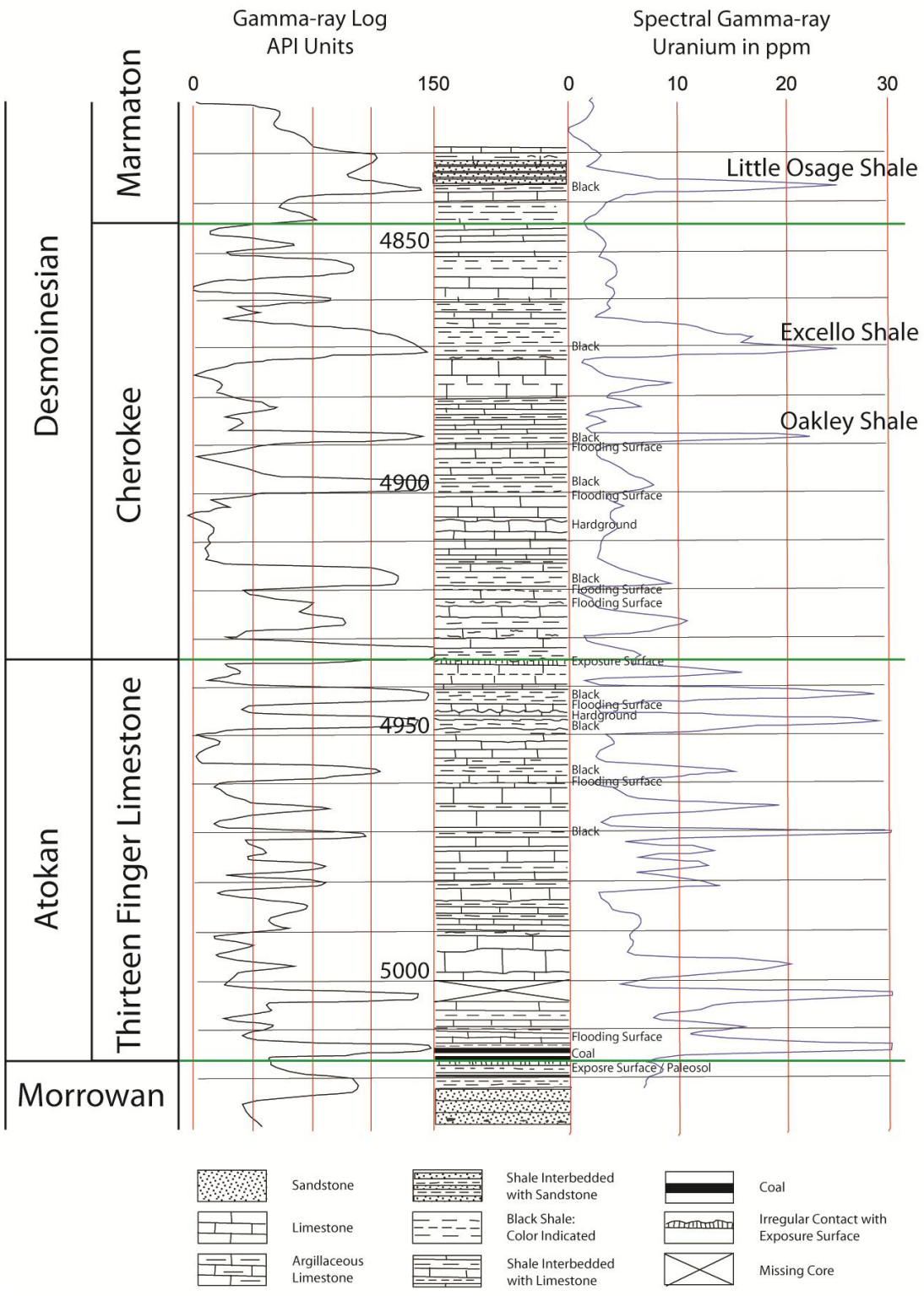

Figure 7: Lithologic column of the Rebecca K. Bounds #1 core including gamma-ray and spectral gamma-ray curves for uranium. Note core depth (used in text) is approximately five (5) feet lower than log depth above 5000'.

4878.5', 4901.5', and 4919'. A thin section at 4928' contains limestone with abundant peloids and open vertical fractures.

The Atokan section extends from an exposure surface at 4939.7' to a basal coal at 5017.5'. It contains nine (9) significant dark gray to black shales (Figs. 8 and 9) with ten (10) interbedded mud- to wackestones, some dolomitized. Many of the carbonates are clay-rich and often contain shale-rich fossil hash zones that contain abundant brachiopods and crinoids. Good examples of these can be found at 4949.5' and 4961'. Peloids are found in thin section at 4944'. From 4987' to 4996' is a nodular limestone in a dark gray mud matrix. Near the base of the Atokan are three shales that transition from carbonized to coaly shale ending with a coal at the base. These units contain three (3) interbedded micrites. Limestones at 4946', 4956-4958', 4961', and 4965' contain open vertical fractures (Fig 10). Limestones at 4944', 4951', 4955', 4966', 4970', 4973', and 5005' show numerous open and healed fractures in thin section (Fig 11). In thin section these fractures range between 6 μm to 18 μm wide.

Below the Atokan is a Morrowan paleosol at 5017.5'. Below this is a dark gray to black shale, sandstone and a dark shale that continues to the bottom of the core where analysis ended at 5073'. Detailed description of the core, including core and thin section photos, are in Appendix I.

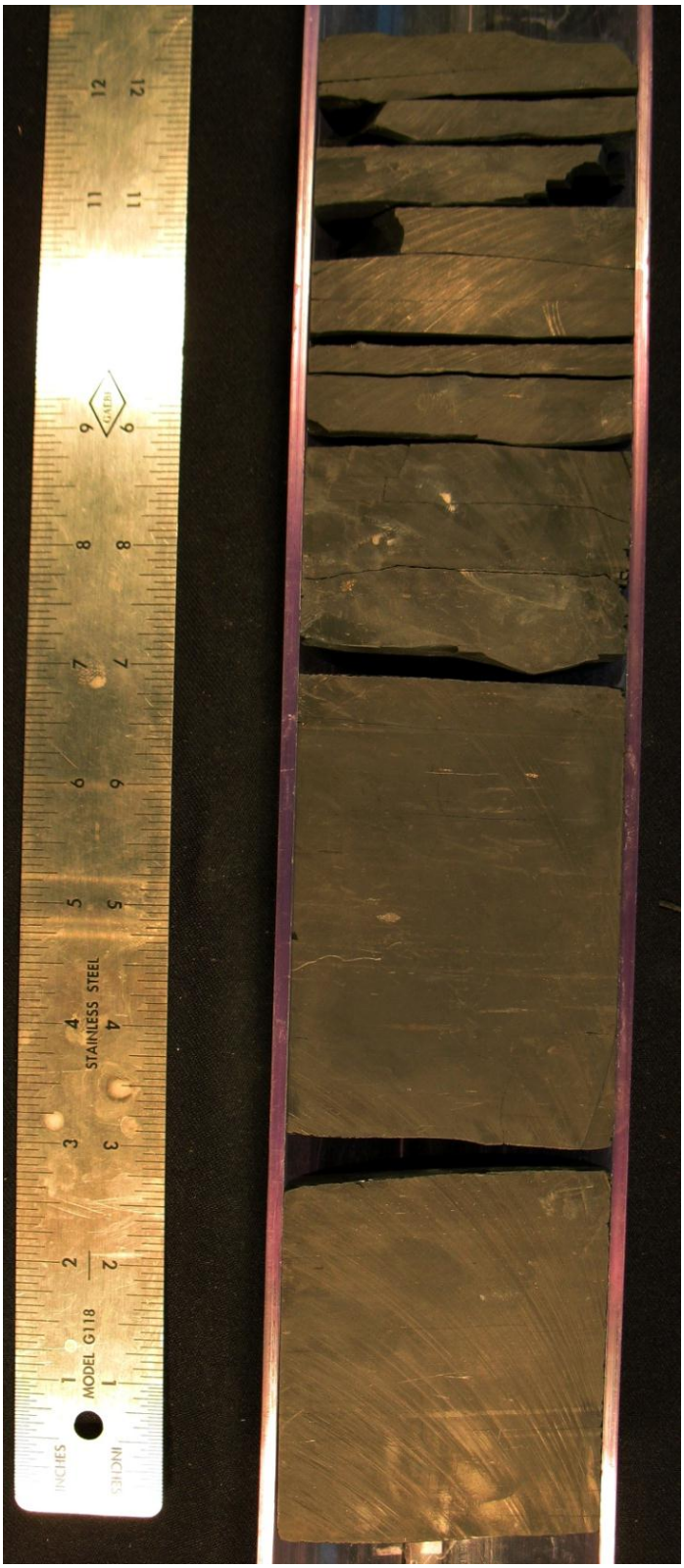

Figure 8: Core photo for depth 4952' showing a black shale with rare marine macroinvertebrates. TOC = 7.1%

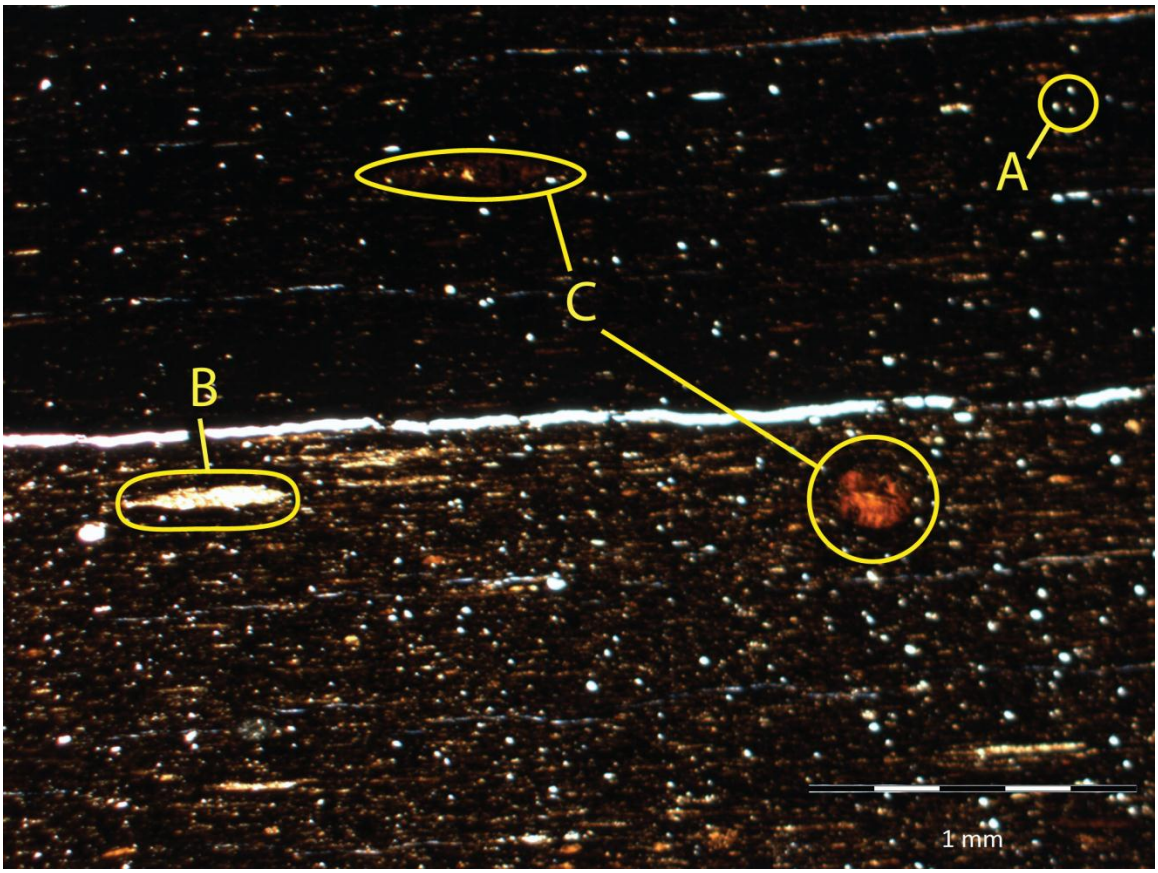

Figure 9: Thin section photo for depth 4952' showing eolian silt (A), silica replacement of bioclasts (B), and phosphate nodules (C) in a black shale matrix.

Figure 10: Core photo for depth 4955' showing a highly fractured clay-rich micrite with abundant marine invertebrate fossils including crinoids.

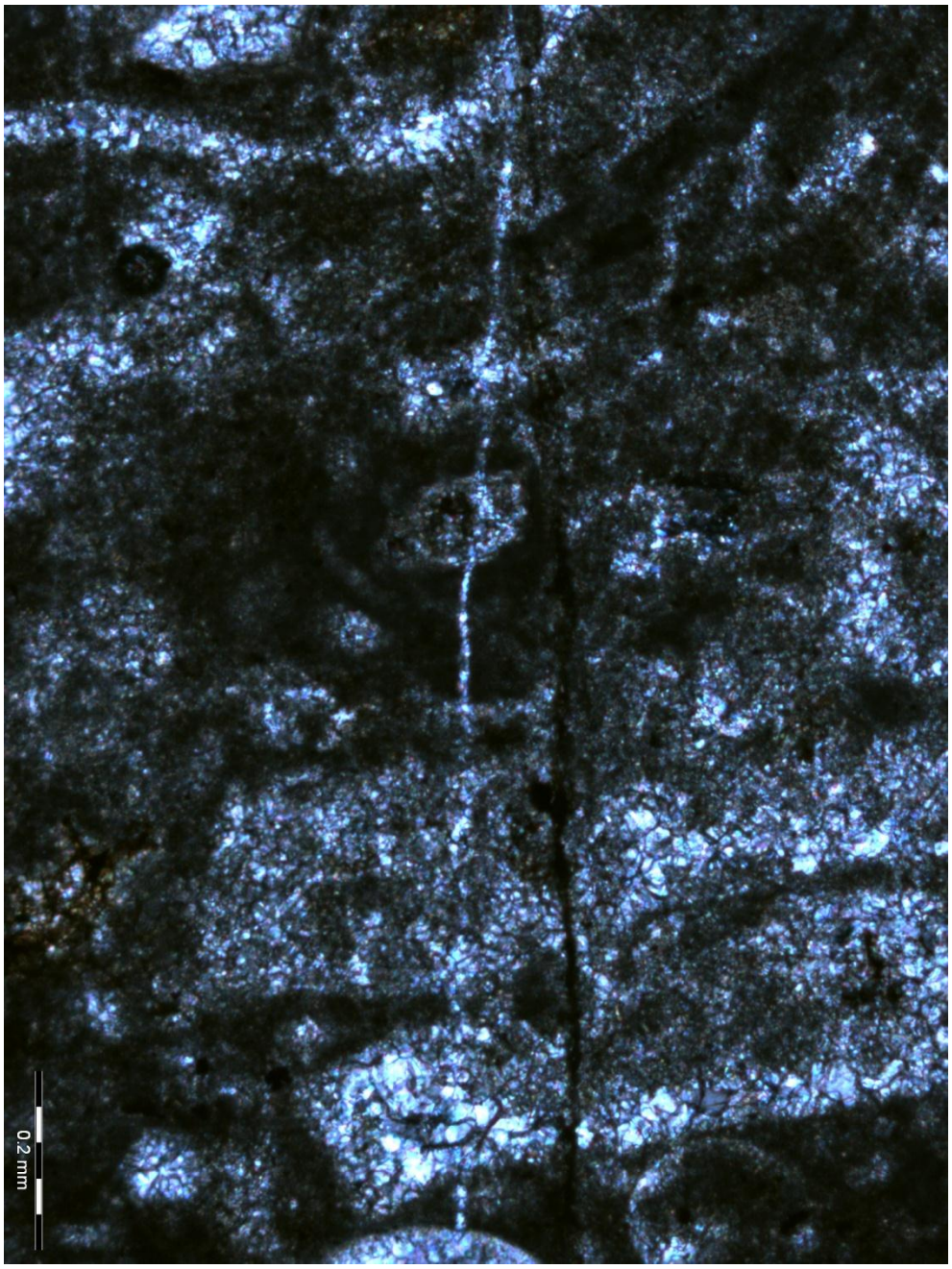

Figure 11: Thin section photo for depth 4966' showing bioclasts in a micrite matrix. The open (dark colored linear feature) and healed (light colored linear feature) factures are approximately 10 µm wide.

CHAPTER V

BIOSTRATIGRAPHY

Due to the interpreted basinal setting, numerous limestones and shales and their dark color; an initial hypothesis was that the Thirteen Finger Limestone of the Rebecca K. Bounds #1 core would contain multiple condensed sections. Initially, the core was to be biostratigraphically constrained and then correlated to other "Atokan" sections. One major difficulty facing this project was acquiring adequate volume of core to complete a detailed micropaleontological study. Only a few samples of core representing the different lithofacies were allowed to be collected for destructive analysis. This limitation in sampling has contributed to the difficulty in establishing the precise location of time boundaries between the Morrowan, Atokan, and Desmoinesian using micropaleontological analysis.

All of the collected shale and carbonate samples were processed. The shale samples were slow to disaggregate and the work is ongoing. As a result, biostratigraphic work was only completed on carbonate samples. The core samples that were dated are upper Atokan based on the co-occurrence of the conodonts *Idiognathodus gibbus* and *Idiognathodus amplificus*. More data is necessary before an interpretation of the depositional environment can be completed.

Future biostratigraphic work includes complete digestion of all shale samples from the Rebecca K. Bounds #1 core. Once completed, biostratigraphic analysis of other cores in the area will commence and the results correlated to the Rebecca K. Bounds #1 well to interpret the depositional environments during Atokan time.

CHAPTER VI

GEOCHEMICAL ANALYSIS

Total Organic Carbon

Total Organic Carbon (TOC) content is used to decipher the type of environment that existed during the time of deposition and a rock's potential to be a source for hydrocarbons. Three major controls determine TOC: organic-rich sediment supply, high organic productivity, and preservation of organic matter. Preservation of organic matter is controlled by anoxia, which occurs through the following three marine controls: restriction of lateral circulation in the deep-water column, thermohaline stratification, and high levels of primary productivity and export of organic carbon from surface waters such that respiratory oxygen demand in lower levels of the water column exceeds renewal (Cruse and Lyons, 2004).

Ronov (1958) determined that petroliferous shales of the Russian Platform have a mean TOC content of 1.37%, compared to 0.5% for carbonates. He states "These figures indicate an existence of a certain minimum of organic substance in the major sedimentary complexes below which the transformations of disseminated organic carbon cannot be conductive to the development of economic accumulations of petroleum. This critical level lies somewhere between the organic carbon averages for the petroliferous and the nonpetroliferous areas, that is, between 1.4 and 0.4 percent and it is probably closer to the first one of these two figures." (Ronov, 1958).

The minimal percentage of TOC required for economical oil and gas production is debated. Some geochemists contend that 0.4 to 1% is sufficient, while others contend that 1 to 1.5% is needed to compensate for recycled carbonized material (Hunt, 1976). Two samples from the Rebecca Bounds core, 4877' and 4947.5, contain notably carbonized shales and represent our highest TOC values, 17.0% and 20.3% respectively. Carbonized matter is unable to produce petroleum (Hunt 1976) and therefore must be accounted for in TOC evaluation.

Ettensohn (1994) states, "dark marine shales that are organic-rich and have a total organic carbon content in excess of one percent … typically form source rocks in which kerogen types I and II predominate." Hunt (1976) warns that not all dark shales are organic rich; they may owe their color to more ferrous sulfides or other heavy metal sulfides or oxides. The Thirteen Finger Limestone contains abundant pyrite and so TOC must be measured.

Twenty shale samples from the Thirteen Finger Limestone were tested for TOC. Measured values of TOC content vary from approximately 1% up to 20.2% (Figs. 12 and 13). The mean content was 6.16% for non-carbonized shales. These values are comparable to values from the Marcellus Shale that ranges from 0.6% to 11% in northeastern Pennsylvania (Laughrey et al. 2011). The Excello Shale, a Pennsylvanian (Desmoinesian) source rock, has TOC values of 1 to 17% with an average of 10% (Ece, 1989). The Excello Shale measured 17.03% TOC in the Rebecca K. Bounds core. The shales of the Thirteen Finger Limestone are rich enough to produce hydrocarbons and evidence shows the viability of extracting natural gas out of shale (Nelson, 2009). This is evident in Morton County, Kansas where there has been gas production from Atokan carbonates in the Pan American #1 Perkins well located at Sec. 28, T.31S., R.40W. in the Kinsler Field (Davis, 1964)

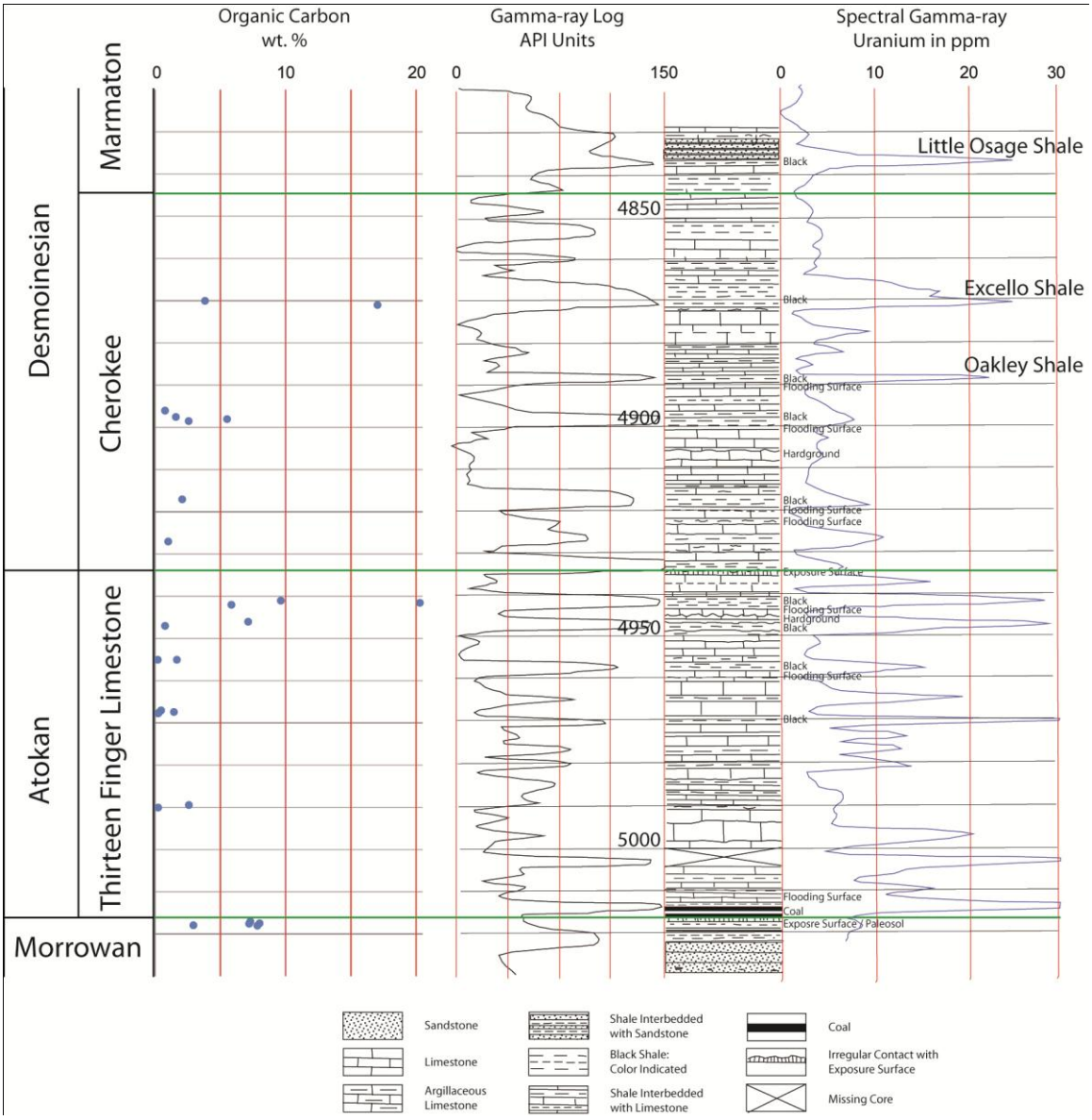

Figure 12: Lithologic column of the Rebecca K. Bounds #1 core including TOC, gamma-ray, and spectral gamma-ray for uranium.

		Sample	wt% C_{total}	wt% C_{inorg}	wt% C_{org}
Desmoinesian	Marmoton	4828'	2.86	0.00	2.86
	Cherokee	4876'	3.89	0.07	3.82
		4877'	17.69	0.67	17.03
		4902'	7.55	6.80	0.75
		4903.5'	2.32	0.74	1.58
		4904'	6.16	0.65	5.51
		4904.5'	2.95	0.38	2.57
		4907.4'	11.13	11.15	-0.02
		4923'	2.92	0.85	2.07
		4933'-34.5'	2.48	1.48	1.00
Atokan	Thirteen Finger Limestone	4944'	11.70	11.73	-0.03
		4947'	9.81	0.18	9.63
		4947.5'	20.41	0.14	20.27
		4948'	6.02	0.18	5.84
		4952'	7.35	0.23	7.12
		4953'	2.11	1.36	0.76
		4961'-63' Shaly Hash	3.36	1.70	1.66
		4961'-63'	11.73	11.53	0.19
		4973'	1.84	1.39	0.45
		4973.4'	6.20	4.77	1.43
		4973.5'	11.78	11.50	0.28
		4973.7'	10.33	10.09	0.23
		4995.4'	7.41	4.83	2.58
		4996'	11.43	11.20	0.23
Morrowan		5023'	7.28	0.00	7.28
		5023.4'	7.99	0.00	7.99
		5023.5'	7.20	0.00	7.20
		5023.9'	2.92	0.00	2.92
		5024'	7.83	0.00	7.83

Figure 13: Weight percent total carbon (C_{total}), total inorganic carbon (C_{inorg}), and total organic carbon (C_{org}) for selected samples of the Rebecca K. Bounds #1 core.

X-Ray Fluorescence

Along with organic carbon, trace metals can be used to interpret depositional environments. The Rebecca K. Bounds #1 core was sampled at forty-eight different depths using a Niton handheld x-ray fluorescence (XRF) device. Using this data, changes in base metal concentration were determined. The concentration of thirty-five elements from magnesium to uranium was measured to ppm.

Transition metals come from both detrital and authigenic sources (Cruse and Lyons, 2004). Concentrations influenced by changes in water-column conditions are authigenic. Following the steps of Cruse and Lyons (2004) to compensate for detrital sources, the data has been normalized to aluminum. Van der Weijden (2002) showed that uncorrelated variables may cause spurious correlations when normalization is used. Comparing the reported and measured values for Al of the NIST 2780 and USGS SCo-1 standards, the reported values were 2.5 times and 2.1 times the values measured using the Niton XL3t XRF analyzer, respectively. Using Sr and Mn for carbonates (Fig 14) and the transition metals for shale (Figs 15 and 16), it was determined that only the trends of the plots will be useful in confirming changes in paleoenvironments determined from microfossil and core analysis. Since the samples were not powdered, the only possible sources for contamination would be the coring and slabbing processes.

The data was plotted verses depth and expressed in a metal/Al ratio and compared to the Post-Archean Average Shale (PAAS; Taylor and McClennan, 1985; Figs 15 and 16) which is indicated by a red line. This calculated standard is an approximate baseline for the continental (detrital) mean that generally follows oxic gray shales in the Midcontinent (Cruse and Lyons, 2004) and is a good indicator of oxic (depleted) and anoxic (enriched) conditions. Analysis of the

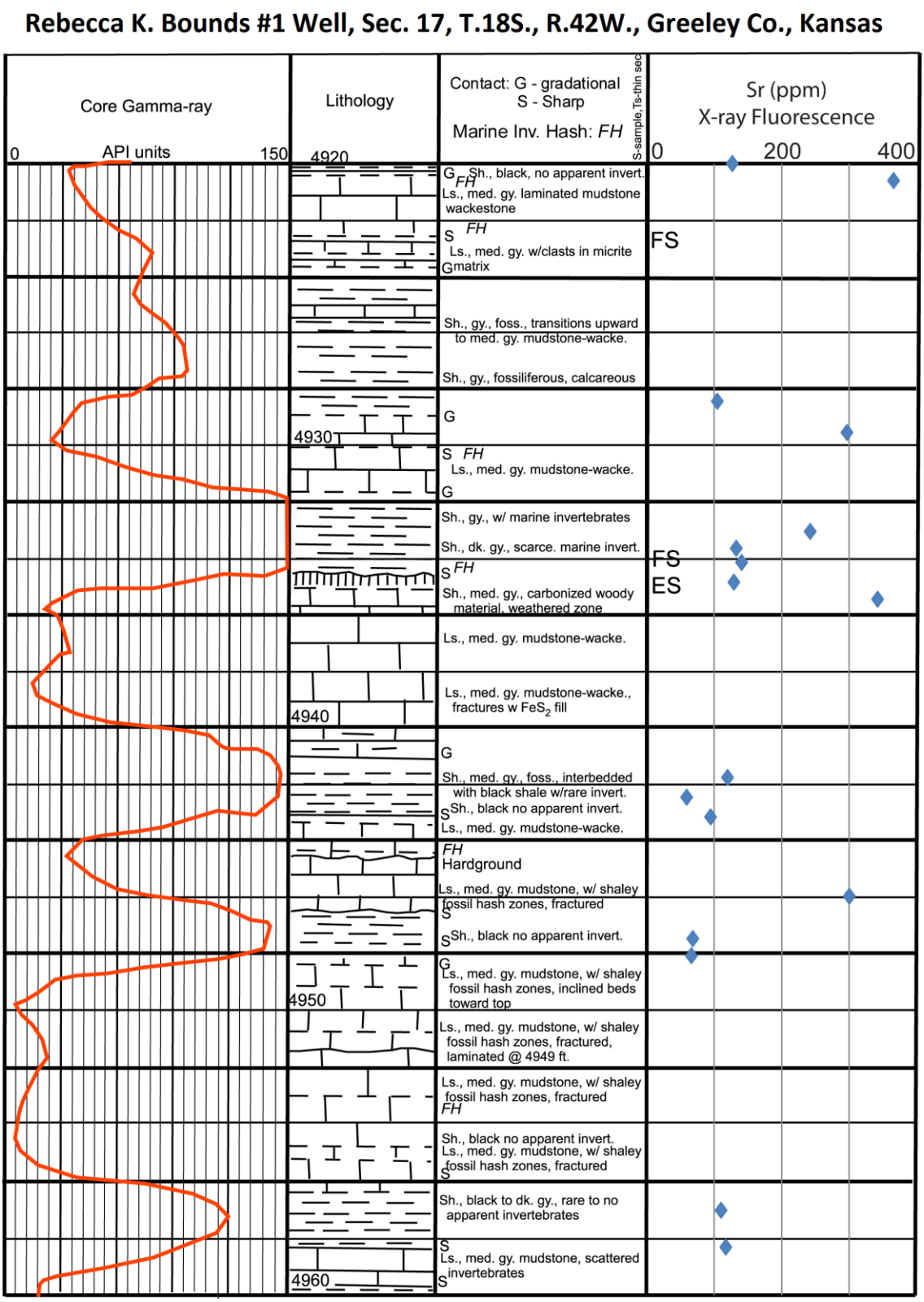

Figure 14: Lithologic column, core descriptions, and core gamma-ray with XRF Sr plotted. Higher values in Sr and Mn correlate with carbonates.

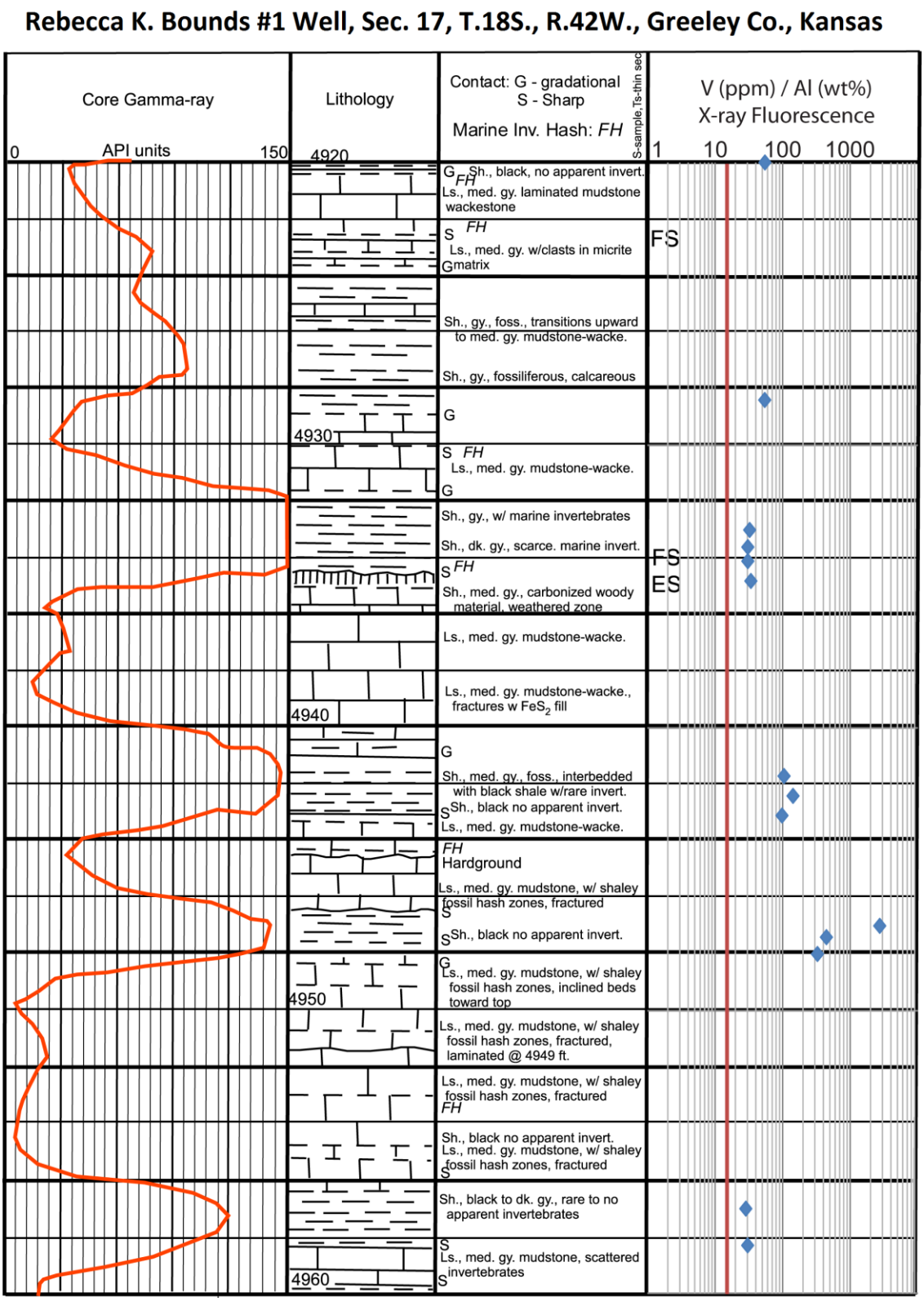

Figure 15: Lithologic column, core descriptions, and core gamma-ray with XRF V/Al ratio plotted. Higher values in transition metals correlate with dark shales. Scale is logarithmic. Red line represents the PAAS standard (Taylor and McClennan, 1985).

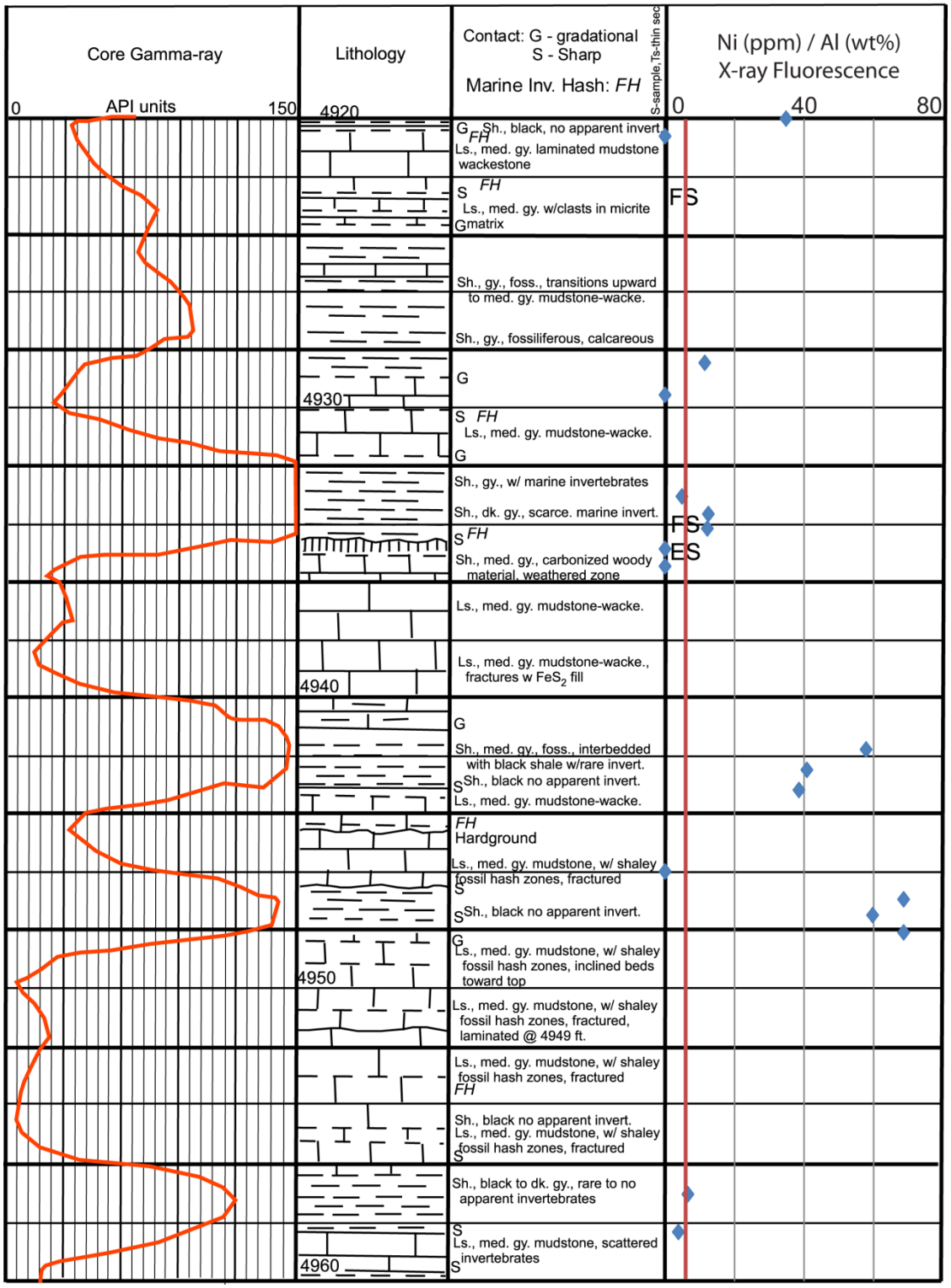

Figure 16 Lithologic column, core descriptions, and core gamma-ray with XRF Ni/Al ratio plotted. Higher values in transition metals correlate with dark shales and anoxic conditions. Red line represents the PAAS standard (Taylor and McClennan, 1985).

data show a strong correlation between "enriched" values of V, Cu, Ni, Zn, and Zr with the dark gray to black shales of the Thirteen Finger Limestone.

Analysis of the metal/Al ratio of Cu, Ni, and V show higher values in shale compared to the relatively low values in carbonates (Fig. 17). This is more obvious in transitional beds from shale to carbonate and vice versa. However, when these same values are compared for gray, dark gray and black shales, there is no apparent trend. In units transitioning from gray to black shale, the black shale does show higher values (Fig. 18), but this same relationship doesn't always apply to separate beds of gray and black shale (Fig. 17). This same trend exists with fossil abundance. Trace metal values increase as fossil content decreases within the same bed, but not between separate beds. Detailed plots of V, Ni, and Cu can be found in Appendix I, pages 132-146.

Dark-gray to black shales of the Thirteen Finger Limestone are considered "hot". Spectral gamma-ray values of uranium for some of these shales range from 20 ppm to 30 ppm. Thorium values range from 3 ppm to 9 ppm. X-ray fluorescence values for uranium are significantly higher than the spectral gamma-ray values (60 ppm to 372 ppm) while thorium values are below the level of detection (<15 ppm) for the Niton XL3t. Even though spectral gamma-ray values average values over several feet while XRF is averaging over 8 mm, the accuracy of the Niton XL3t XRF analyzer becomes questionable (Fig 19).

A study conducted at the University of California at Berkeley (Lin, 2009) sought to determine what factors could decrease the accuracy of the Niton XL3t by measuring samples from California and Chile and comparing those values to those measured by either inductively coupled plasma spectroscopy or plasma mass spectroscopy. It was determined that partical size, length of analysis, and soil chemistry had little or no effect on XRF, but organic matter and water had a significant effect on the accuracy of the Niton XL3t (Lin, 2009). Lin (2009) also noted that

Rebecca K. Bounds #1 Well, Sec. 17, T.18S., R.42W., Greeley Co., Kansas

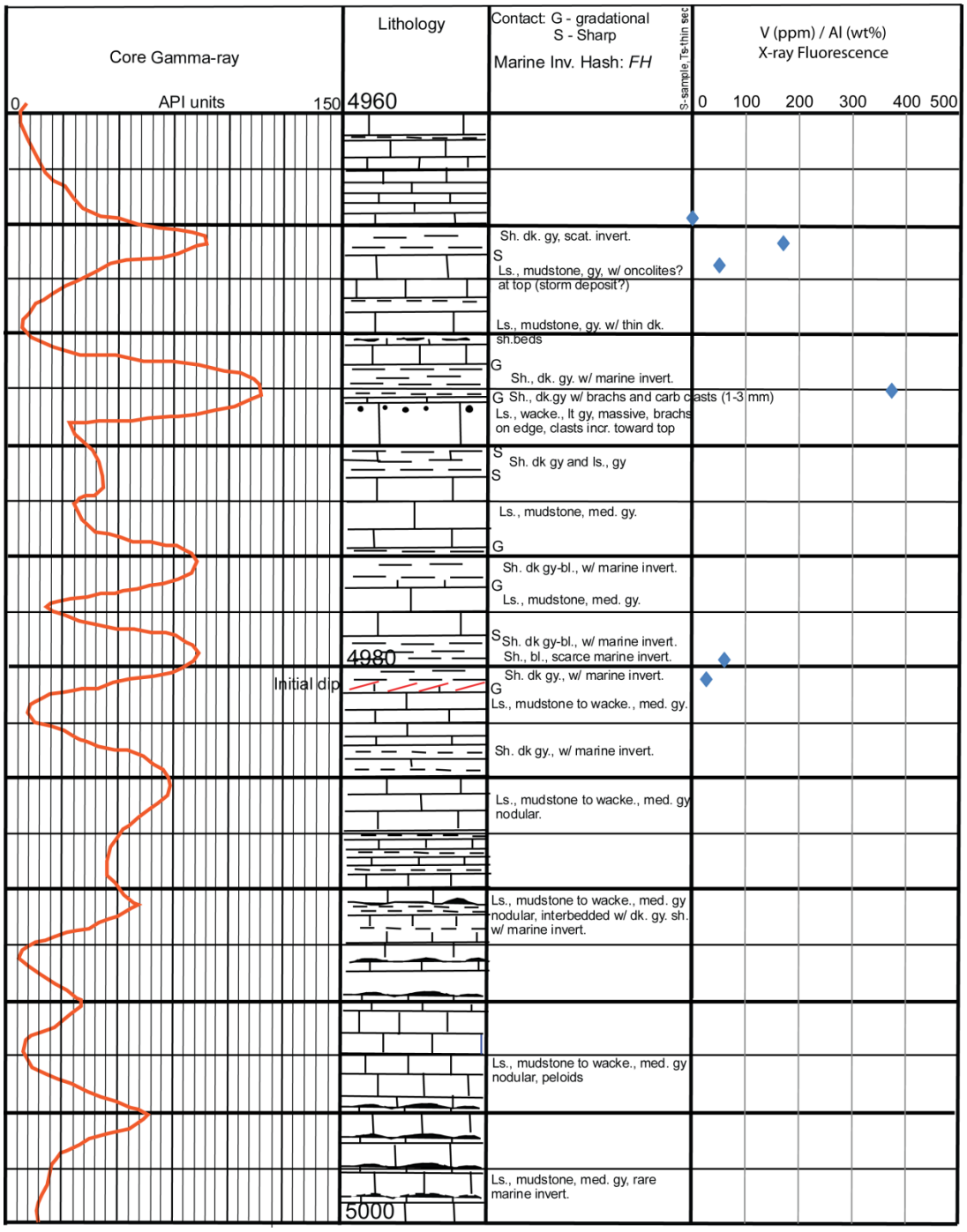

Figure 17: V/Al ratio plotted against the lithologic column for core depths 4960' to 5000'. Note the lower values for carbonates compared to shales. Shale at 4980' shows relative values in a shale that transitions from dark gray to black. But the dark gray shale at 4970' has a higher ratio compared to the black shale at 4980'.

Rebecca K. Bounds #1 Well, Sec. 17, T.18S., R.42W., Greeley Co., Kansas

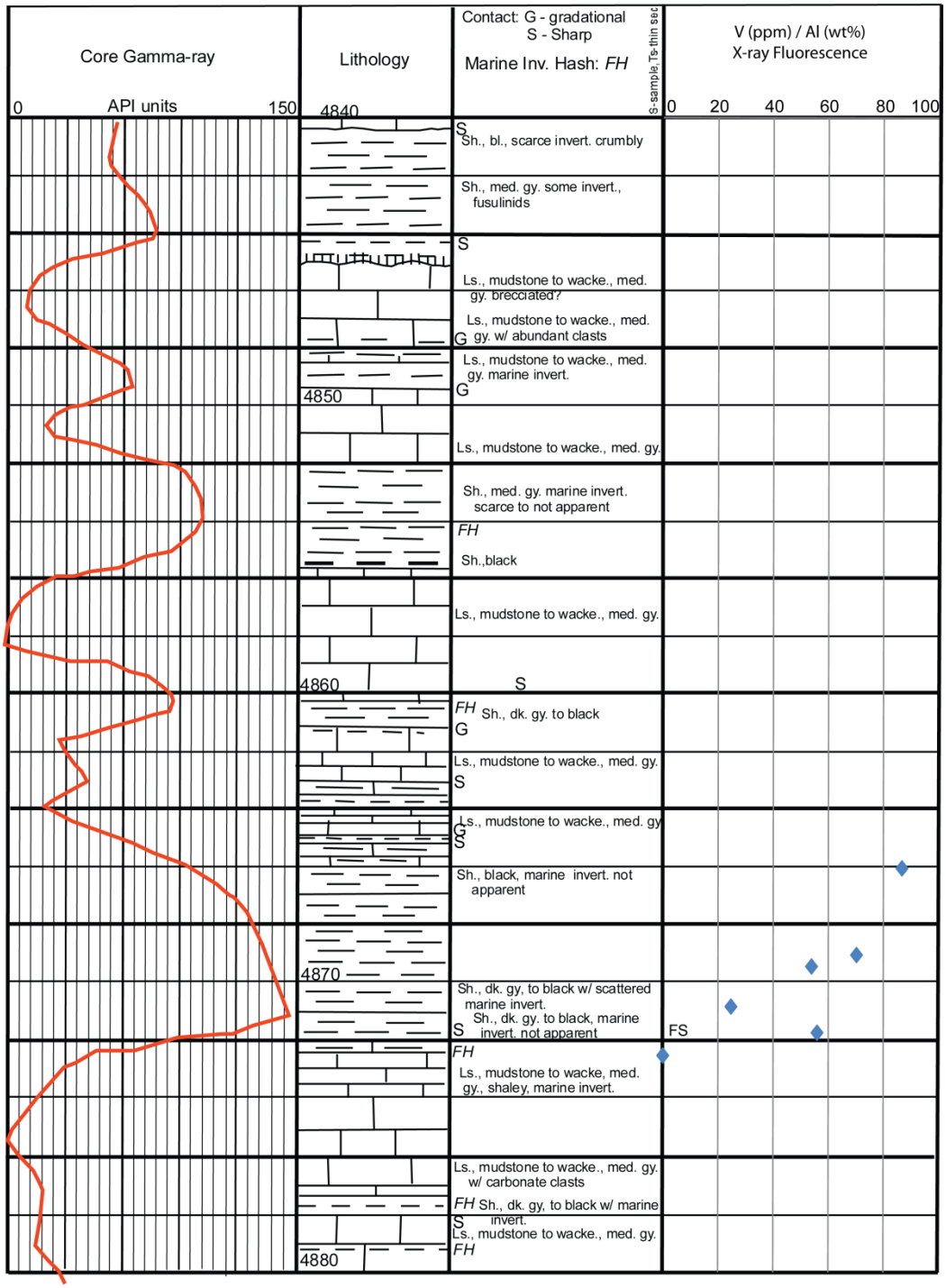

Figure 18: V/Al ratio plotted against the lithologic column for core depths 4840' to 4880'. Note the increasing values in a shale that transitions from dark gray to black.

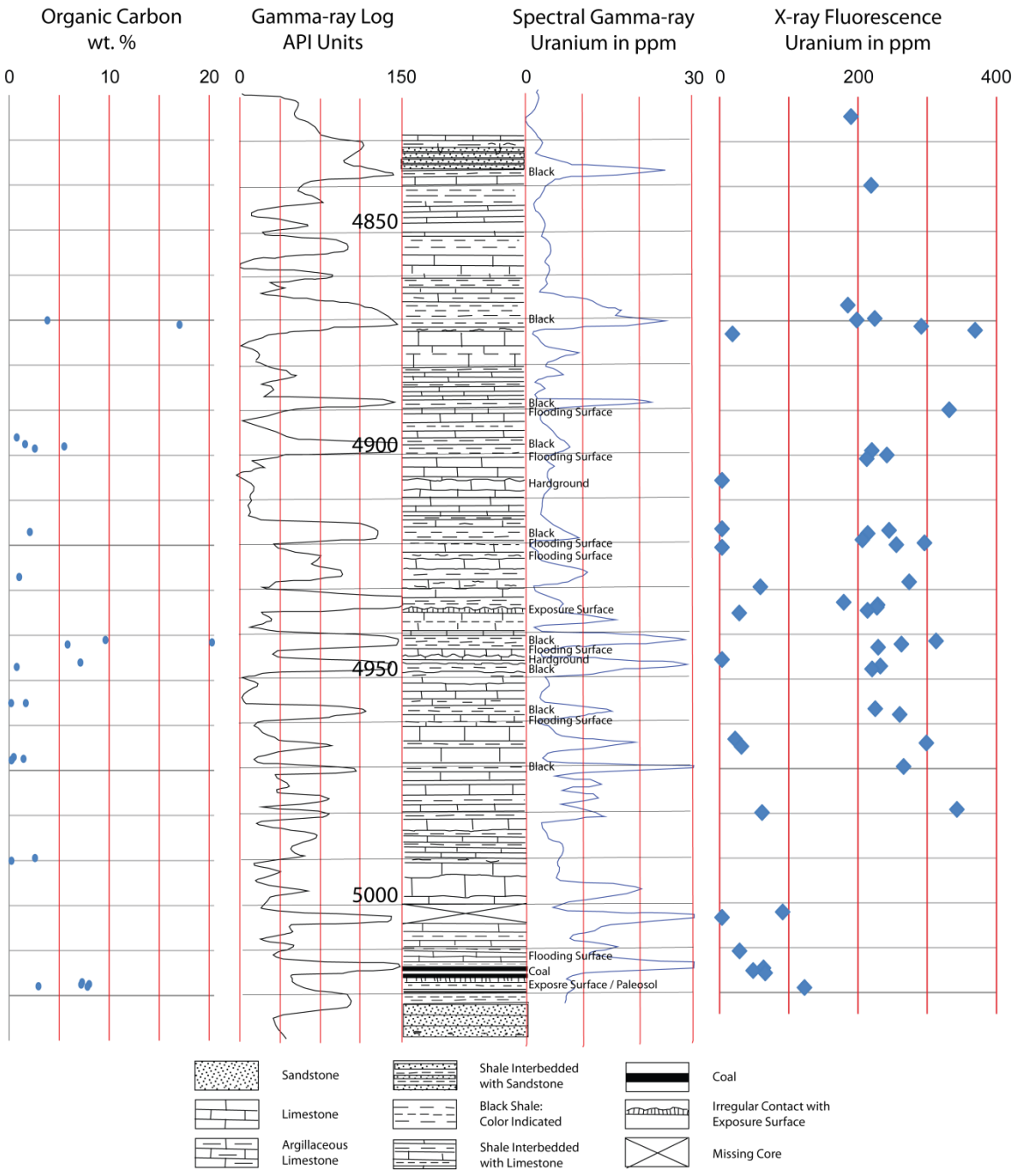

Figure 19:.Lithologic column, TOC, gamma-ray, and spectral gamma-ray for uranium plotted against XRF data for U. The apparent discrepancy between uranium values from spectral gamma-ray (max approximately 30 ppm) and XRF (max approximately 390 ppm) is obvious. Interestingly, though the absolute values for XRF were used, the plots of relative abundance of uranium determined by both methods are similar shape.

increasing the length of analysis increases the accuracy of the readings, but not significantly. Eccles and Murphy (2005) came to the conclusion that analyzing powdered samples with the Niton XL3t produced more accurate results than analysis of crushed or whole rock samples. Since XRF analysis was completed using whole core samples and many of the shale samples are rich in organic matter (<20.2 wt% C), the accuracy of the measurements comes into question.

According to Lin (2009), Eccles and Murphy (2005), the error should be no more than 20%-50%. Analysis of the standards used in this project show that values of uranium detected by the Niton XL3t were on average 71 times and 52 time higher than the actual amounts of the NIST 2780 and USGS SCo-1 standards respectively. This means that the exact values measured by the XRF analyzer are not useful, but the general pattern is still useful for finding peaks of concentrations. Comparing the XRF values with the spectral gamma-ray values for uranium, the XRF values are roughly 2 to 18 times higher than the spectral gamma-ray values in the black shales of the Thirteen Finger limestone. This means that we cannot use the uranium values acquired through XRF. XRF readings of NIST 2780 and USGS SCo-1 are located in Appendix II.

Adams and Weaver (1958) studied Th/U ratios among sedimentary rocks and determined that continental rocks have values above seven, whereas marine rocks have values below seven. They determined that the reason for this was two-fold: a reducing environment fixes uranium to organic matter or clay causing an increasing the amount of uranium in the sediment, and oxic conditions leach uranium out of sediment causing a reduction in uranium (Adams and Weaver, 1958). Thus, the more oxic the water or shallower and closer to the shoreline, the higher the Th/U ratio. Th/U values for the Thirteen Finger Limestone are below 1 with an average at 0.22 for the five “hottest” black shales (Fig 20).

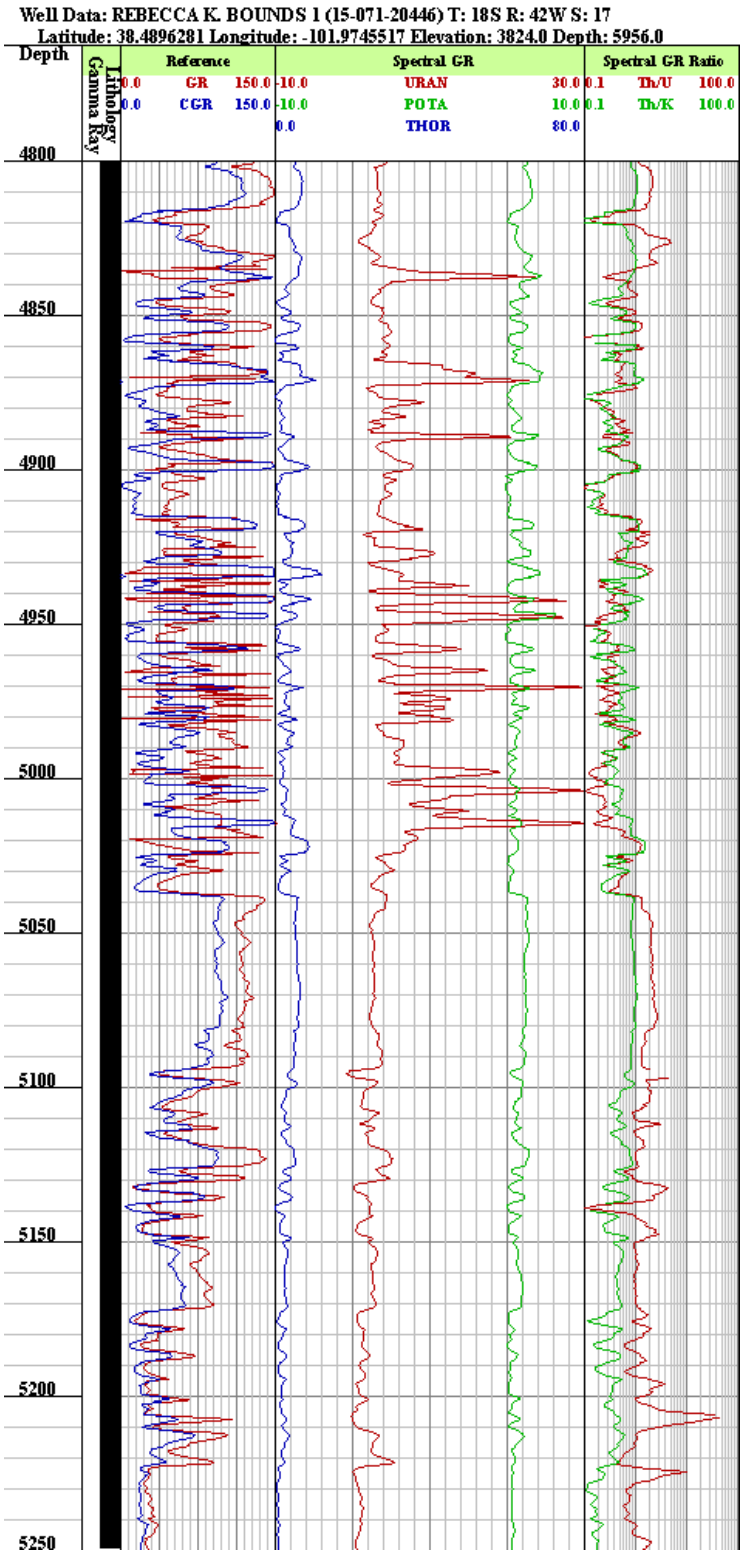

Figure 20: Log gamma-ray, core gamma-ray, and spectral gamma-ray for U, K, and Th provided by the Kansas Geological Survey of the Rebecca K. Bounds #1 well. The column to the right showing the Th/U ratio for the Thirteen Finger Limestone is at or below 1.

X-ray diffractograms of selected samples show that Atokan strata are rich in silica. Clays include illite, kaolinite, and sericite. Albite, muscovite, and biotite represent the influence of the eroding craton on sediment supply. Calcite and dolomite were also detected in some shale samples. Thin sections from 4955' and 4966' contain sphaerosiderite, microcrystalline siderite nodules signifying an anoxic environment with little to no dissolved sulfides, but abundant iron and bicarbonate (Taylor and Curtis, 1995). XRD results are located in Appendix II, pages 125-128.

CHAPTER VII

DISCUSSION

Lithofacies

The Pennsylvanian Thirteen Finger Limestone (Atokan) is comprised of thirteen (13) mudstones and wackestones interfingered by thirteen (13) dark gray to black shales. Black shales occur as two types: black shale with no apparent macrofossils and black shale with scattered marine macroinvertebrates. The carbonates are typically clay-rich and contain several shale fossil hash zones. A carbonate hardground is located at 4950'. Flooding surfaces have been identified at 4948.5' and 4963.7'. A basal coal overlies an underclay at 5017.5'. This surface is interpreted as the post-Morrowan unconformity. An exposure surface at 4939.7' represents the post-Atokan unconformity.

Geochemical Trends

TOC content for the shales of the Thirteen Finger Limestone measure between 0.76% and 20.27%. Gray shale at 5023.25' measured at 0.76%. Dark gray shale measured 1.43% to 1.66%. Dark gray to black shale measured from 5.84% to 9.63%. A TOC value of 20.27% was measured in black shale at 4947.5. This bed appears to contain recycled carbonized material, such as coal, which is inert and will not produce economical volumes of hydrocarbons. Further analysis will verify and quantify the amount of carbonized matter that needs to be accounted for in estimating

economical potential. The Thirteen Finger Limestone contains sufficient organic matter to favor hydrocarbon production. The highest measured TOC values coincide with spectral gamma-ray uranium peaks (Fig. 21). This supports the hypothesis that uranium spectral gamma-ray measurements are a predictor of nanoporosity. Future work is necessary to explore this idea.

During clastic deposition of the Atokan, organic productivity outpaced organic decomposition. This was triggered by high productivity and/or reduced decomposition. High productivity is often the result of upwelling of nutrient rich deep waters, however there is no evidence for deep water upwelling in the Hugoton Embayment during the Carboniferous. Decomposition of organic matter is directly influenced by dissolved oxygen and decreases under hypoxia and ceases under anoxic marine conditions.

Trace metal analysis of the Thirteen Finger Limestone shows higher concentrations of V, Ni, Zn, and Cu in dark shales compared with carbonates, suggesting hypoxia to anoxic conditions during periods of clay deposition. Anoxia allowed the preservation of organic matter, leading to high TOC values (>1%). During times of carbonate buildup, the waters were oxic, leading to lower concentrations of V, Ni, Zn, and Cu. Little organic matter was preserved (<0.45%).

Trace metal concentrations for gray, dark gray, and black shale varies. Shales of the Thirteen Finger Limestone generally have increasing concentrations of trace metals as color darkens and fossil abundance decreases. This is apparent in beds that transition from gray to black shale and beds where invertebrate fossil abundance varies. However, these relationships are not apparent when comparing separate beds of gray, dark gray, and black shale. This is likely the result of insufficient sampling frequency and the small size of the area scanned by the handheld XRF.

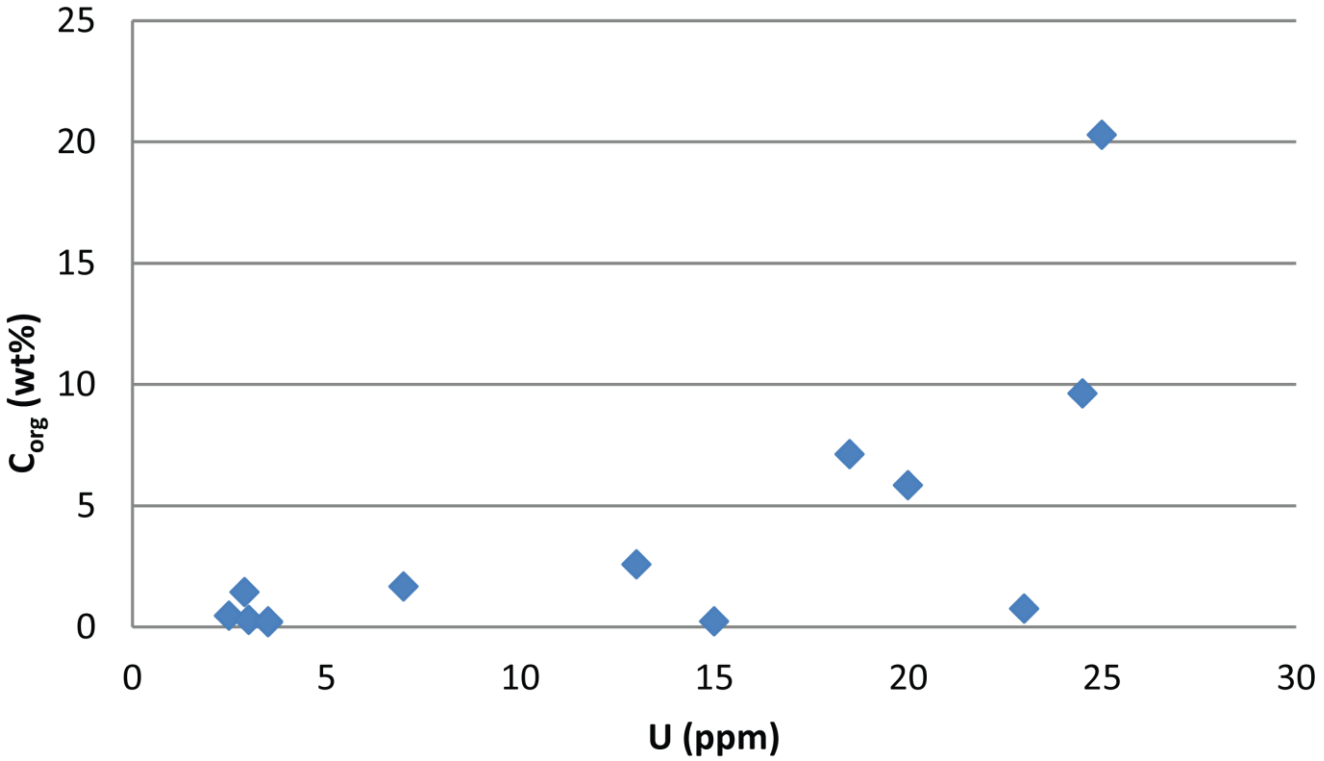

Figure 21: TOC in wt% plotted versus spectral gamma-ray uranium in ppm for shales of the Thirteen Finger Limestone. Higher TOC values correlate with higher uranium values.

Reservoir Assessment

The Atokan Thirteen Finger Limestone in the Rebecca K. Bounds #1 core is 83.5 feet thick and contains 58.3 feet of carbonate, 9 feet of which contains fractures evident in hand specimen; 18.2 feet of shale, almost entirely dark gray to black; 3 feet of coal; and 4 feet of missing core. Thin sections show numerous open and healed fractures in the carbonate. Healed fractures are cemented with calcite and pyrite, suggesting that these fractures are connected, and were the conduits for migration of basin fluids.

Porosity and permeability were tested on four unfractured carbonates at 4954', 4962', 4955', and 5005'. Porosity measured between 0.54% and 1.23%. Permeability measured between 0.1 md and 0.2 md. These measurements do not reflect overall formation porosity and permeability due to the inability to sample fractured rock. Nanoporosity was not measured. The abundance of healed fractures and silica, as measured by XRD and seen in thin section, may favor the creation of permeability through hydraulic fracturing.

TOC values for non-carbonaceous shales vary from 0.76% to 9.63%, averaging 6.16%. These values are higher than the minimum for economical oil and gas production as calculated by Ronov (1958) and discussed by Hunt (1976). Based on mapping by Newell (1997), vitrinite reflectance values of Desmoinesian strata indicate thermal maturation in the early to late stages of oil generation (0.7 to 1.08) (Fig. 22). Thermal maturity in oil producing Morrowan strata in the Stateline Trend range from 0.65 to 0.7 (Burruss et al., 1990). This suggests that the Thirteen Finger Limestone is capable of generating hydrocarbons.

Reconstructed Depositional System

Lithological and geochemical data suggests that the Thirteen Finger Limestone reflects fluctuations of sea-level in a shallow marine environment. Exposure surfaces record times of lowstand. Fine-grained deposition of clay occurred during times of transgression. Black shale

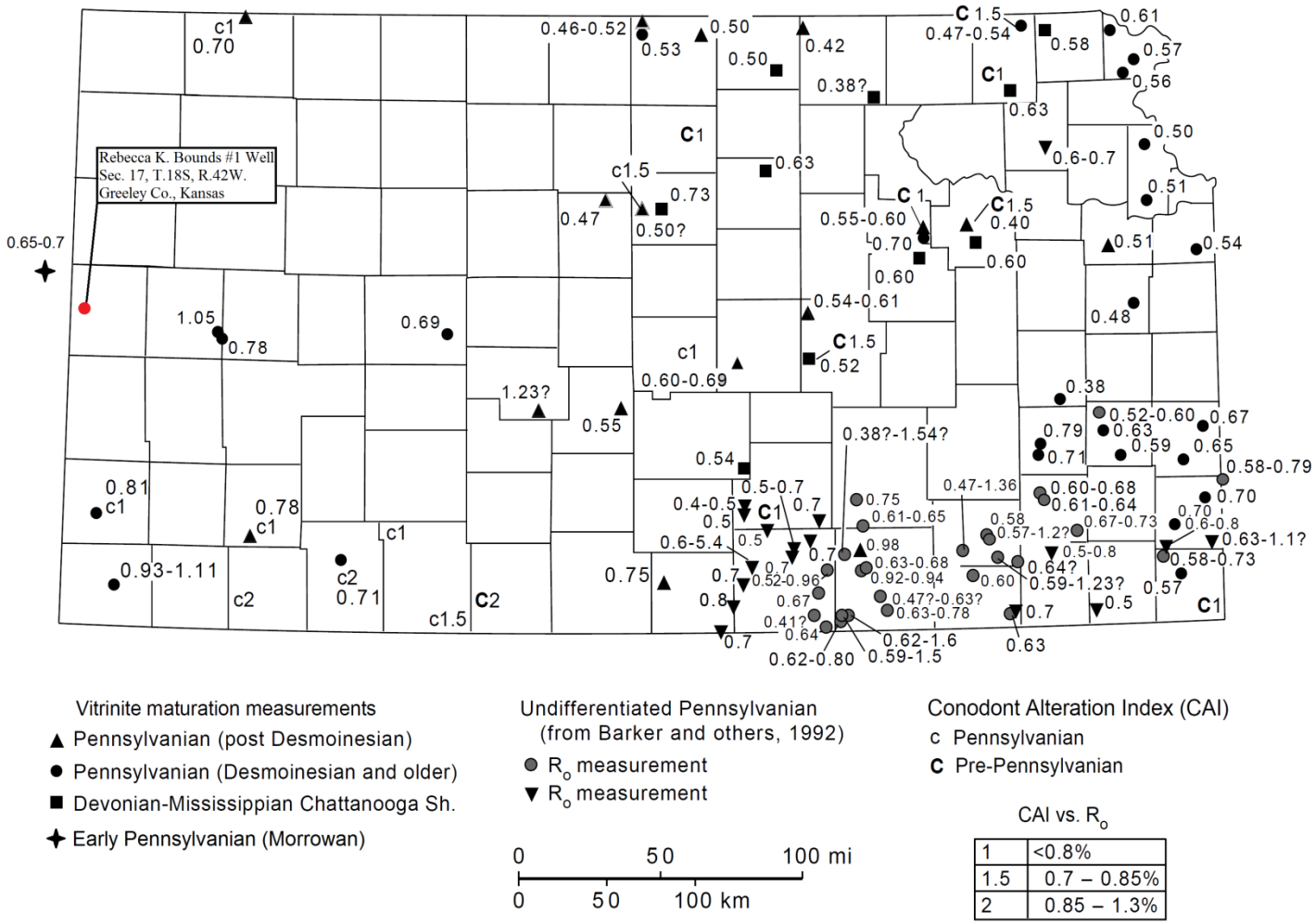

Figure 22: Thermal maturation in Kansas and the Stateline Trend (Burruss et al., 1990) in eastern Colorado based of conodont coloration and vitrinite reflectance. Location of the Rebecca K. Bounds #1 well is in red (Modified from Newell, 1997).

containing phosphate and high uranium concentrations (>20ppm) formed from sediments deposited in stratified, anoxic waters. Dark gray shale containing marine invertebrate fossils formed from sediments deposited in shallowing, hypoxic waters. These beds often transition to carbonate. In contrast, the upper contacts of carbonates with shale are sharp and indicative of flooding and rapid inundation. Th/U ratios of black shales are low (<1) suggests either deeper water anoxia resulting in uranium precipitation or a depositional setting far from any significant continental sediment source.

Carbonates of the Thirteen Finger Limestone contain low concentrations of transition metals, scattered to abundant shallow marine invertebrate fossils including crinoids and brachiopods, and peloids indicative of a higher energy shallow marine enviromnet. These carbonates contain numerous hardgrounds. These carbonates were deposited in a shallow, oxic equatorial sea (Wicander and Monroe, 1989). Th/U ratios of carbonates of the Thirteen Finger Limestone are less than 0.5, suggesting that the input of continental sediments was minimal.

CHAPTER VIII

CONCLUSIONS

The Thirteen Finger Limestone is upper Atokan and contains a record of high frequency sea level fluctuations. It contains thirteen (13) shales that are predominantly dark gray. Medium to dark gray shales have TOC values from 0.76 to 5 wt% C, lower trace metals (Cu, Ni, V) that indicate oxic to hypoxic marine conditions, and abundant macro invertebrates including crinoids. Dark gray to black shales have higher TOC values from 5 to 20 wt% C, higher trace metals (Cu, Ni, V) that indicate hypoxic to anoxic marine conditions, and rare macroinvertebrates.

The Thirteen Finger Limestone contains thirteen (13) carbonates that are predominantly mudstone to wackestone. Several of these carbonates contain numerous open and healed vertical fractures. Healed fractures are cemented with calcite, pyrite, and possibly dolomite. Several carbonates have undergone diagenetic dolomitization. These fractures have served as migration pathways for warm (<50° C), possibly basinal, fluids. XRD shows quartz as a major mineralogical constituent as evident as silica replacement of bioclasts in thin section.

TOC values are well above the recommended minimum for economical oil and gas production of 0.9 wt% C (Ronov, 1958). The Thirteen Finger Limestone is located adjacent to the oil producing Stateline Trend (Morrowan) where vitrinite reflectance values measure 0.65 to 0.7 (Burruss et al., 1990). Vitrinite reflectance values for the Desmoinesian of western Kansas measure 0.7 to 1.08 (Newell, 1997). Porosity and permeability are too low for oil generation and migration, but abundant silica increases the brittleness of the Thirteen Finger Limestone which enhances effectiveness of hydraulic fracturing to create permeability.

CHAPTER IX

FUTURE WORK

Due to the slow process of shale breakdown, further biostratigraphic work on Atokan shales in the Rebecca K. Bounds #1 core will develop depositional and paleoecological models for this area. The Kansas Geological Survey also has provided Oklahoma State University core from the nearby Pendleton/Schauf #1 well (Sec. 16, T.27S., R.26W.) in Gray County, Kansas. This core, along with others that Dr. Darwin Boardman is currently attempting to acquire will be examined to establish biostratigraphy and be correlated to the Rebecca K. Bounds #1 core.

Additional source rock evaluation will improve the understanding of the source potential of the Thirteen Finger Limestone. This work could include kerogen identification, calculating the carbonized organic matter content, and vitrinite reflectance. These will provide further understanding of the types of hydrocarbons to expect, productive TOC content, and thermal maturity.

Further high frequency sampling for TOC and trace metals will better constrain the changes in water chemistry during deposition. This information would expand the knowledge of Atokan sea level fluctuations and help establish possible causes. This is particularly useful as the Anadarko Atokan strata are much different than the well known siliciclastics that outcrop in the Arkoma Basin.

REFERENCES

Adams, J. A. S., and Weaver, C. E., 1958, Thorium-to-Uranium Ratios as Indicators of Sedimentary Processes: Examples of Concept of Geochemical Facies: AAPG Bulletin, Vol. 42, no. 2, pp. 387-430.

Adler, F. J., et al., 1971, Future petroleum provinces of the midcontinent, region 7, *in* I. H. Cram, ed., Future petroleum provinces of the Unived States – Their geology and potential: AAPG Memoir 15, Vol. 2, pp. 985-1123.

Barby, B. G., 1956, Subsurface Geology of Pennsylvanian and Upper Mississippian of Beaver County, Oklahoma: Oklahoma City Geological Society Shale Shaker, Vol. 6, no. 10, pp. 133-154.

Boler, M. E., 1959, Pre-Desmoinesian isopach and paleogeographic study of northwestern Oklahoma: Oklahoma City Geological Society Shale Shaker, Vol. 9, no. 10, pp. 6-18.

Bowen, D. W., and Weimer, P., 2003, Regional sequence stratigraphic setting and reservoir geology of Morrow incised-valley sandstones (lower Pennsylvanian), eastern Colorado and western Kansas: AAPG Bulletin, Vol. 87, pp. 781-815.

Branson, C. C., 1962, Pennsylvanian System of the Mid-continent: AAPG Special Volumes, Vol. SP 23, pp. 431-460.

Buijs, G. J. A., Golstein, R. H., Hasiotis, S. T., and Roberts, J. A., 2004, Preservation of Microborings as Fluid Inclusions: The Canadian Mineralogist, Vol. 42, pp. 1563-1581.

Burruss, R. C., Blakeney, B. A., Castle, R. A., and Kirkby, K. C., 1990, Petroleum Source Rock Potential and Thermal Maturation of the Mississippian "Harrison" and Spergen Formations and Pennsylvanian Morrow Formation and Marmaton Group, Southeastern Colorado *in* Morrow Sandstones of Southeast Colorado and Adjacent Areas: Rocky Mountain Association of Geologists, Denver, Colorado, pp. 59-66.

Cecil, C. B., 1990, Paleoclimate controls on stratigraphic repetition of chemical and siliciclastic rocks: Geology, Vol. 18, pp. 533-536.

Cheney, M. G., 1940, Geology of north-central Texas: AAPG Bulletin, Vol. 24, no. 1, pp. 65-118.

Clark, S. L., 1987, Seismic Stratigraphy of Early Pennsylvanian Morrowan Sandstones, Minneola Complex, Ford and Clark Counties, Kansas: AAPG Bulletin, Vol. 71, no. 11, pp. 1329-1341.

Coveney, R. M., Jr., Watney, W. L., and Maples, C. G., 1991, Contrasting depositional models for Pennsylvanian black shale discerned from molybdenum abundances: Geology, Vol. 19, pp. 147-150.

Cruse, A. M., and Lyons, T. W., 2004, Trace metal records of regional paleoenvironmental variability in Pennsylvanian (Upper Carboniferous) black shales: Chemical Geology, Vol. 206, no. 3-4, pp. 319-345.

Curtis, B. F., and Ostergard, D., 1982, Subsurface Stratigraphy of the Morrow Formation in southeastern Texas County, Oklahoma: Oklahoma City Geological Society Shale Shaker Digest 20, Vol. 30-32, pp. 116-146.

Davis, H. G., 1964, Kinsler Morrow Gas Field, Morton County, Kansas: Oklahoma City Geological Society Shale Shaker, Vol. 14, no. 8, pp. 2-20.

Dean, W. E., Arthur, M. A., Sageman, B. B., and Lewan, M. D., 1995, Core descriptions and preliminary geochemical data for the Amoco Production Company Rebecca K. Bounds #1 Well, Greeley County, Kansas; USGS Open-File Report 95-209, pp. 1-243.

Eccles, D. R., and Murphy, E. E., 2005, Comparison of field-portable X-ray fluorescence analyzer and conventional geochemical analysis: EUG/AGS Geo-Note 2004-04 (March 2005), pp. 1-16.

Ece, O. I., 1989, Organic Maturation and Paleoceanographic/Paleogegraphic Implications of the Desmoinesian Cyclothemic Excello Black Shale of the Midcontinent, USA: Oklahoma City Geological Society Shale Shaker Digest 12, Vol. 36-39, pp. 273-287.

Eddleman, M. W., 1961, Tectonics and geologic history of the Texas and Oklahoma panhandles, *in* Oil and gas fields of the Texas and Oklahoma panhandles: Amarillo, Texas, Panhandle Geological Society, pp. 61-68.

Fort Smith Geological Society, 1960, A subsurface correlation of the gas-producing formations of northwest Arkansas: chart.

Galloway, J. J., and Ryniker, C., Foraminifera from the Atoka Formation of Oklahoma: Oklahoma Geological Society Circular, Vol. 21, pp. 1-37.

Gibbons, K. E., 1964, Pennsylvanian of the North Flank of the Anadarko Basin: Oklahoma City Geological Society Shale Shaker 4, Vols. 12-14, pp. 71-87.

Heckel, P. H., 1986, Sea-level curve for Pennsylvanian eustatic marine transgressive-regressive depositional cycles along midcontinent outcrop belt, North America: Geology, Vol. 14, pp. 1676-1680.

Huffman, G. G., 1959, Pre-Desmoinesian Isopachous and Paleogeologic Studies in central Mid-continent Region: AAPG Bulletin, Vol. 43, no. 11, pp. 2541-2574.

Hunt, J. M., 1979, Petroleum Geochemistry and Geology, San Francisco, W. H. Freeman and Co., pp. 268-271.

Jordan, L., 1957, Subsurface stratigraphic names of Oklahoma: Oklahoma Geological Survey Guidebook 6, pp. 220.

Klein, G. D., and Willard, D. A., 1989, Origin of the Pennsylvanian coal-bearing cyclothems of North America: Geology, Vol. 17, pp. 152-155.

Kansas Geological Survey, 2011, Specific Well—15-071-20493: KGS Oil and Gas Well Database, Accessed November 2011. <http://www.kgs.ku.edu/Magellan/Qualified/index.html>

Laughrey, C.D., Ruble, T. E., Lemmens, H., Kostelnik, J., Butcher, A. R., Walker, G., and Knowles, W., 2011, Black Shale Diagenesis: Insights from Integrated High-Definition Analysis of Post-Mature Marcellus Formation Rocks, Northeastern Pennsylvania: AAPG Search and Discovery Article #110150.

Lin, J., 2009, Performance of the Thermo Scientific Niton XRF Analyzer: The Effects of Particle Size, Length of Analysis, Water, Organic Matter, and Soil Chemistry, pp. 1-36, Accessed October 2011. <http://nature.berkeley.edu/classes/es196/projects/2009final/LinJ_2009.pdf>

Lyday, J. R., 1985, Atokan (Pennsylvanian) Berlin Field: Genesis of Recycled Detrial Dolomite Reservoir, Deep Anadarko Basin, Oklahoma: AAPG Bulletin, Vol. 69, no. 11, pp. 1931-1949.

Maher, J. C., 1946, Correlation of Paleozoic Rocks Across Las Animas Arch in Baca, Las Animas, and Otero Counties, Colorado: AAPG Bulletin, Vol. 37, pp. 913.

Mannhard, G. W., and Busch, D. A., 1974, Stratigraphic trap accumulation in southwestern Kansas and northwestern Oklahoma: AAPG Bulletin, Vol. 58, pp. 447-463.

McLemore, V. T., and Frey, B. A., 2009, Appendix 8. Quality control and quality assurance report: New Mexico Bureau of Geology and Mineral Resources Open-File Report: 523, pp. 357-421.

Moore, R. C., 1948, Classification of Pennsylvanian rocks in Iowa, Kansas, Missouri, Nebraska, and northern Oklahoma: AAPG Bulletin, Vol. 32, no. 11, pp. 2011-2040.

Moriarty, B. J., 1990, Stockholm Northwest extension; effective integration of geochemical, geological, and seismic data *in* Morrow Sandstones of Southeast Colorado and Adjacent Areas: Rocky Mountain Association of Geologists, Denver, Colorado, pp. 143-152.

National Institute of Standards & Technology Certificate of Analysis, 2003, Standard Reference Material 2780, Hard Rock Mine Waste.

Nelson, P. H., 2009, Pore-throat sizes in sandstones, tight sandstones, and shales: AAPG Bulletin, Vol. 93, no. 3, pp. 329-340.

Newell, K. D., 1997, Comparison of Maturation Data and Fluid-inclusion Homogenization Temperatures to Simple Thermal Models: Implications for Thermal History and Fluid Flow in the Midcontinent: Current Research in Earth Sciences, Kansas Geological Survey, Bulletin 240, part 2. http://www.kgs.ku.edu/Current/1997/newell/newell1.html (September 2011).

Potts, P. J., Tindle, A. G., and Webb, P. C., 1992, Geochemical reference material compositions: rocks, minerals, sediments, soils, carbonates, refractories & ores

used in research & industry: Whittles Publishing, Latheronwheel, United Kingdom, pp. 1-317.

Prescott, G.C., Jr., Branch, J.R., and Wilson, W.W., 1954, Geology and ground-water resources of Wichita and Greeley counties, Kansas: Kansas Geological Survey Bulletin 108, pp. 134.

Rascoe Jr., B., and Adler, F. J., 1983, Permo-Carboniferous Hydrocarbon Accumulations, Mid-Continent, U.S.A.: AAPG Bulletin, Vol. 67, pp. 979-1001.

Ronov, A. B., 1958, Organic carbon in sedimentary rocks (in relation to the presence of petroleum): Geokhimiya, Vol. 5, pp. 409-423.

Smith, D. B., 1995, USGS Certificate of Analysis Cody Shale, SCo-1, Accessed November 2011, <http://minerals.cr.usgs.gov/geo_chem_stand/codyshale.pdf>.

Swanson, D. D., 1979, Deltaic deposits in the Pennsylvanian Upper Morrow Formation of the Anadarko Basin: Tulsa Geological Society Special Publication, no. 1, pp. 115-168.

Taylor, K. G., and Curtis, C. D., 1995, Stability and facies association of early diagenetic mineral assemblages: an example from a Jurassic ironstone-mudstone succession, UK: Journal of Sedimentary Petrology, Vol. 65, pp. 358-368.

Taylor, S.R., and McClennan, S.M., 1985. The Continental Crust: Its Composition and Evolution; An Examination of the Geochemical Record Preserved in Sedimentary Rocks Geoscience texts. United Kingdom: Blackwell Science Publication: Oxford, United Kingdom.

Tribovillard, N., Algeo, T. J., Lyons, T., and Riboulleau, A., 2006, Trace metals as paleoredox paleoproductivity proxies: An update: Chemical Geology, Vol. 232, pp. 12-32.

Van der Weijen, C. H., 2002, Pitfalls of normalization of marine geochemical data using a common divisor: Marine Geology, Vol. 184, pp. 167-187.

Weaver, C. E., 1958, Clay petrology of Upper Mississippian-Lower Pennsylvanian sediments of central United States: AAPG Bulletin, Vol. 42, pp. 272-309.

Wicander, R., and Monroe, J. S., 1989, Historical Geology – Evolution of the Earth and Life through Time: St. Paul, Minnesota, West Publishing Company, pp. 578.

Worden, J. A., 1961, Pre-Desmoinesian Isopachous and Paleogeologic Studies of the Armarillo-Hugoton Area: Oklahoma City Geological Society Shale Shaker Digest 3, Vol. 9-11, pp. 285-309.

Zurfluh, F. J., Hoffmann, B. A., Gnos, E., and Eggenberger, U., 2011, Evaluation of the utility of handheld XRF in meteoritics: X-Ray Spectrometry, Vol. 40, pp. 449-463.

APPPENDIX I

DETAILED DESCRIPTION OF THE REBECCA K. BOUNDS CORE

Core Description

4825’-4831.6’

Dark Gray/Black shale with a gradational contact with underlying limestone. Sampled for XRF, TOC, and biostratigraphy.

4831.6’-4836.5’

Upper gradational contact from shale to wackestone with a sharp lower contact. Contains three 2”-4” clay-rich zones.

4836.5’-4843.7’

Highly burrowed light- to medium-gray sandy shale with a sharp lower contact.

4843.7’-4844.2’

Highly fissile black shale with a sharp lower contact. Sampled for XRF.

4844.2’-4845.25’

Gray calcareous mudstone. Clay-rich marine fossil hash at upper contact grading into clean mudstone. Lower contact is sharp.

4845.25’-4846

Crumbly black shale with a sharp lower contact.

4846’-4850’

Medium-gray shale with flattened carbonate clasts with a clastic-like fabric showing possible soft sediment deformation. Lower section developes into a punky zone with a sharp eroded lower contact. Fusilinids and carbonized material throughout.

4850.5’-4853’

Brecciated limestone with a possible exposure surface at upper contact. Sharp lower contact.

4853’-4855.6

Clay-rich limestone with shaly intervals and abundant marine invertebrates. Sharp lower contact.

4855.6’-4857’

Medium-gray wackestone with sharp upper and lower contacts.

4857’-4860.25’

Medium-gray shale. Marine invertebrates scarce or lacking near top becoming abundant at base.

4860.25‘-4860.65’

Fissile black shale with scarce marine invertebrates and sharp upper and lower contacts.

4860.65’-4861’

Medium-gray shale with abundant marine invertebrates. Sharp upper and lower contacts.

4861’-4865.3’

Medium-gray mud- to wackestone becoming factured near base. Marine invertebrates common. Grads into a clay-rich marine hash at the base. Sharp upper and lower contacts.

4865.3’-4866.3’

A dark-gray shale with sharp upper contact and a gradational lower contact.

4866.3’-4868’

Transitions from a dark-gray calcareous shale to gray shaly limestone to light-gray limestone and back. Marine invertebrate abundance high at the top, becoming scarce in the middle, then high near the base with a fossil hash found at the upper contact.

4868’-4868.5’

Medium- to dark-gray shale with a fossil hash at the base. Sharp upper and lower contacts.

4868.5’-4871’

A fractured, dark-gray limestone that gradually becomes shaly near the base. Marine invertebrates are scattered throughout and become more abundant near the base where we have a fossil hash. Sharp upper and lower contacts.

4871’-4871.85’

A black to dark gray shale with no apparent marine fossils. Sharp upper and lower contacts. Sampled for XRF.

4871.85’-4876’

A black to dark gray shale with pyrite and scattered invertebrate fossils. Sharp upper and lower contacts. Sampled for XRF.

4876’-4877’

A black shale with no apparent marine fossils. Sharp upper and lower contacts. Sampled for XRF.

4877’-4877.6’

Gray limestone with a fossil hash zone representing a flooding surface with sharp upper lower contacts. Lower contact is erosional. Sampled for XRF, XRD, TOC, and biostratigraphy.

4877.6’-4879’

A light-gray limestone with a shaly zone including carbonate clasts separated by a marine fossil hash. Sharp upper and lower contacts.

4879’-4882.6’

Gray micrite with a zone of clastic-like appearance. Transitions from micrite to wackestone to micrite with a shale flux at the base. Sharp upper and lower contacts.

4882.6’-4882.8’

A thin dark-gray shale with sharp upper and lower contacts.

4882.8’-4885.6’

A medium- to dark-gray mudstone/wackestone with a marine fossil hash in the middle of the section. Sharp lower and upper contacts.

4885.6’-4888’

Dark-gray shaly limestone with scattered marine invertebrates at the top, becoming a medium-gray limestone, a dark-gray to black shale marine fossil hash, and a dark gray limestone at the base. Sharp upper and lower contacts.

4888-4889’

Dark gray shale with medium (<0.5 cm) burrows at the top and scattered marine invertebrate fossils. Sharp upper and lower contacts.

4889’-4891.35’

Light- to medium-gray, clay-rich limestone. Soft sediment deformation with banding disrupted by fluid escape is found at the top followed by parallel laminae that are horizontal then become slightly angled (<10°). Large (>1 cm) burrows with carbonate clasts and soft sediment deformation near the base with an unconformable, sharp lower contact.

4891.35’-4891.9’

Medium-gray limestone with sharp upper and lower contacts.

4891.9’-4894’

Limestone that is dark-gray and clay-rich near the top and becomes cleaner near the base. Abundant marine invertebrates throughout. Sharp upper and lower contacts. Sampled for TOC and biostratigraphy.

4894’-4895.7’

Dark gray to black shale with a sharp upper contact and a gradational contact with limestone below. Marine fossil hash at the bottom representing a flooding surface.

4895.7’-4901.6’

Light- to medium-gray micrite with transitional upper and lower contacts. Occasional marine invertebrates, including oncolites, that become more abundant near the base. Marine hash zone in the middle of the section. A thin section at 4896’ was made of the micrite showing a fine mud matrix, occasional marine invertebrates, and pyrite.

4901.6’-4901.8’

Shaly limestone with abundant marine invertebrates. Transitional upper and lower contacts.

4901.8’-4903’

Medium-gray limestone with marine fossil hash zones in the middle and the base of the section. Transitional upper contact and sharp lower contact. Sampled for TOC and biostratigraphy.

4903’-4906.4’

Dark-gray to black shale. Marine invertebrate fossils initially scattered near the top, becoming scarce in the middle, and becoming abundant with a fossil hash near the base representing a flooding surface. Sampled for XRF, TOC, and biostratigraphy.

4906.4’-4921.5’

Gray wackestone turning to packstone rich in coral. Varies from mud- to wackestone. Hardground at 4912.75’. Marine invertebrates mainly corals near the top, becoming rich in foraminifera. Lower half of this section is fractured and contains fossil hash zones. Base is rich in clay with a fossil hash zone at the contact with the next lower section. Thin sections were made from the wackestone at 4907’ and the packstone at 4921’. The thin section at 4907’ shows zones of clay matrix, silica replacement of bioclasts, and calcite infilling of marine invertebrates. The thin section at 4921’ shows silica replacement of bioclasts, calcite infilling of marine invertebrates, and clasts of shale.

4921.5’-4925.45’

Black shale with sharp upper and lower contacts. Lacks normal marine invertebrate fauna. Possible pyritized burrows. Sampled for XRF.

4925.45’-4927.5’

Light-gray limestone transitioning to a shaly hash at the upper and lower contacts. Upper contact is sharp while the lower contact is gradational. Sampled for XRF.

4927.5’-4927.85’

Dark gray shale rich in marine invertebrate fossils. Gradational upper contact. Lower contact is sharp and posiibly a flooding surface.

4927.85’-4930’

Light- to medium-gray clay-rich limestone with shaly zones. Broken along bedding planes. Sharp upper and lower contacts. A thin section was made at 4928’ showing scattered marine invertebrates, oncolites, healed and open fractures, and occasional dolomite in crystalline zones.

4930’-4930.5’

Massive light gray limestone with sharp upper and transitional lower contacts.

4930.5’-4934.4’

Calcareous gray shale transitioning to a limestone near the top and to a dark gray at the base. Shaly hash at the base grades into lower unit. Sampled for XRF.

4934.4’-4934.9’

Gray limestone which grades into a shaly hash at both the top and bottom. Sharp lower contact. Samlped for XRF.

4934.9’-4936.7’

Medium gray limestone with possible burrow or dissolution feature filled with grainy textured carbonate. Sharp upper contact and gradational lower contact into gray shale. No apparent invertebrate fauna.

4936.7’-4939.6’

Medium-gray shale at the top becoming dark-gray half way down section. Marine invertebrate fauna is abundant and becomes scarce with the color change. Gradational upper contact. Sharp lower contact with a fossil hash. A possible sequence boundary with carbonized wood on the bedding plane.

4939.6’-4943.2’

Exposure surface at the top in a gray shale transitioning to a medium- to light-gray limestone with a few shaly zones and a sharp lower contact.

4943.2’-4945’

Light- to medium-gray fractured limestone. Some fractures have been filled with pyrite. Upper and lower contacts are sharp. Sampled for TOC and biostratigraphy. A thin section was made at 4944’ that contain abundant marine invertebrates, oncolites, pyrite, and healed fractures.

4945’-4946.45’

Medium- to dark-gray clay-rich limestone with scattered marine invertebrate fossils. Upper contact is sharp and lower contact is gradational to shale.

4946.45’-4946.65’

Thin bedded dark gray shale with fossil hash. Upper and lower contacts are gradational.

4946.65’-4948.55’

Black shale with no apparent marine invertebrates. Upper contact is gradational and lower contact is sharp. A dark gray shaly hash is found at the base. Sampled for XRF, XRD, TOC, and biostratigraphy.

4948.55’-4849.4’

Medium gray limestone becoming shaly at the top and bottom. Marine invertebrates are abundant. Upper and lower contacts are sharp. Sampled for TOC and biostratigraphy.

4949.4’-4949.6’

Dark gray shaly hash with a sharp upper contact and gradational lower contact into limestone. Marine invertebrates are abundant. Lower contact is erosional.

4949.6’-4950.5’

Medium gray limestone with a burrowed hardground at the upper contact. Lower contact is gradational into shale. Sampled for TOC and biostratigraphy.

4950.5’-4950.6’

Thin dark gray fissile shale with gradational upper and lower contacts.

4950.6’-4951.5’

Medium gray dolomitic limestone with gradational upper contact and sharp lower contact. Marine invertebrates are not apparent. Has been sampled for XRF, TOC, and biostratigraphy. Thin section made at 4951’ shows occasional marine invertebrates with dolomite infill and a grainy dolomitic texture.

4951.5’-4951.7’

Dark gray clay-rich limestone with thin laminations. Sharp upper and lower contacts. Sampled for TOC and biostratigraphy.

4951.7’-4953.25’

Black shale with sharp upper and lower contacts. Top of section is a fine shaly hash. Sampled for XRF, XRD, TOC, and biostratigraphy. Thin section made at 4952’ show unidentifiable silica replaced bioclasts, eolian silt, phosphate nodules, and phosphatic layering.

4953.25’-4954’

A gray shale fossil hash is located at the top transitioning into a parallel laminated limestone followed by dipping laminations, possibly indicating currents. Upper and lower contacts are sharp. Sampled for TOC, XRD, and biostratigraphy. Thin section made at 4954’ showing abundant marine invertebrates, pyrite, clay-rich zones, and crystalline carbonate zones. Porosity = 0.88101 %, Permeability = 0.2 md.

4954’-4955.85’

Medium- to dark-gray limestone with fossiliferous shaly intervals. Parallel laminations throughout. Sharp upper contact and quick grade to shale at the base. Sampled for TOC and biostratigraphy. Thin section made at 4955’ shows a fine mud matrix, abundant marine invertebrates, abundant fossil fragments, sphaerosiderite, and occasional crystalline dolomite. Porosity = 0.54427, Permeability = 0.1 md.

4955.85’-4957.2’

Fractured medium- to dark-gray limestone. Quick grade from shale to limestone at upper contact. Sharp lower contact with thin basal shale. Limestone becomes shaly and clay-rich near the base. Sampled for TOC and biostratigraphy.

4957.2’-4958.5’

Dark gray clay-rich limestone with healed and open fractures and scattered marine invertebrates. Healed fractures have been filled with calcite and shaly intervals are rich in marine invertebrates. Sharp upper and lower contacts. Sampled for TOC and biostratigraphy.

4958.5’-4959.9’

Fractured medium- to dark-gray limestone with scattered marine invertebrates. Shaly interval in the middle of the section. Upper contact is sharp and lower contact grades into a dark gray shale.

4959.9’-4960.2’

Dark gray fossil-rich shale transitioning to black shale with rare marine invertebrates. Upper contact is gradational and lower contact is sharp.

4960.2’-4961.75’

Medium gray micrite with two fossiliferous shaly hash zones in the upper half of section. Lower half consists of open fractured micrite. Upper and lower contacts are sharp. Sampled for TOC and biostratigraphy. Thin section made at 4961’ shows occasional marine invertebrates and a clay matrix with crystalline calcite fragments. Porosity = 0.539735%, Permeability = 0.1 md.

4961.75’-4962.4’

Dark gray shaly micrite with rare marine invertebrates. Sharp upper and lower contacts. Sampled by XRF.

4962.4’-4962.65’

Dark gray shale fossil hash zone. Sharp upper and lower contacts. Sampled for TOC and biostratigraphy.

4962.65’-4963.75’

Dark gray to black shale with rare marine invertebrates. Upper and lower contacts are sharp. Sampled by XRF.

4963.75’-4965.8’

Medium gray fractured micrite with scattered marine fossils. Clay-rich interval in the middle of the section. Sharp upper and lower contacts. Sampled for TOC and biostratigraphy.

4965.8’-4967.75’

Dark gray clay-rich limestone with a dark gray fossiliferous shaly zone at the top of the section and two more in the middle of the section. Lowest shaly interval consists of coaly black shale. Laminations start dipping in the lower half of the section. Thin section at 4966’ shows muddy matrix, abundant marine invertebrates, abundant fossil fragments, spaerosiderite, silica replacement of bioclasts, and open and calcite-healed fractures.

4967.75’-4969’

Dark gray micrite transitioning into a thinly laminated dark gray shale at the top where marine invertebrates are scattered. Upper and lower contacts are sharp. Sampled by XRF.

4969’-4970.2’

Dark gray shale with scattered marine invertebrates. Upper and lower contacts are sharp. Sampled by XRF.

4970.2’-4970.35’

Clay-rich oncolite limestone. Upper contact is sharp and lower contact grades into a dark gray shale. Sampled for TOC and biostratigraphy.

4970.35’-4972.95’

Medium- to dark-gray dolomitic micrite with several shaly fossil zones. Upper and lower contacts quickly grade to dark gray shale. Sampled for XRF, TOC, and biostratigraphy. A thin section from 4970’ shows a grainy texture of dolomite rhombohedra which contain pyrite, shale fragments, and open fractures.

4972.95’-4974’

Medium- to dark-gray fractured limestone with abundant marine invertebrates. Fractures are healed with calcite. Upper and lower contacts grade into dark gray shales. The lower gradational contact into shale is more abrupt than the upper contact. Sampled for TOC, XRD, and biostratigraphy. Thin section at 4973’ shows a mud matrix with abundant marine invertebrates, abundant fossil fragments, healed fractures, silica replaced bioclasts, and shale clasts.

4974’-4975.4’

Horizontally bedded dark gray shale with scattered marine invertebrates grading into a limestone at the base of the section. Lower section consists of horizontally bedded marine invertebrate fragments and carbonate clasts between 1 mm and 3mm in diameter. The upper contact is gradational and the lower contact is sharp. Sampled by XRF.

4975.4’-4977’

Medium- to dark-gray wackestone with a clastic appearance with soft sediment deformation. There is no apparent bedding. Carbonate “clasts” are initially pebble size grading into sand size. Upper and lower contacts are sharp.

4977’-4977.75’

Dark gray limestone grading into a dark gray shale in the middle of the interval and then back into limestone. Marine invertebrates are scattered but not abundant. Gravel size carbonate “clasts” are found in the shaly interval. Upper and lower contacts are sharp.

4977.75’-4978.3’

A thin dark gray fossiliferous shale with sharp upper and lower contacts.

4978.3’-4980.6’

A medium gray micrite with clay-rich intervals becoming more clay-rich near the base. The upper contact is sharp. Micrite transitions into shale with a gradational lower contact with the underlying shale.

4980.6’-4981.4’

Dark gray to black shale with scatterd marine invertebrate fossils. The upper and lower contacts are gradational into micrite.

4981.4’-4982.65’

Long transition from a fossiliferous dark gray shale at the top of the section to a light gray micrite with rare marine invertebrates at the base of the section. The upper contact is gradational and the lower contact is sharp.

4982.65’-4984’

Light gray micrite with rare marine invertebrates. Upper and lower contacts are sharp.

4984’-4985’

Transitional from a dark gray shale with scattered marine invertebrates to a black shale with rare marine invertebrates. The upper and lower contacts are sharp. Sampled by XRF.

4985’-4985.5’

Dipping dark gray shale with abundant marine invertebrates. The upper and lower contacts are sharp. Sampled by XRF.

4985.5’-4988.45’

Medium- to dark-gray micrite with fossil-rich shaly and wacke zones. The upper contact is sharp and the lower contact grades into the underlying dark gray shale.

4988.45’-4989’

Horizontally bedded dark gray shale with abundant marine invertebrates. The upper contact is gradational into the above micrite. The lower contact is sharp.

4989’-4993.4’

Medium gray nodular limestone in a clay-rich matrix. Shaly matrix contains scattered marine invertebrates. The upper and lower contacts are sharp. Thin section at 4999’ shows a transition from clean micrite to grainy calcite with rare marine invertebrates and pyrite.

4993.4’-4993.9’

Dark gray shale with parallel laminations. Upper and lower contacts are sharp.

4993.9’-4994.25’

Medium- to dark-gray wackestone with abundant marine invertebrates. Notable constituents include oncolites and gastropods. Upper and lower contacts are sharp.

4994.25’-4994.5’

Parallel laminated dark gray shale with abundant marine invertebrates. Upper and lower contacts are sharp.

4994.5’-4996’

Dark gray nodular micrite in a dark gray fissile clay matrix. Shaly matrix contains scattered marine invertebrates. The upper and lower contacts are sharp. Sampled for TOC and biostratigraphy.

4996’-5006’

Light olive green micrite with no apparent marine invertebrates with several zones of dark gray shale. Upper and lower contacts are both sharp.

5004’-5005.8’

Dark gray clay-rich limestone that transitions into a nodular limestone near the base. Upper section is burrowed with shale filling the burrows. The upper and lower contacts are sharp. Thin section of 5005’ show calcite mud matrix with abundant pyrite, extremely rare marine invertebrates, and healed fractures. Porosity = 1.2%, Permeability = 0.1 md.

5005.8’-5007’

Dark gray shale rich in marine invertebrates that transitions into a black marine shale, into a coaly shale, back into a marine shale, and then back into a coaly shale. Upper and lower contacts are sharp.

5007’-5008.25’

Dark gray nodular limestone transitioning into a parallel-laminated dark gray limestone with abundant marine invertebrates and clay. The lower half of the section transitions into a dark gray shale with 1-7 mm diameter carbonate clasts. Sharp upper and lower contacts. Sampled by XRF.

5008.25’-5009.25’

Medium gray nodular limestone in gray clay-rich matrix. Upper and lower contacts are sharp. Sampled by XRF.

5009.25’-5010.5’

Dark gray shale with thin, wavy laminations and scattered marine invertebrates. The upper contact is sharp. The lower contact is gradational into the underlying, clay-rich micrite.

5010.5’-5012.5’

Dark gray micrite with a high clay content. Upper contact is gradational from the above shale. The lower contact is sharp. A fault is located near the base of the section. The amount of displacement for this fault is uncertain.

5012.5’-5013.85’

Gray shale with scattered marine invertebrates transitioning into a dark gray shale. A dark gray to black shaly hash seperates the gray shale from the dark gray shale. The upper and lower contacts are sharp.

5013.85’-5014.85’

Dark gray to black carbonaceous shale at the top the quickly becomes a coal. Sulfide discoloration of the coal is found near the base. The upper and lower contacts are sharp. Sampled by XRF.

5014.85’-5015.5’

Highly fractured light gray shale with sharp upper and lower contacts.

5015.5’-5017.2’

Black coal with a sharp upper contact and a gradational lower contact.

5017.2’-5019.4’

A transitional section starting with coal that grades into a paleosol and then light gray shale. A structureless zone is found near the base of the section. The upper contact is gradational from the above coal. The lower contact is sharp. The base of this section is believed to be the base of the Thirteen Finger Limestone in accordance with descriptions of the lower contact by Curtis and Ostergard (1982) and Gibbons (1964).

5019.4’-5020.1’

Light gray calcareous siltstone to silty micrite with no apparent marine invertebrates. Upper and lower contacts are sharp.

5020.2’-5022.75’

Dark gray carbonized shale. Marine invertebrates are scarce at the top of the section and then entirely disappear by the middle of the section. Carbonized plant matter is present along bedding planes at the base of the section. The upper and lower contacts are sharp. Sampled for XRF, XRD, TOC, and biostratigraphy.

5022.75’-5024.4’

Finely laminated silty shale with carbonaceous material along bedding planes. No marine invertebrates are evident in the rock. Upper and lower contacts are sharp. Sampled for XRF, TOC, and biostratigraphy.

5024.4’-5027’

Light gray to yellow medium- to coarse-grained sandstone. Upper and lower contacts are sharp.

5027’-5027.7’

Dark gray shale with no apparent marine invertebrates. Upper and lower contacts are sharp.

5027.7’-

Light yellow coarse-grained sandstone with gravel size clay clasts and shaly intervals.

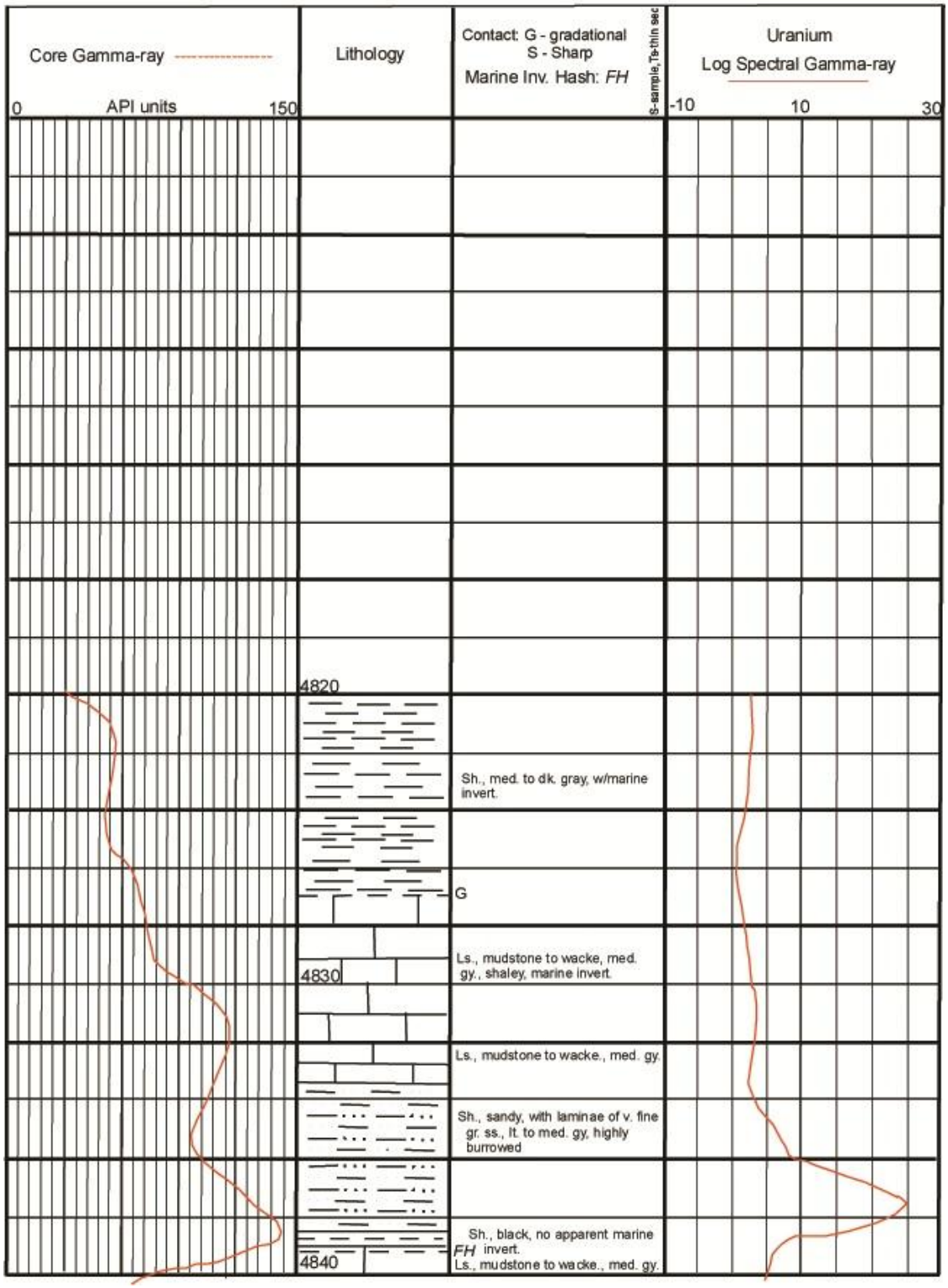

Figure 23: Detailed Lithologic Column with gamma-ray and spectral gamma-ray for uranium for depths 4820' through 4840'.

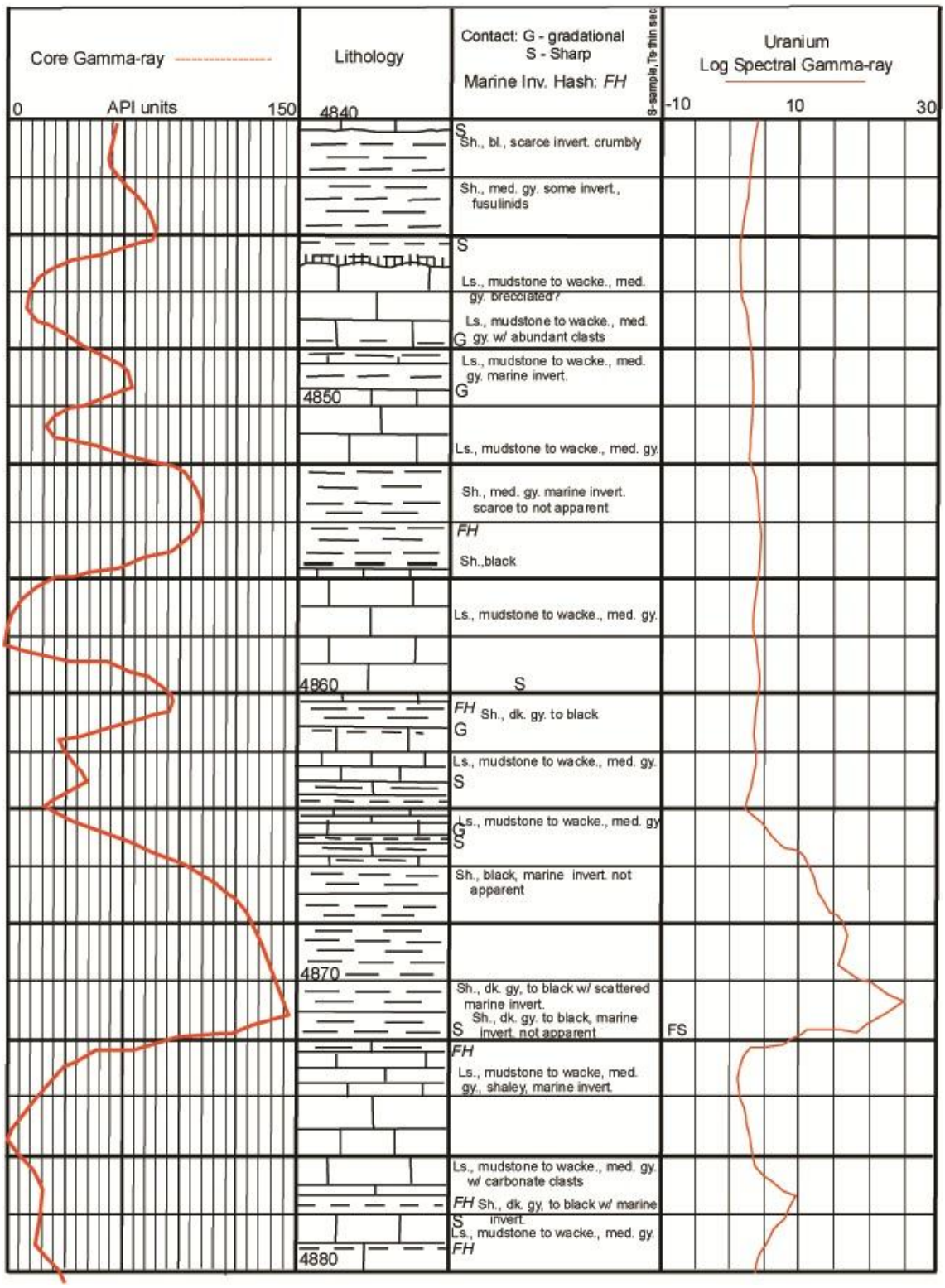

Figure 24: Detailed Lithologic Column with gamma-ray and spectral gamma-ray for uranium for depths 4840' through 4880'.

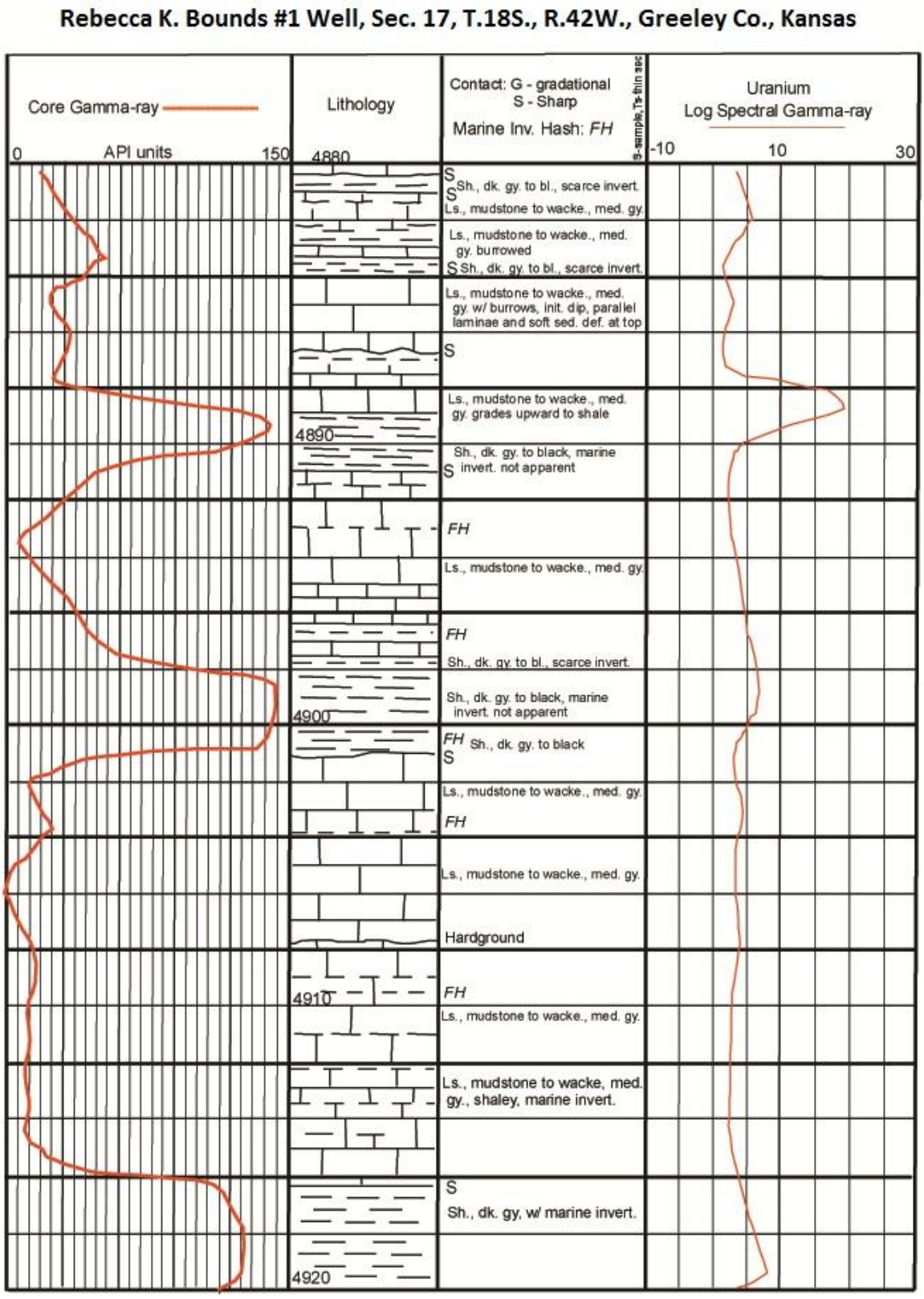

Figure 25: Detailed Lithologic Column with gamma-ray and spectral gamma-ray for uranium for depths 4880' through 4920'.

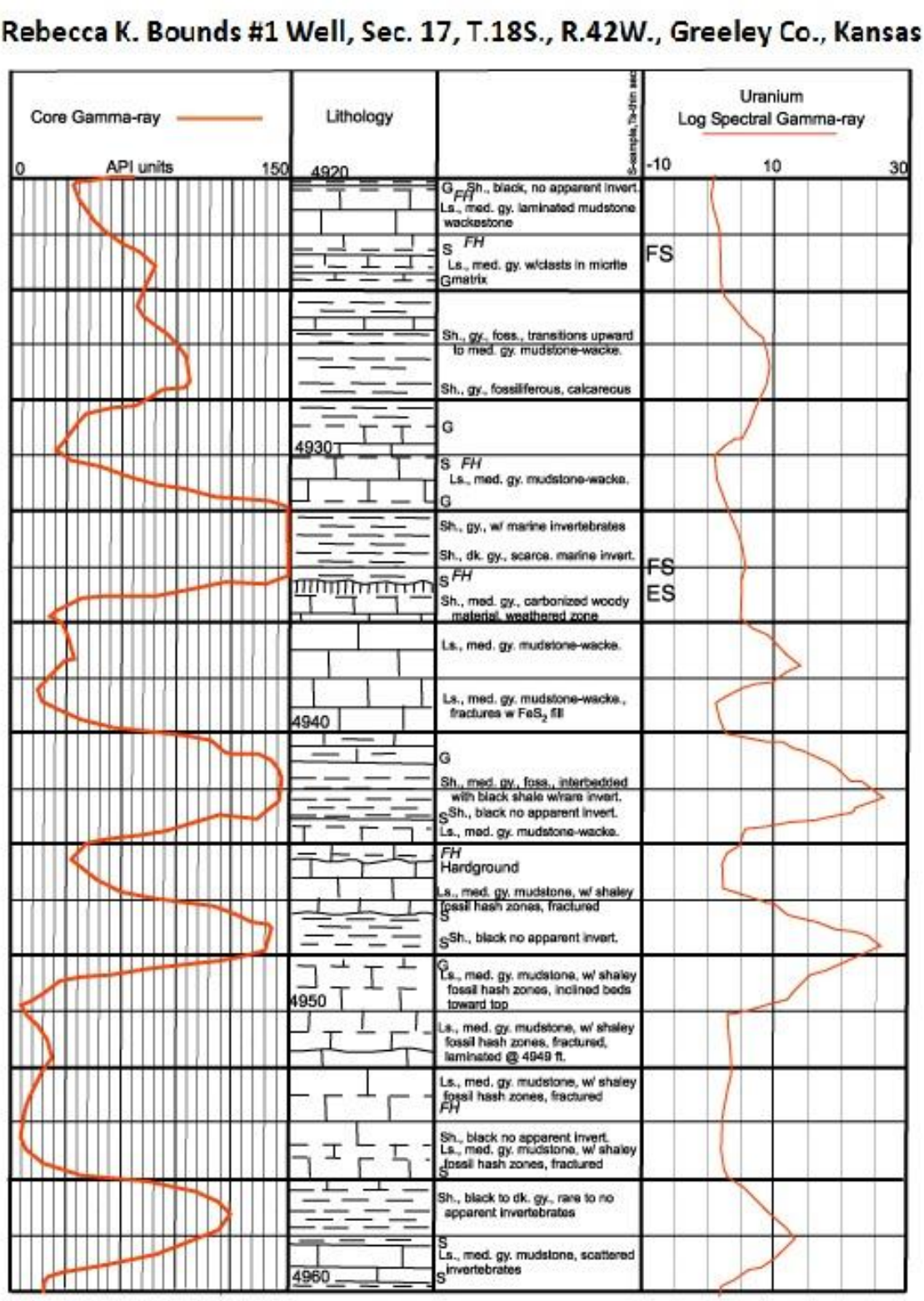

Figure 26: Detailed Lithologic Column with gamma-ray and spectral gamma-ray for uranium for depths 4920' through 4960'.

Rebecca K. Bounds #1 Well, Sec. 17, T.18S., R.42W., Greeley Co., Kansas

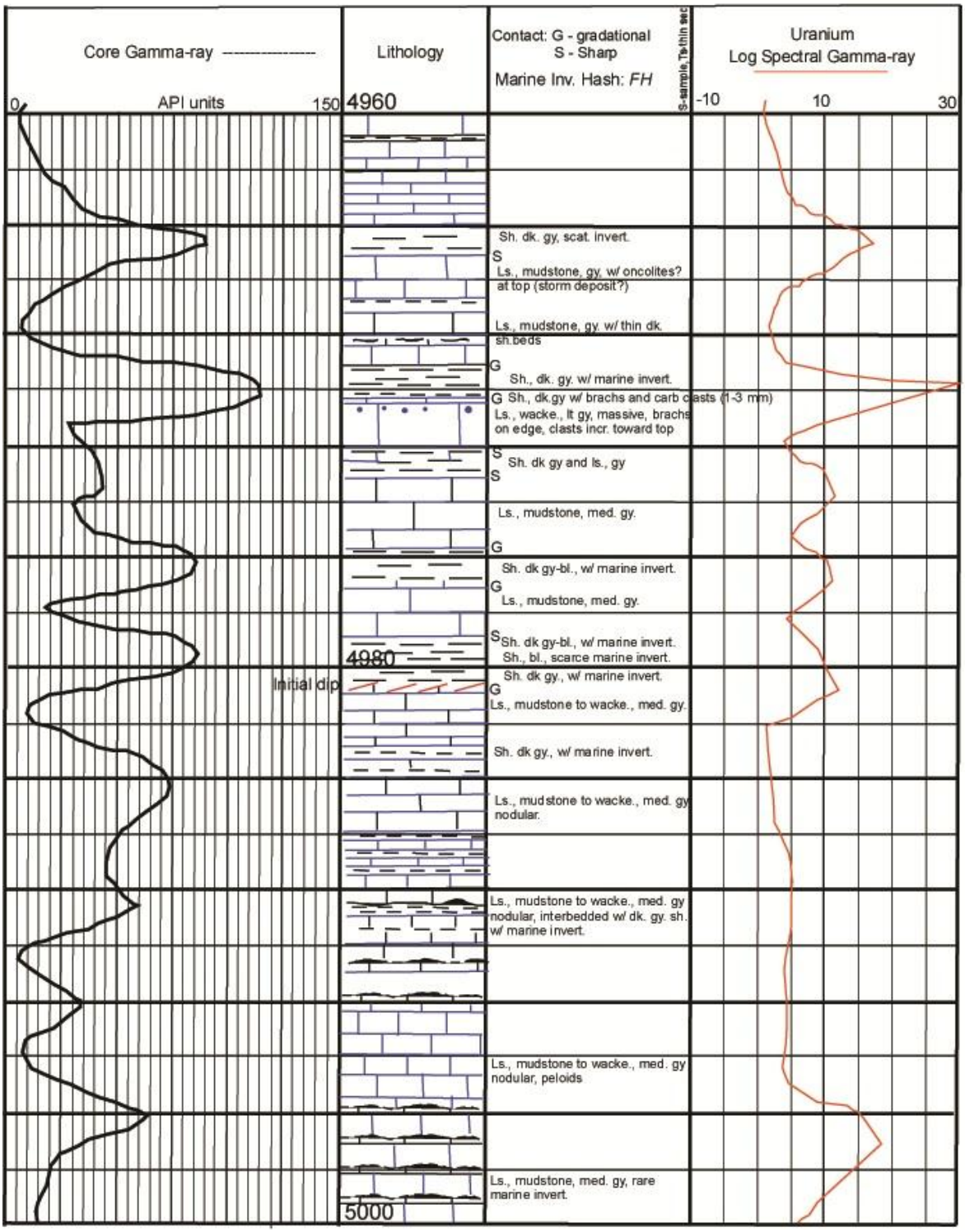

Figure 27: Detailed Lithologic Column with gamma-ray and spectral gamma-ray for uranium for depths 4960' through 5000'.

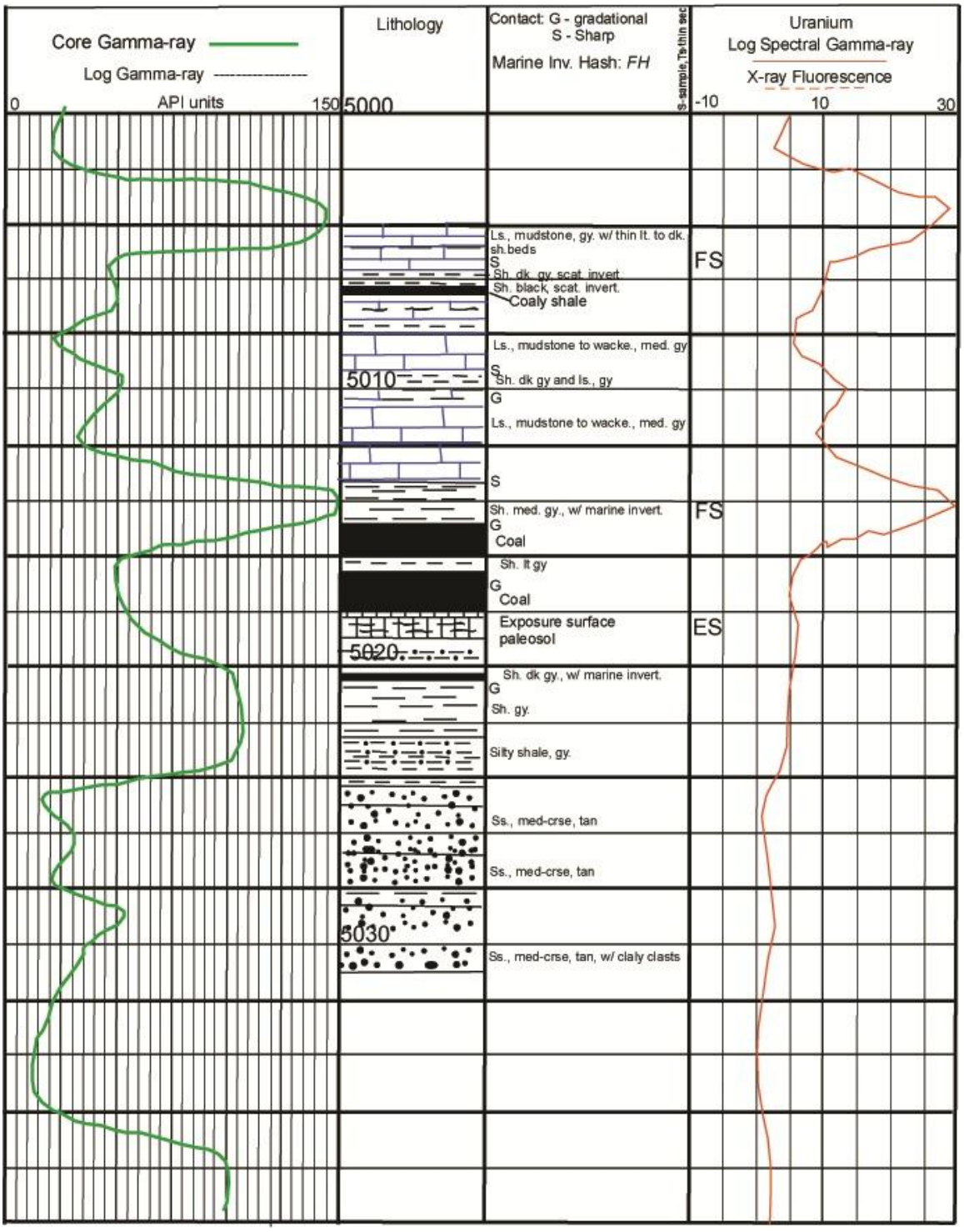

Figure 28: Detailed Lithologic Column with gamma-ray and spectral gamma-ray for uranium for depths 5000' through 5031'.

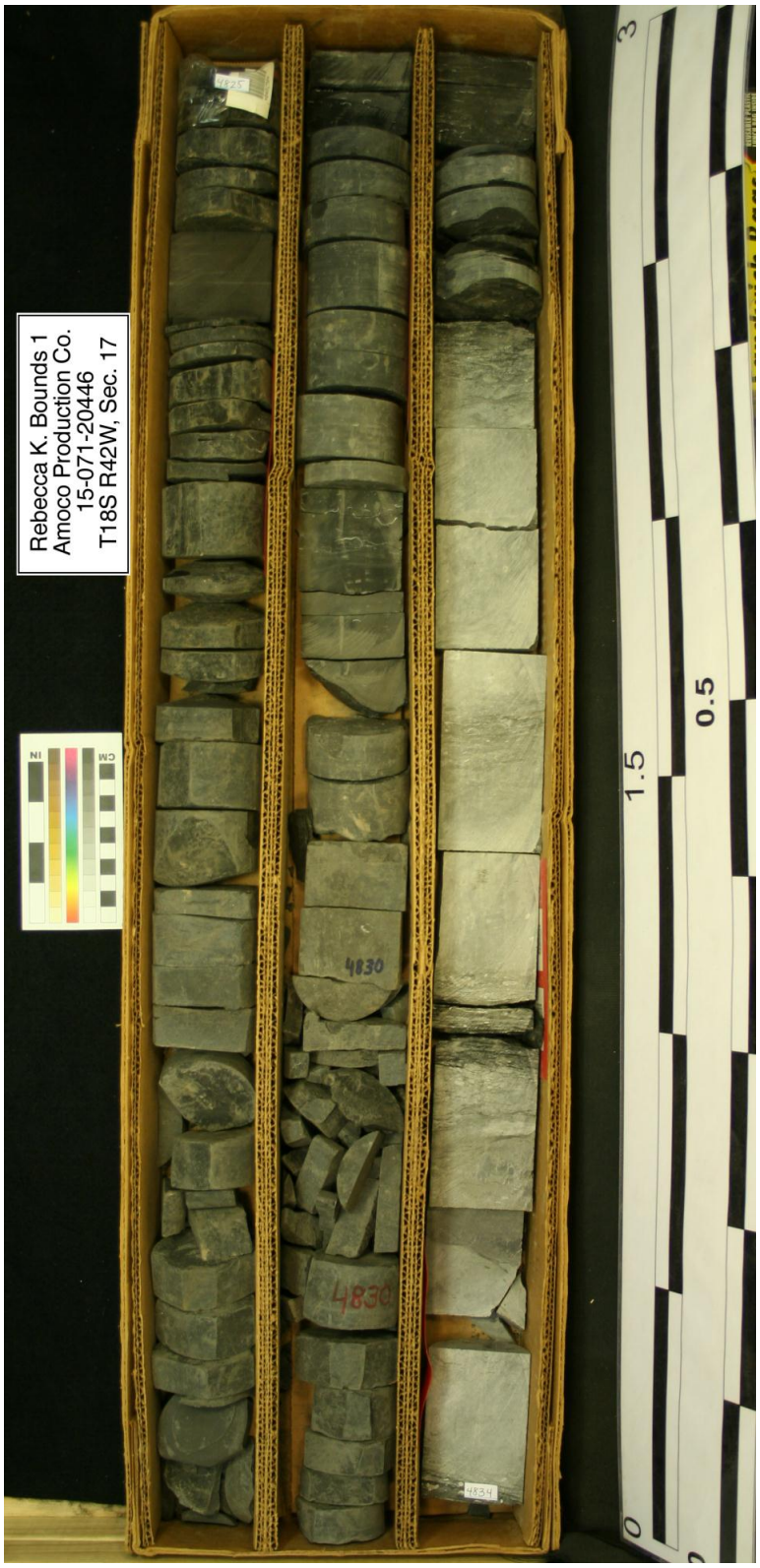

Photograph 1: Photo of the Rebecca K. Bounds #1 core for depths 4825' to 4834' taken by the Kansas Geological Survey.

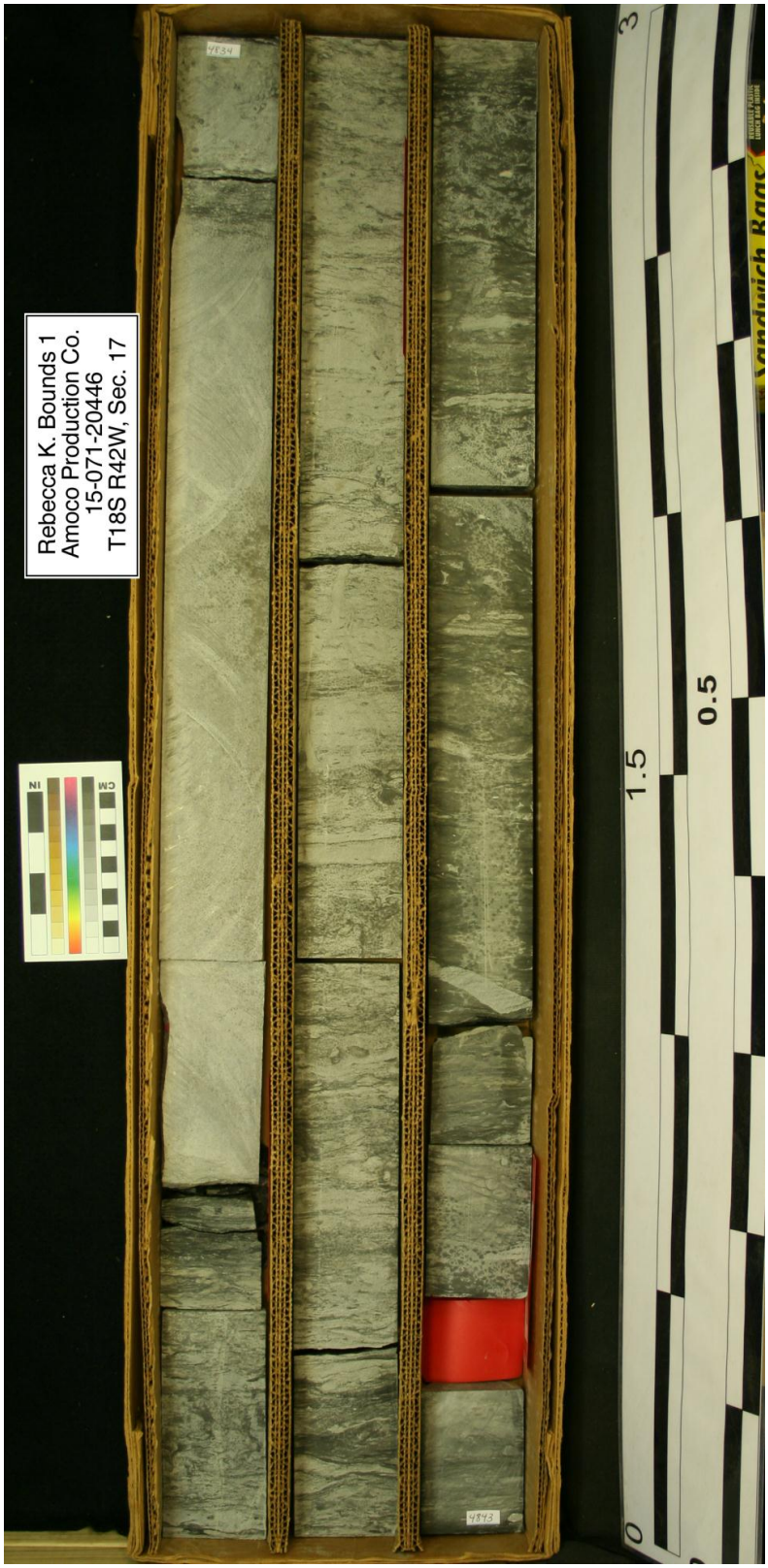

Photograph 2: Photo of the Rebecca K. Bounds #1 core for depths 4834' to 4843' taken by the Kansas Geological Survey.

Photograph 3: Photo of the Rebecca K. Bounds #1 core for depths 4843' to 4852' taken by the Kansas Geological Survey.

Photograph 4: Photo of the Rebecca K. Bounds #1 core for depths 4852' to 4861' taken by the Kansas Geological Survey.

Photograph 5: Photo of the Rebecca K. Bounds #1 core for depths 4861' to 4870' taken by the Kansas Geological Survey.

Photograph 6: Photo of the Rebecca K. Bounds #1 core for depths 4870' to 4879' taken by the Kansas Geological Survey.

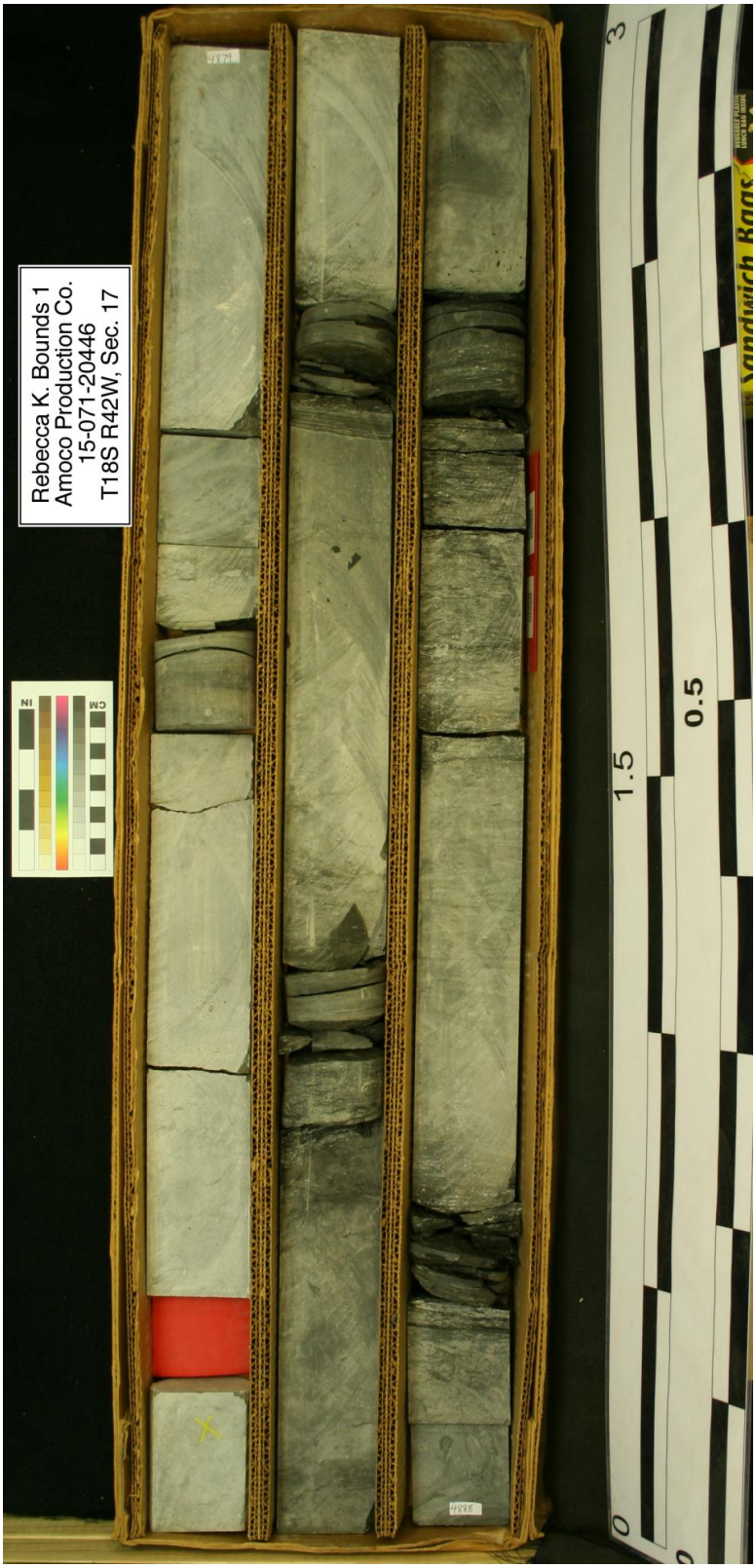

Photograph 7: Photo of the Rebecca K. Bounds #1 core for depths 4879' to 4888' taken by the Kansas Geological Survey.

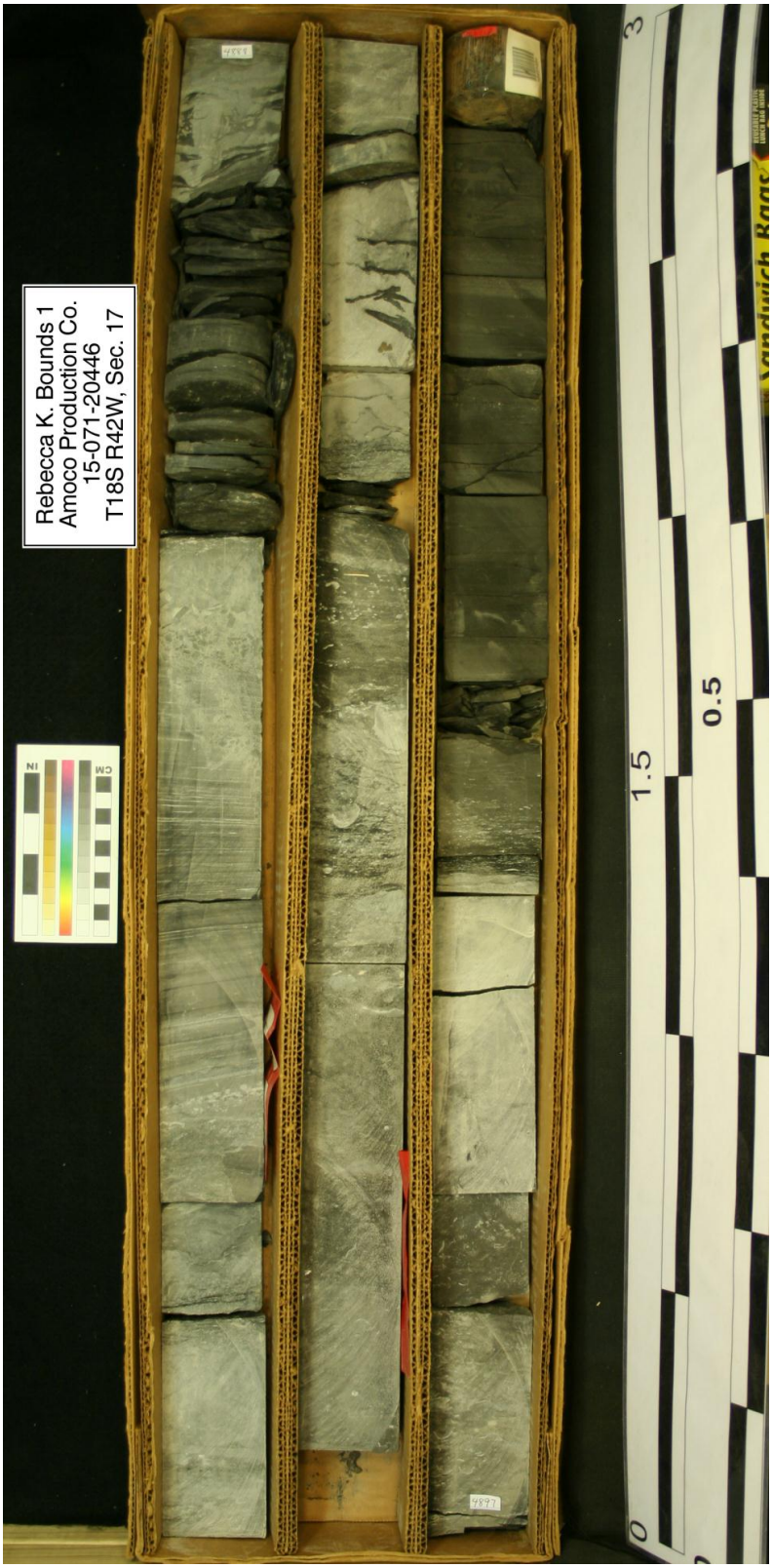

Photograph 8: Photo of the Rebecca K. Bounds #1 core for depths 4888' to 4897' taken by the Kansas Geological Survey.

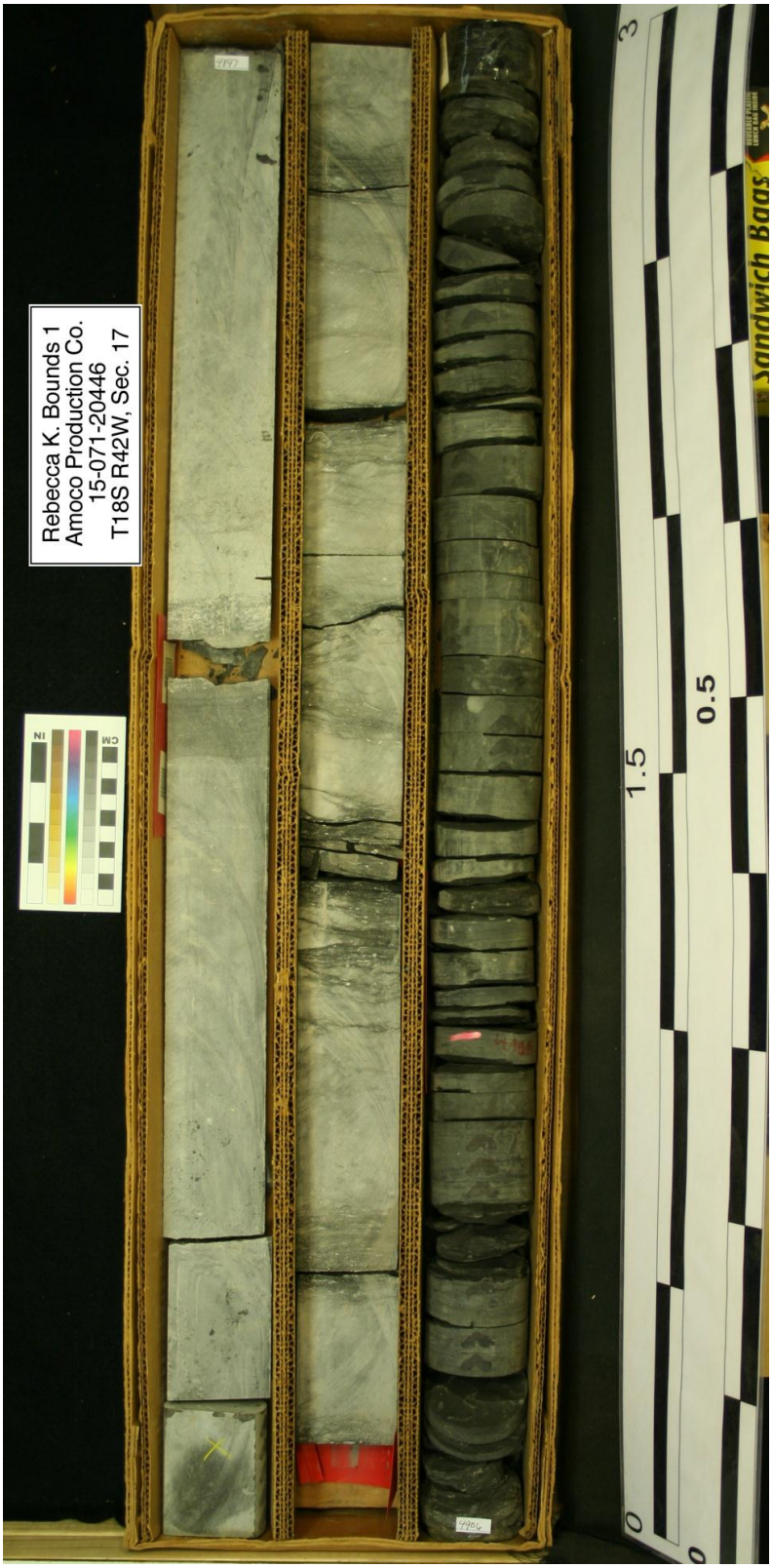

Photograph 9: Photo of the Rebecca K. Bounds #1 core for depths 4897' to 4906' taken by the Kansas Geological Survey.

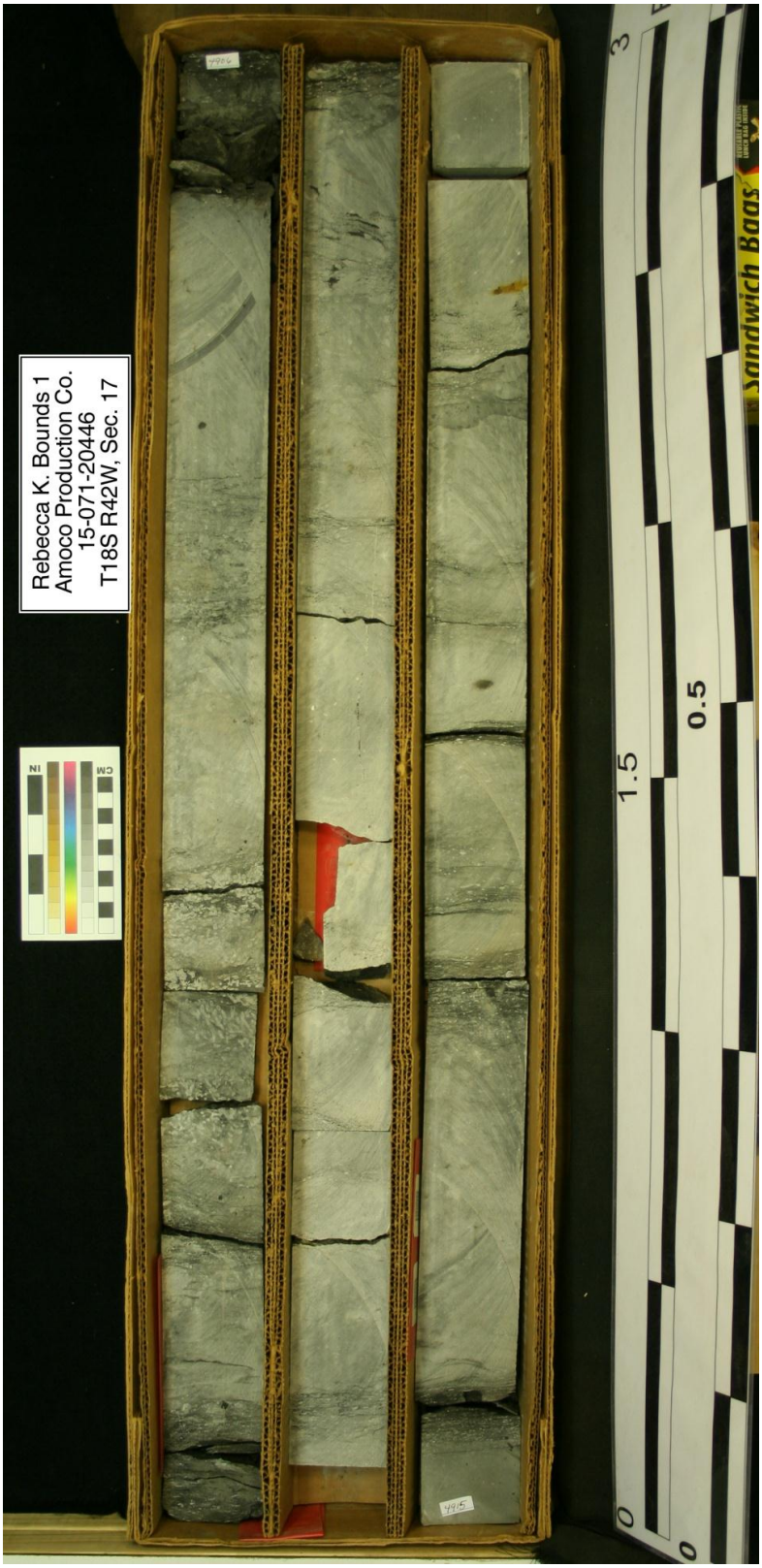

Photograph 10: Photo of the Rebecca K. Bounds #1 core for depths 4906' to 4915' taken by the Kansas Geological Survey.

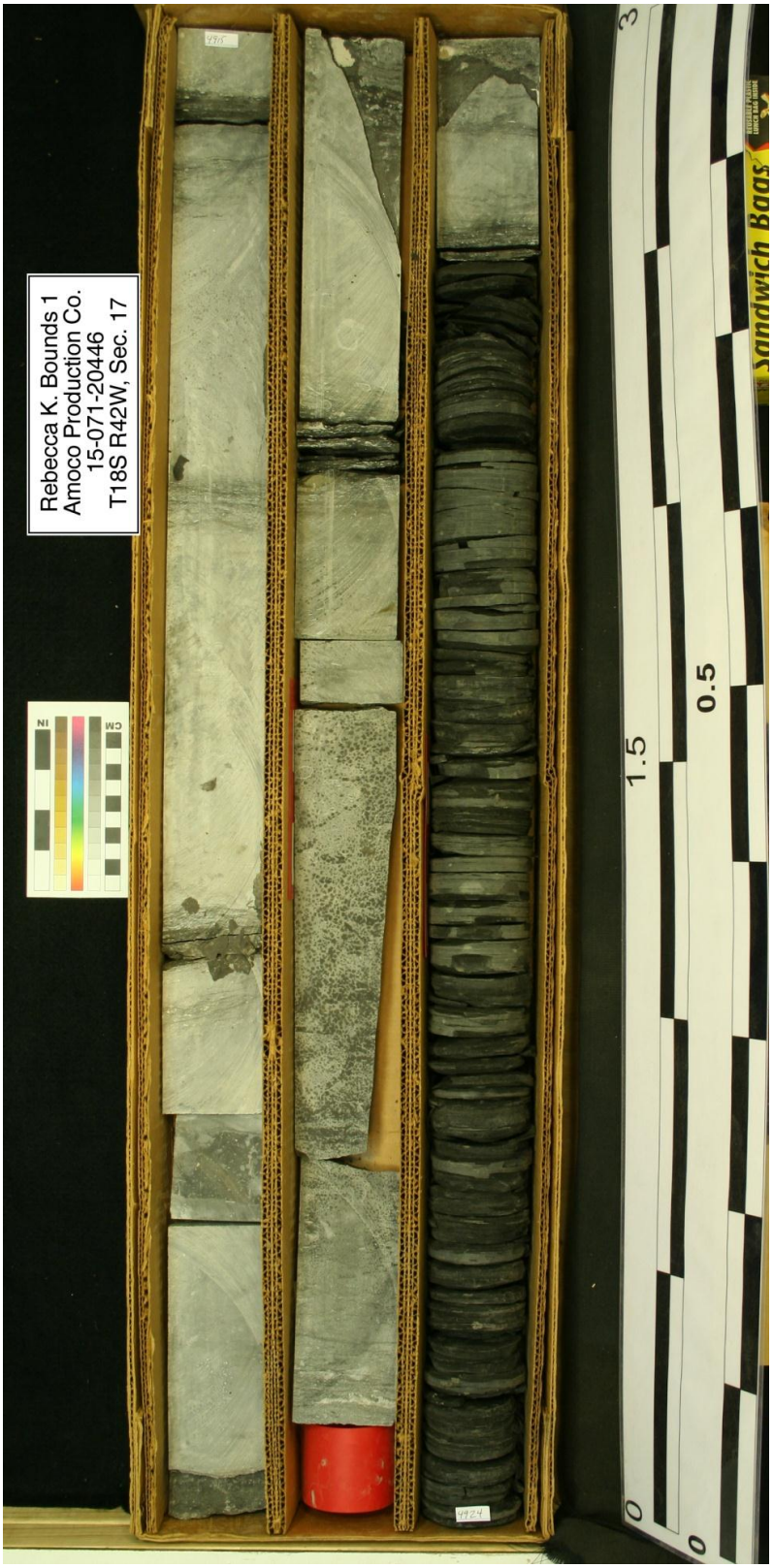

Photograph 11: Photo of the Rebecca K. Bounds #1 core for depths 4915' to 4924' taken by the Kansas Geological Survey.

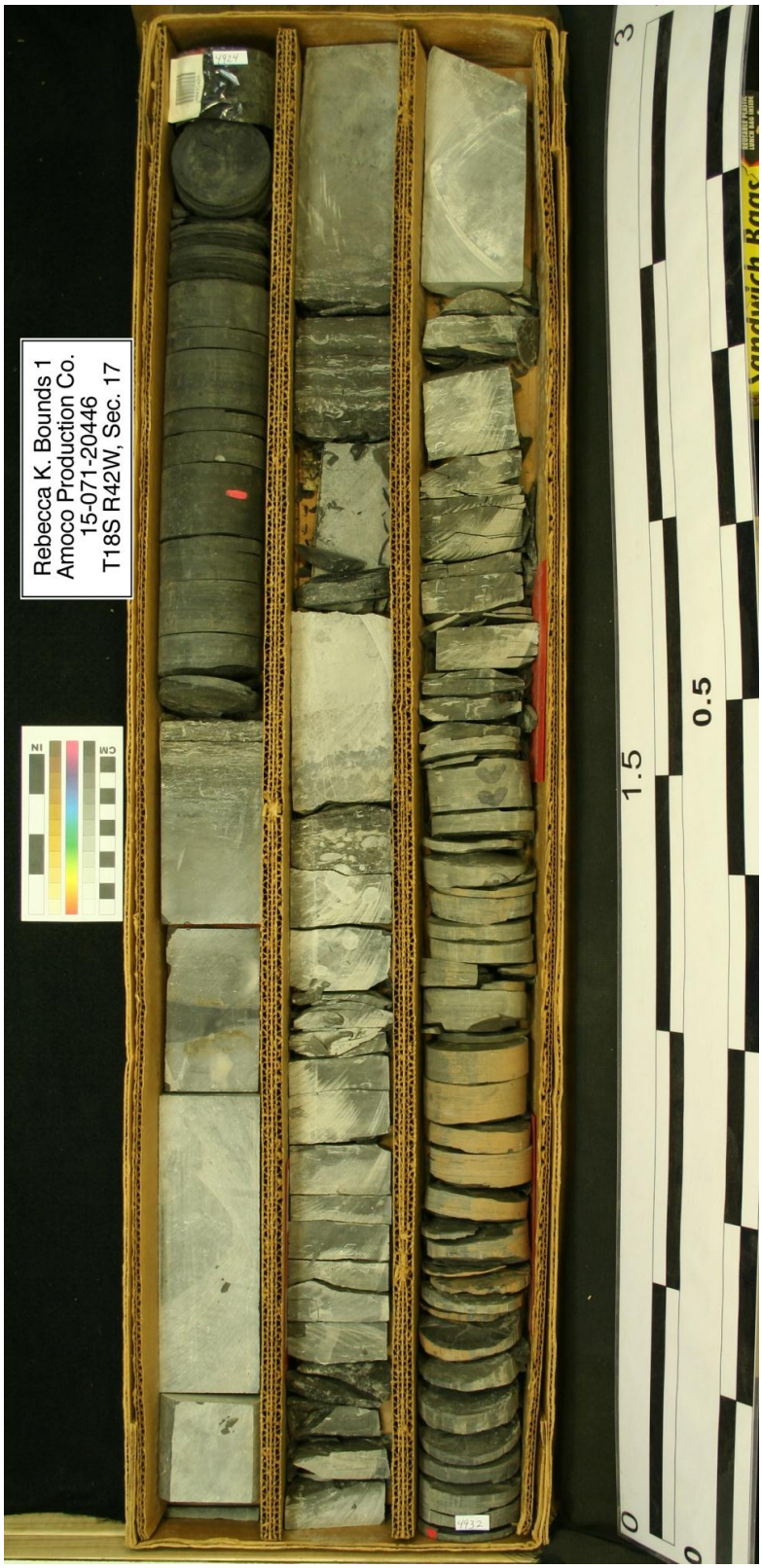

Photograph 12: Photo of the Rebecca K. Bounds #1 core for depths 4924' to 4933' taken by the Kansas Geological Survey.

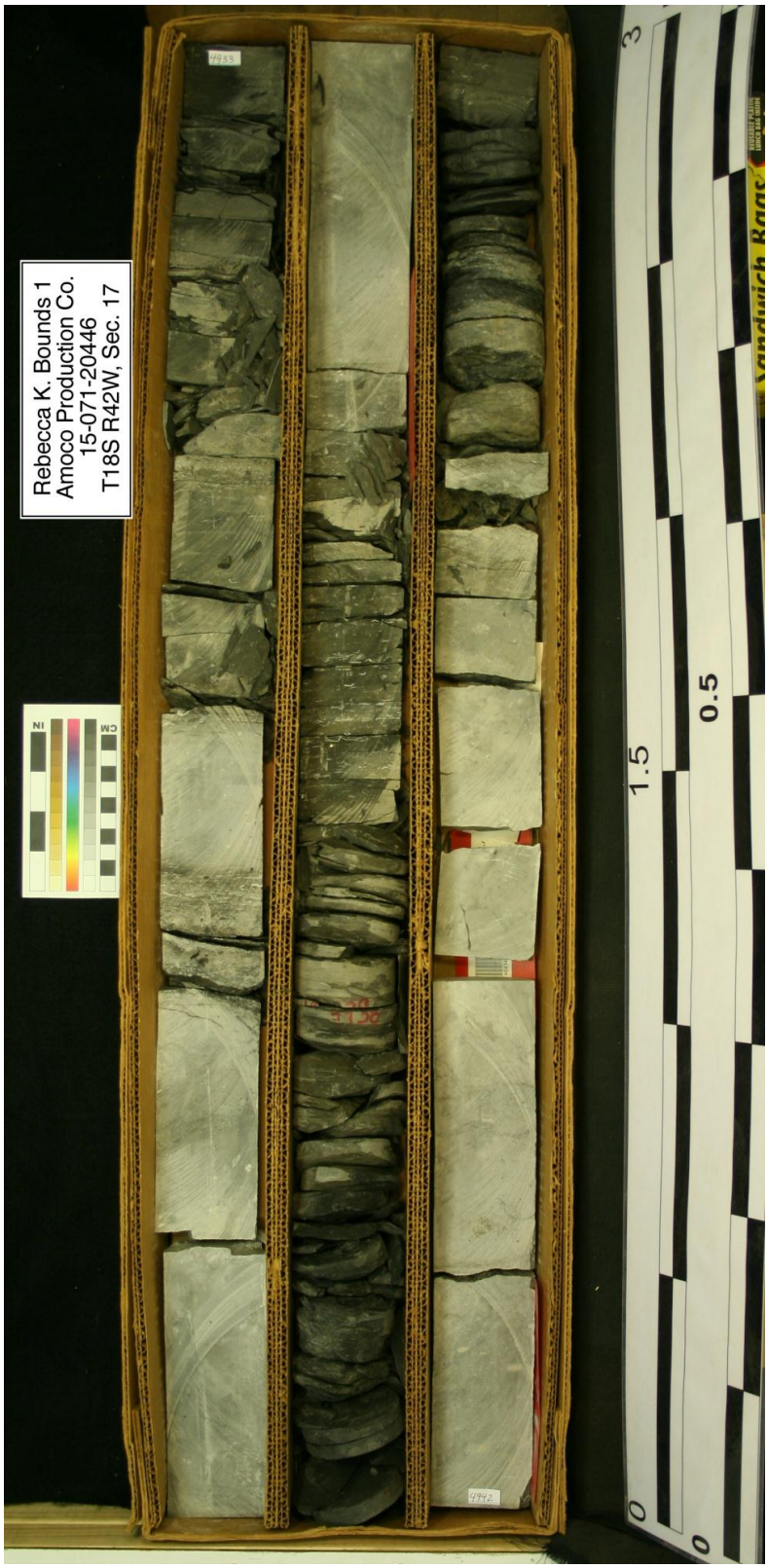

Photograph 13: Photo of the Rebecca K. Bounds #1 core for depths 4933' to 4942' taken by the Kansas Geological Survey.

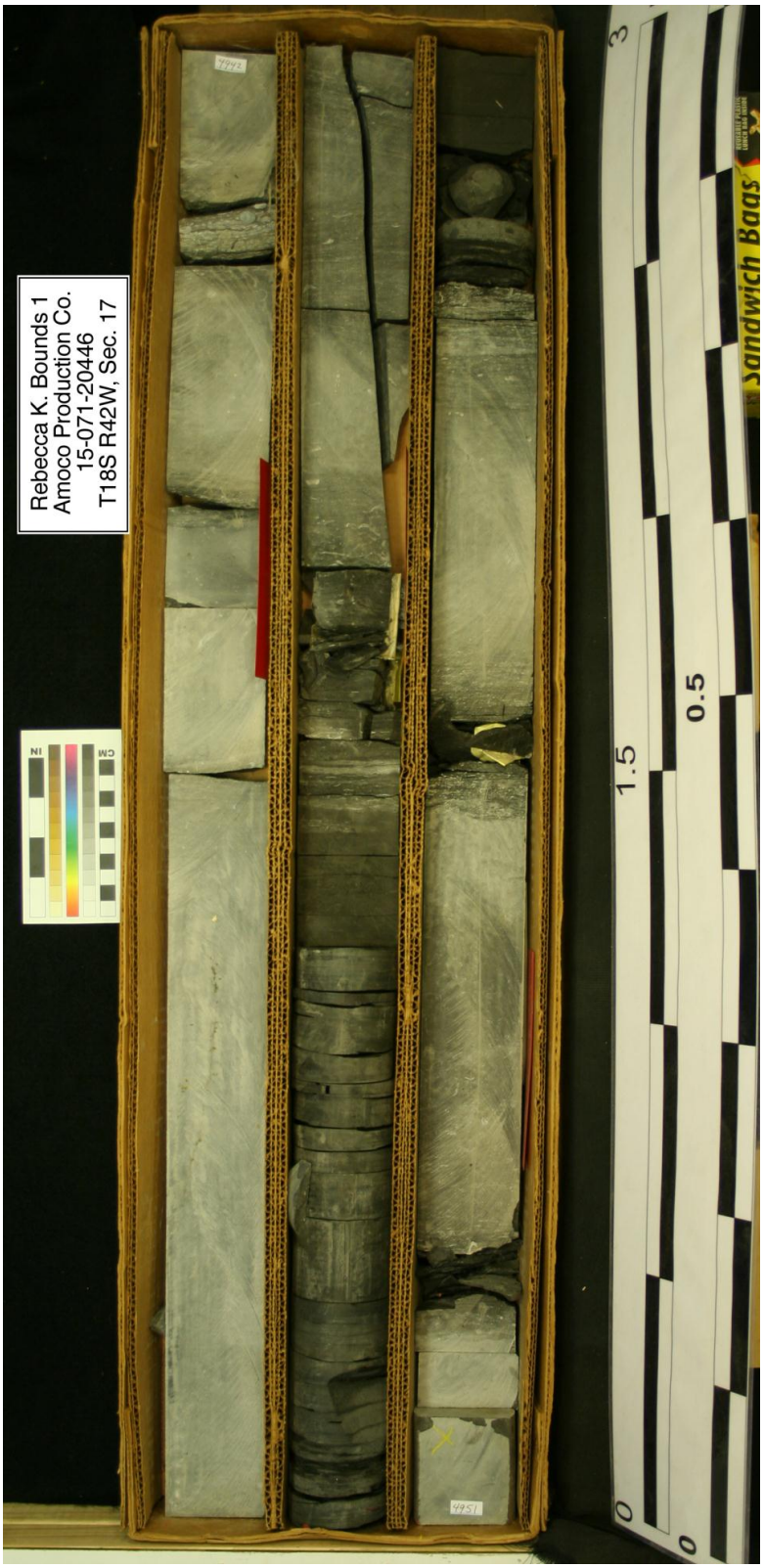

Photograph 14: Photo of the Rebecca K. Bounds #1 core for depths 4942' to 4951' taken by the Kansas Geological Survey.

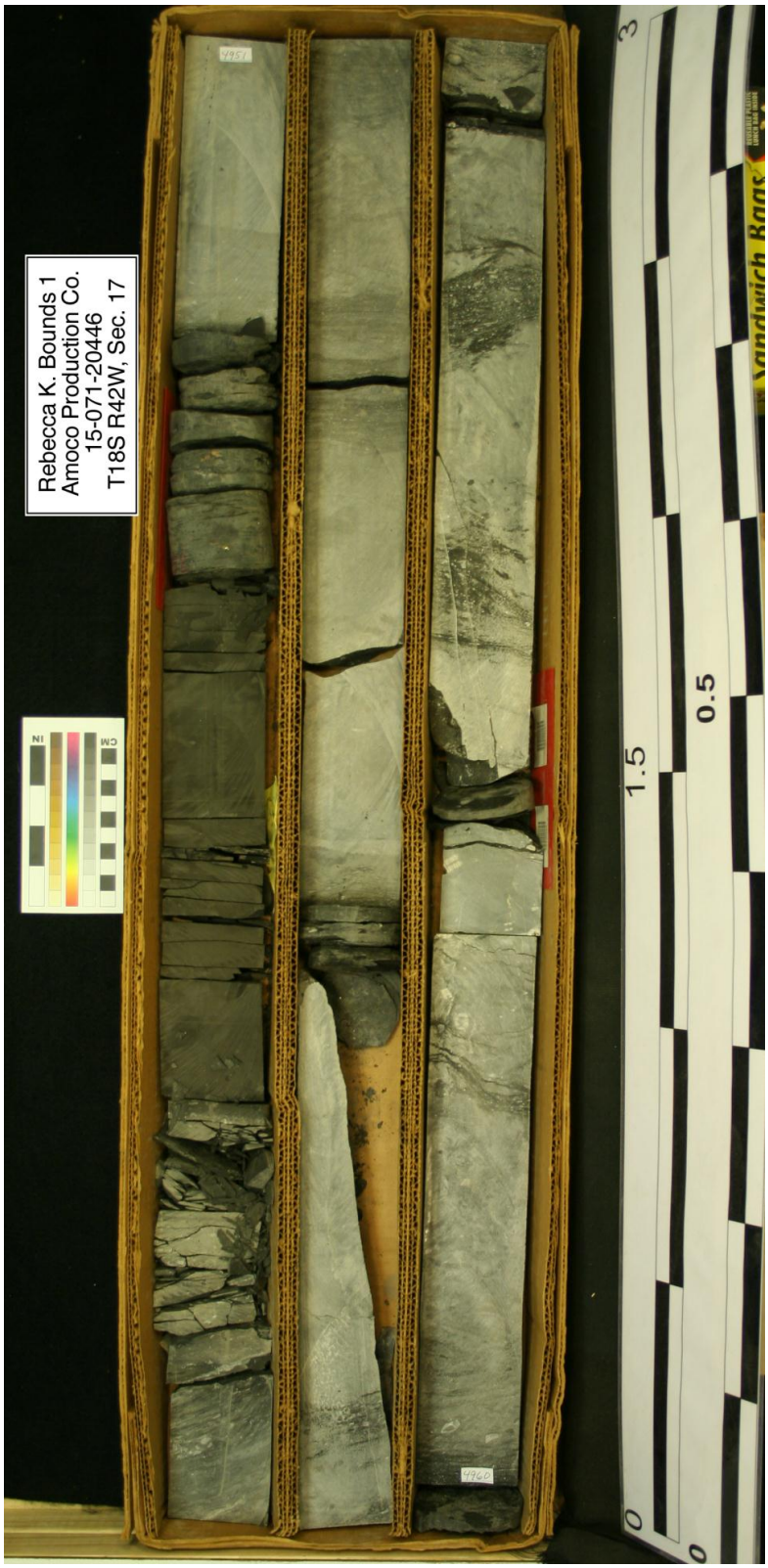

Photograph 15: Photo of the Rebecca K. Bounds #1 core for depths 4951' to 4960' taken by the Kansas Geological Survey.

Photograph 16: Photo of the Rebecca K. Bounds #1 core for depths 4960' to 4969' taken by the Kansas Geological Survey.

Photograph 17: Photo of the Rebecca K. Bounds #1 core for depths 4969' to 4978' taken by the Kansas Geological Survey.

Photograph 18: Photo of the Rebecca K. Bounds #1 core for depths 4978' to 4987' taken by the Kansas Geological Survey.

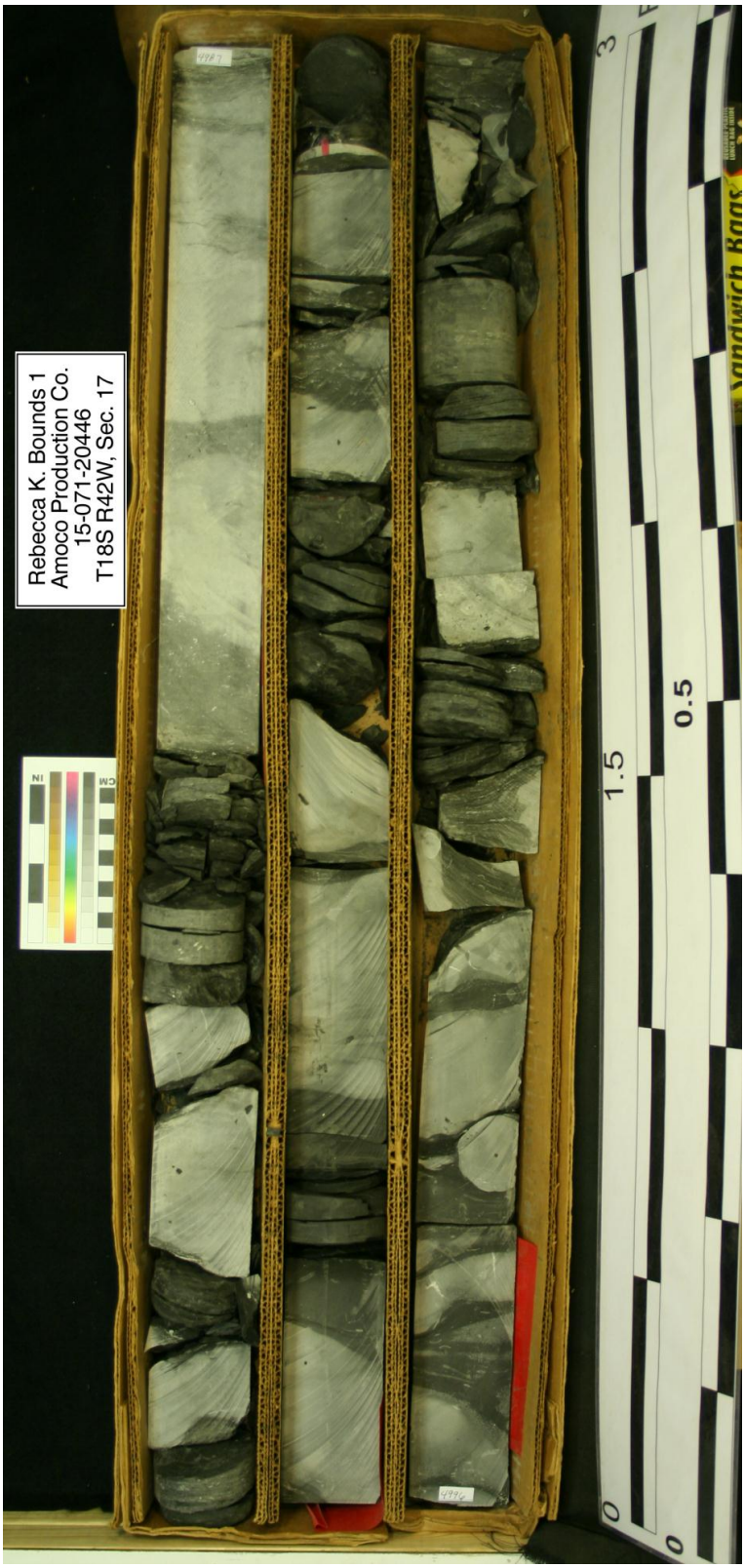

Photograph 19: Photo of the Rebecca K. Bounds #1 core for depths 4987' to 4996' taken by the Kansas Geological Survey.

Photograph 20: Photo of the Rebecca K. Bounds #1 core for depths 4996' to 5006' taken by the Kansas Geological Survey.

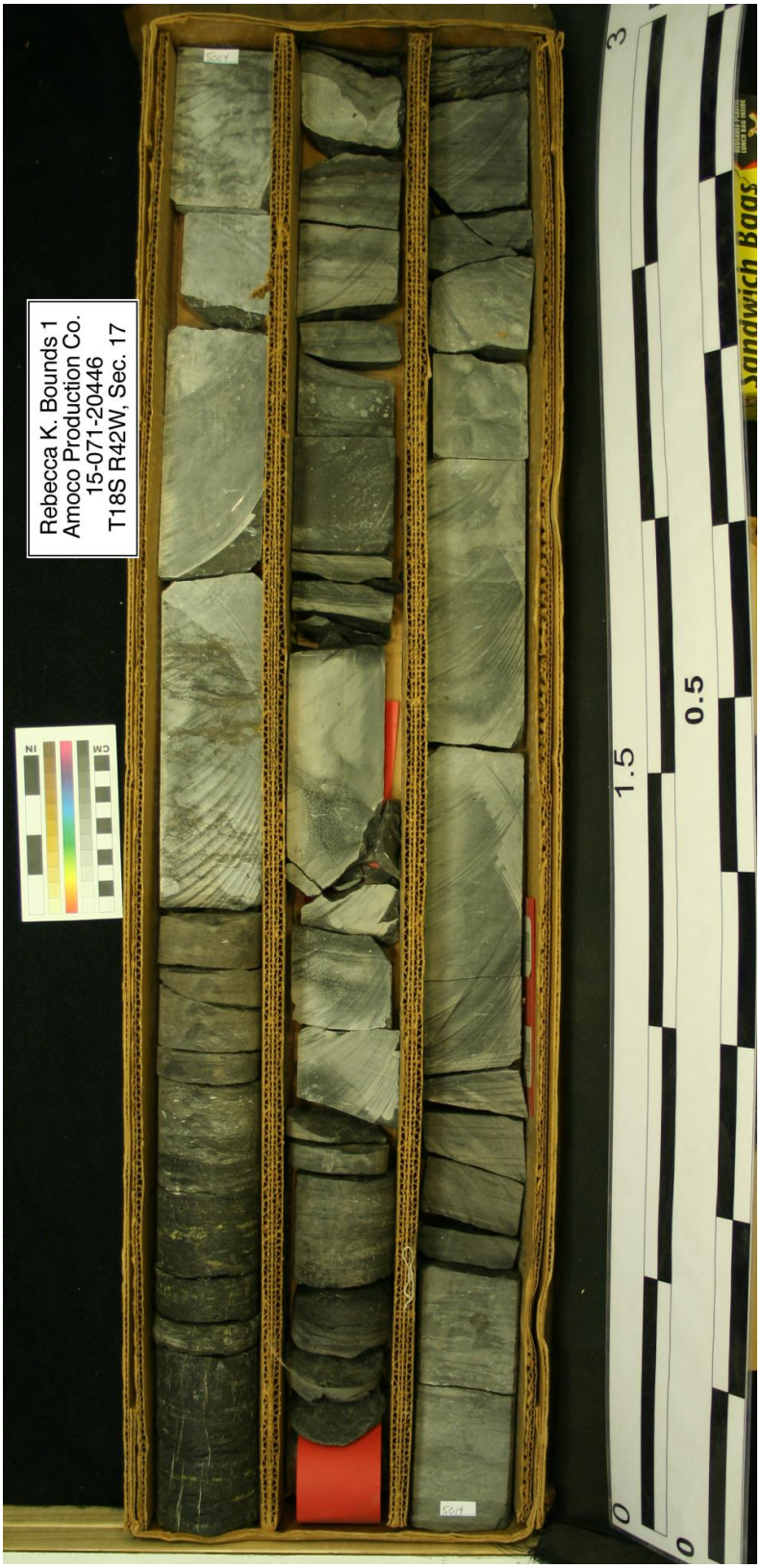

Photograph 21: Photo of the Rebecca K. Bounds #1 core for depths 5004' to 5013' taken by the Kansas Geological Survey.

Photograph 22: Photo of the Rebecca K. Bounds #1 core for depths 5013' to 5022' taken by the Kansas Geological Survey.

Photograph 23: Photo of the Rebecca K. Bounds #1 core for depths 5022' to 5032' taken by the Kansas Geological Survey.

Photograph 24: Photo of the Rebecca K. Bounds #1 core for depths 5032' to 5046' taken by the Kansas Geological Survey.

Photograph 25: Photo of the Rebecca K. Bounds #1 core for depths 5046' to 5055' taken by the Kansas Geological Survey.

Photograph 26: Photo of the Rebecca K. Bounds #1 core for depths 5055' to 5064' taken by the Kansas Geological Survey.

Photograph 27 Photo of the Rebecca K. Bounds #1 core for depths 5064' to 5073' taken by the Kansas Geological Survey.

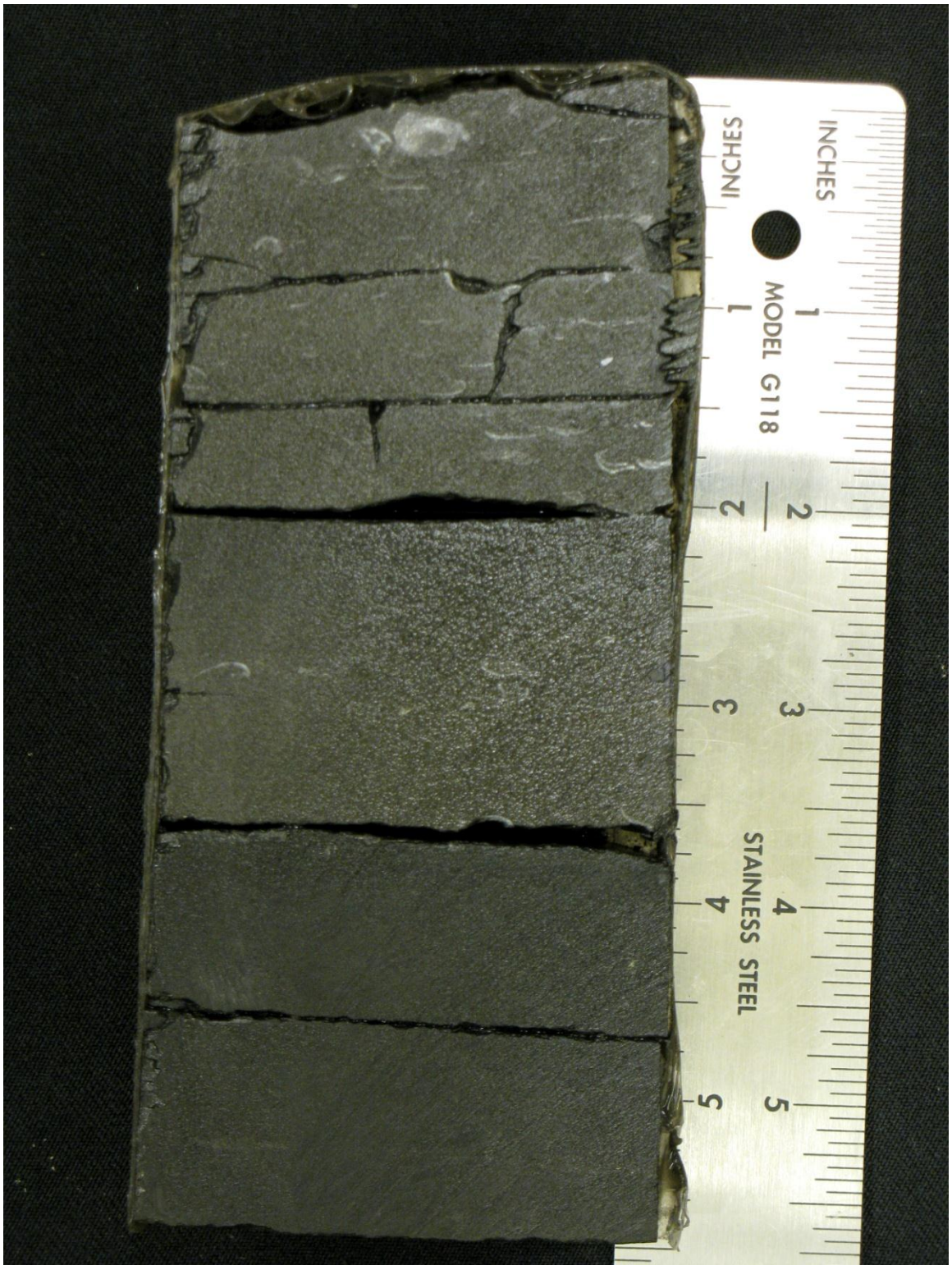

Photograph 28: Collected core sample for depths 4828-4829'.

Photograph 29: Collected core sample for depths 4903.5-4904.5'.

Photograph 30: Collected core sample for depth 4923'.

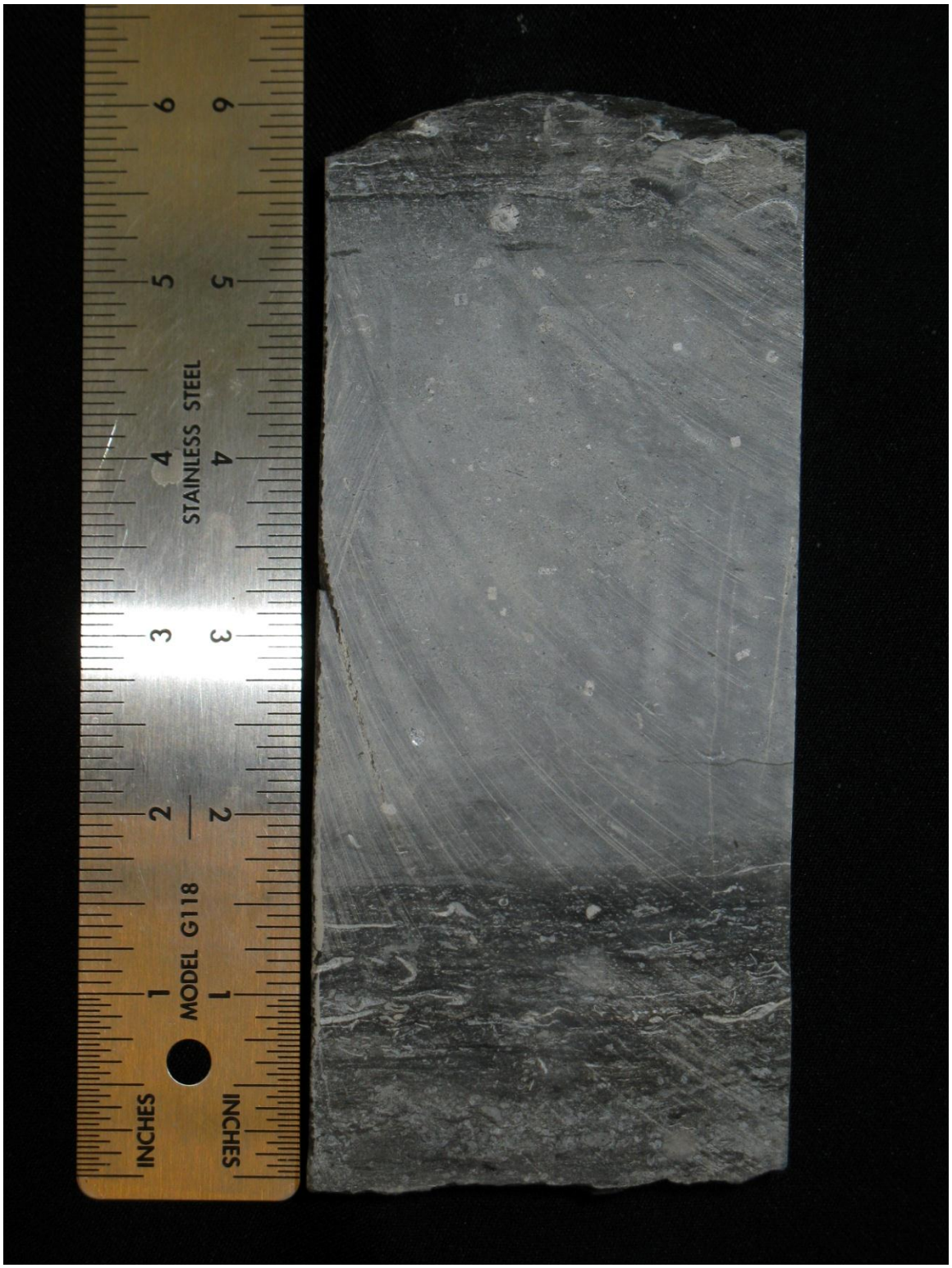

Photograph 31: Collected core sample for depths 4933-34.3'.

Photograph 32: Collected core sample for depth 4944'.

Photograph 33: Collected core sample for depths 4947-4948'.

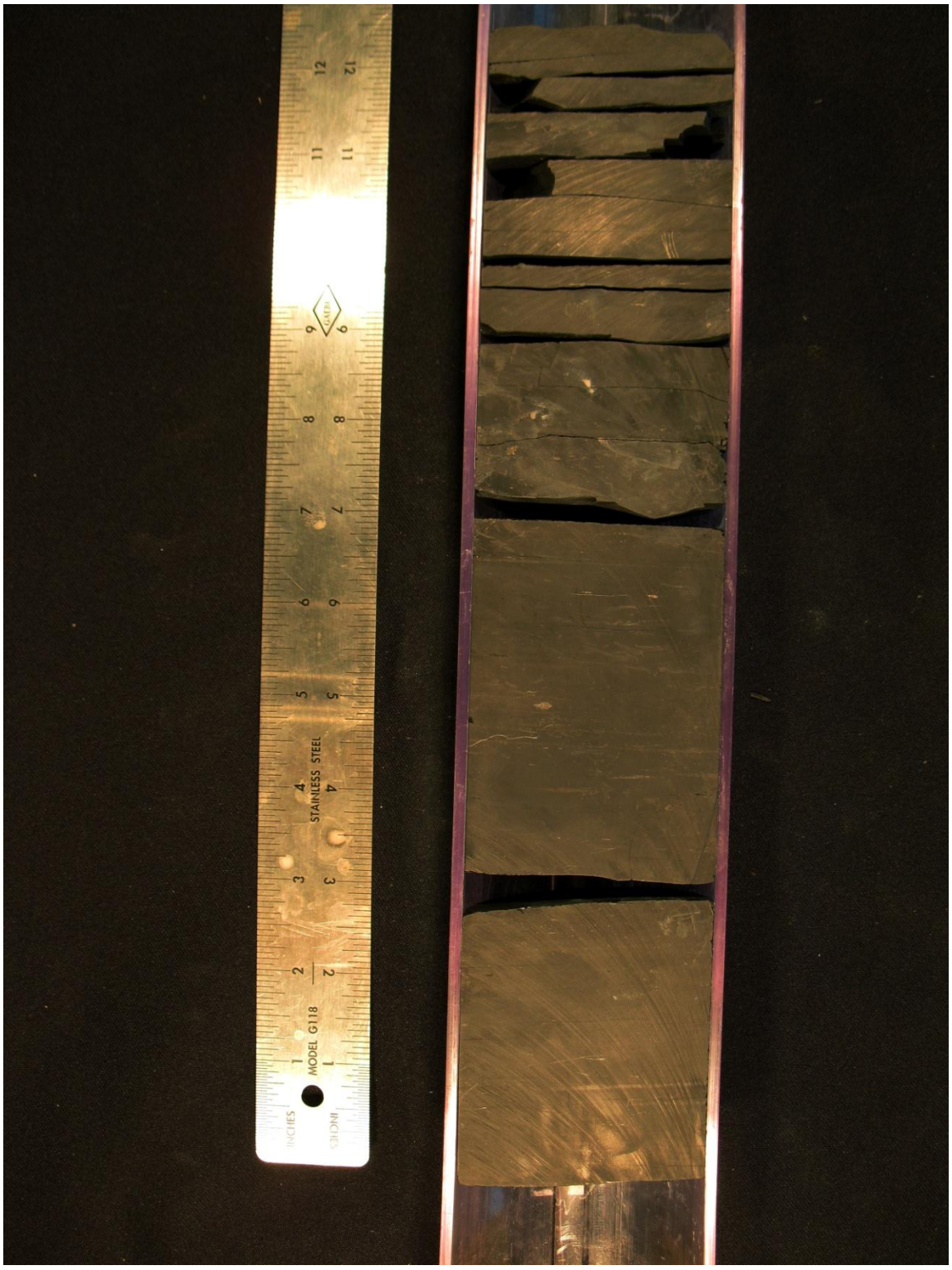

Photograph 34: Collected core sample for depth 4952'.

Photograph 35: Collected core sample for depths 4957.5-4958.5'.

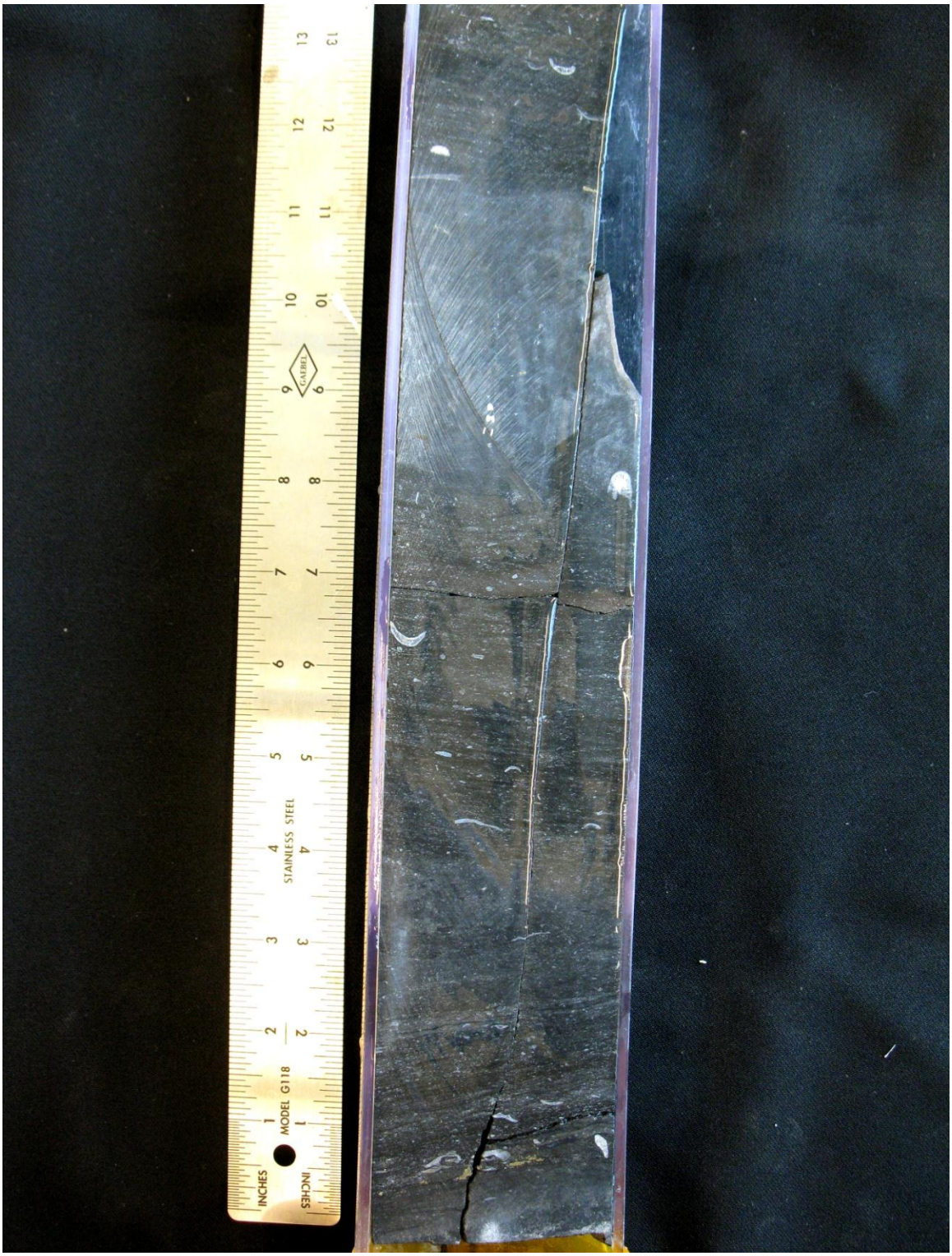

Photograph 36: Collected core sample for depths 4973-4974'.

Photograph 37: Collected core sample for depths 4995-4996'.

Photograph 38: Collected core sample for depth 5023'.

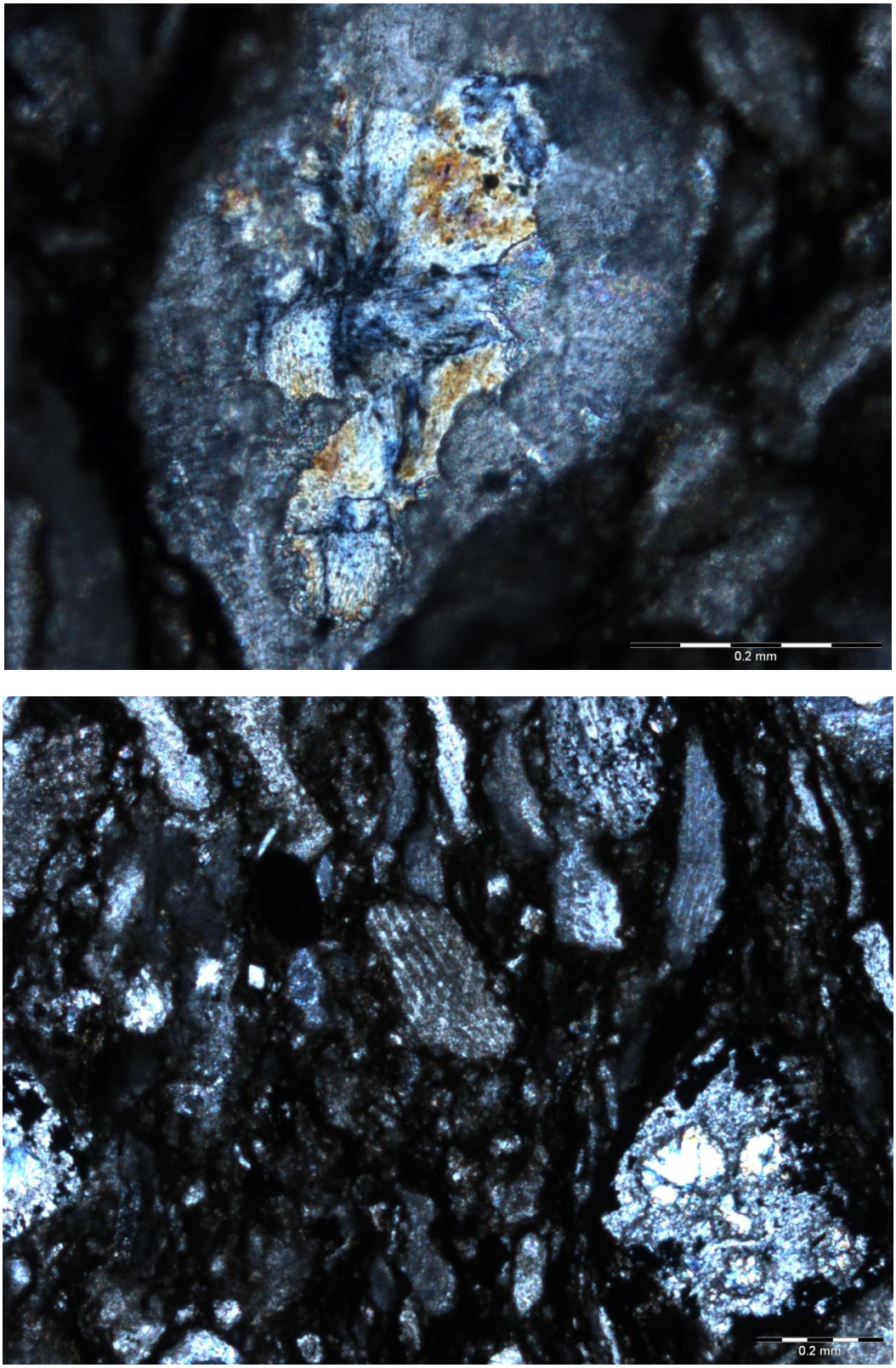

Photograph 39: Thin section photos for depth 4921' showing silica replacement of bioclasts in a fossiliferous micrite host.

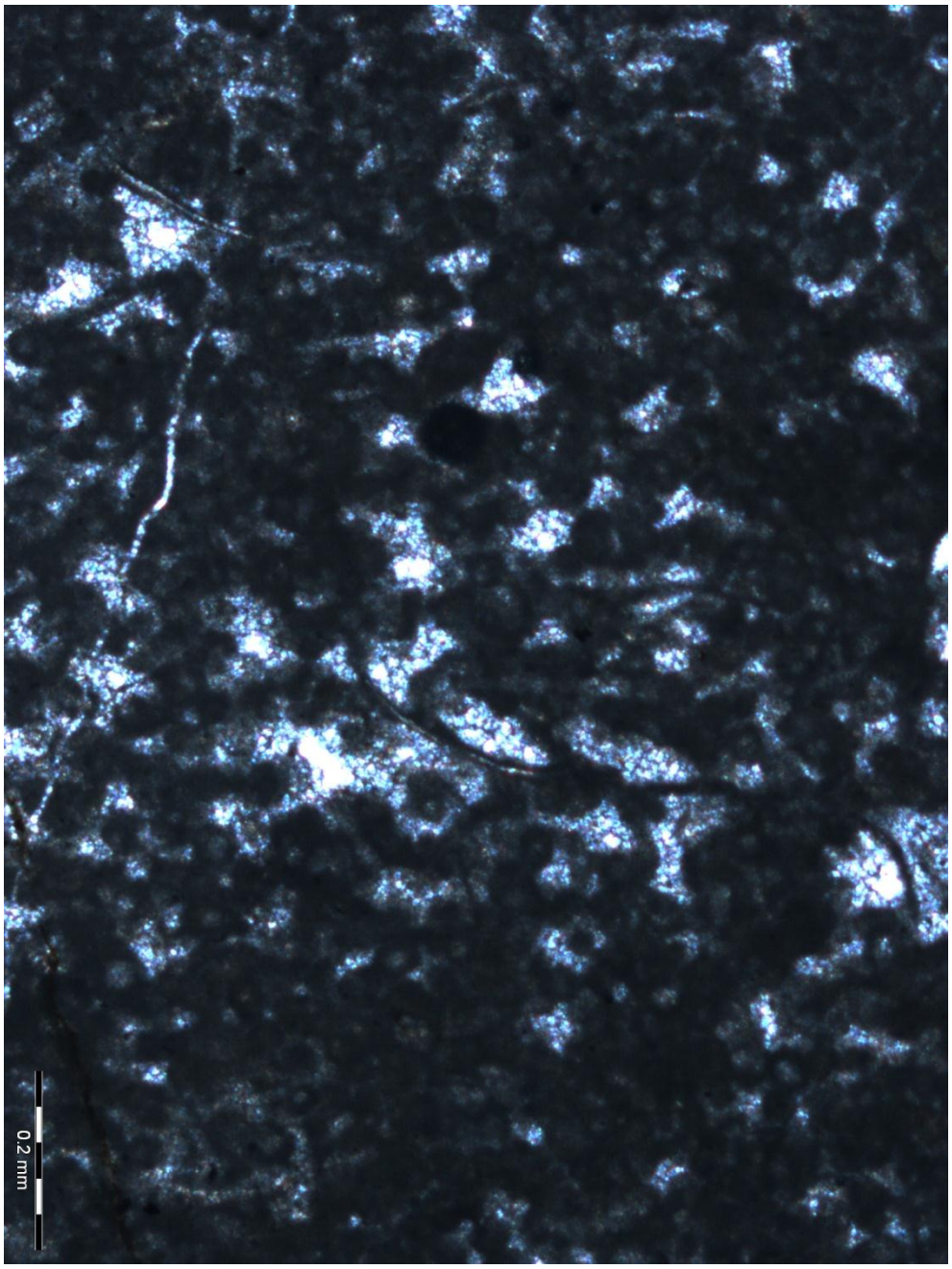

Photograph 40: Thin section photo for depths 4928-4929' showing peloides and healed fractures in microspar. Peloides are approximately 6 µm wide. Fractures are approximately 2 µm wide.

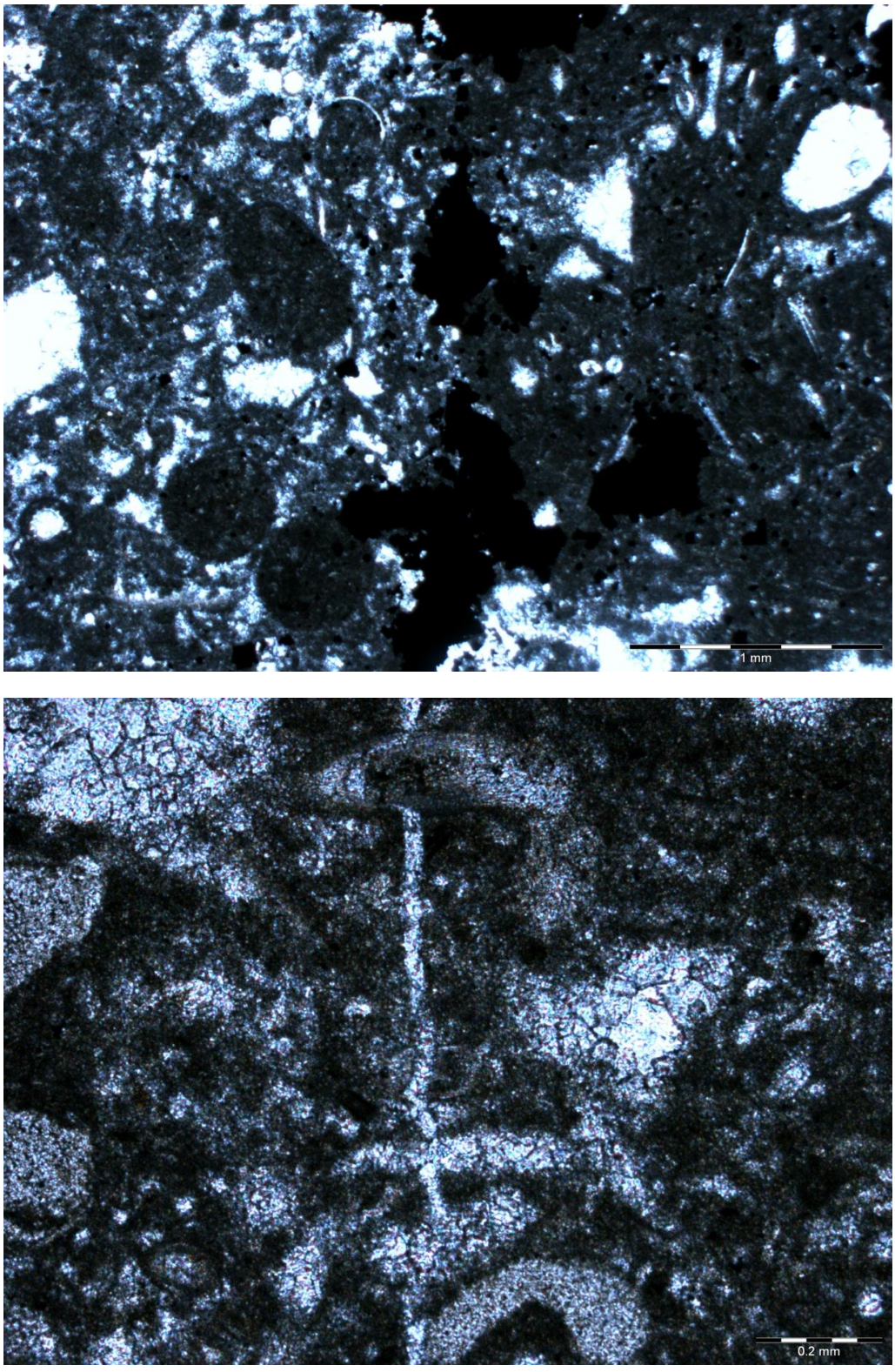

Photograph 41: Thin section photos for depth 4944' showing a bioclastic wackestone with peloides, pyrite, and a healed fracture that is approximately 18 µm wide.

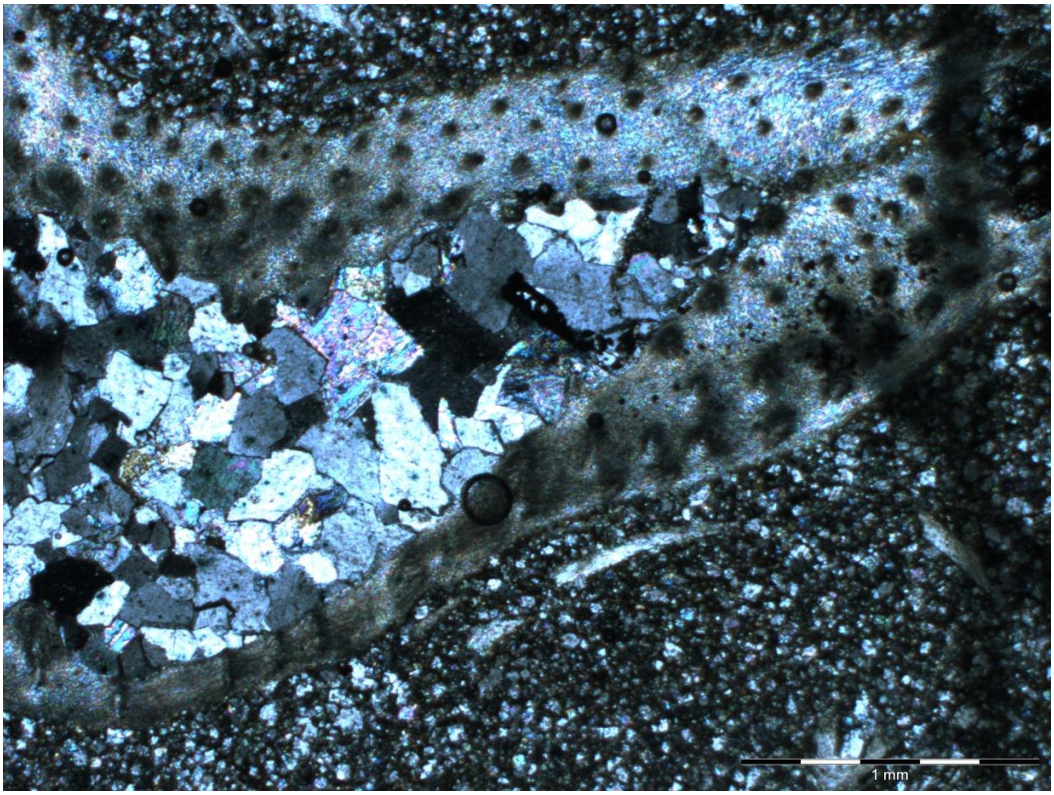

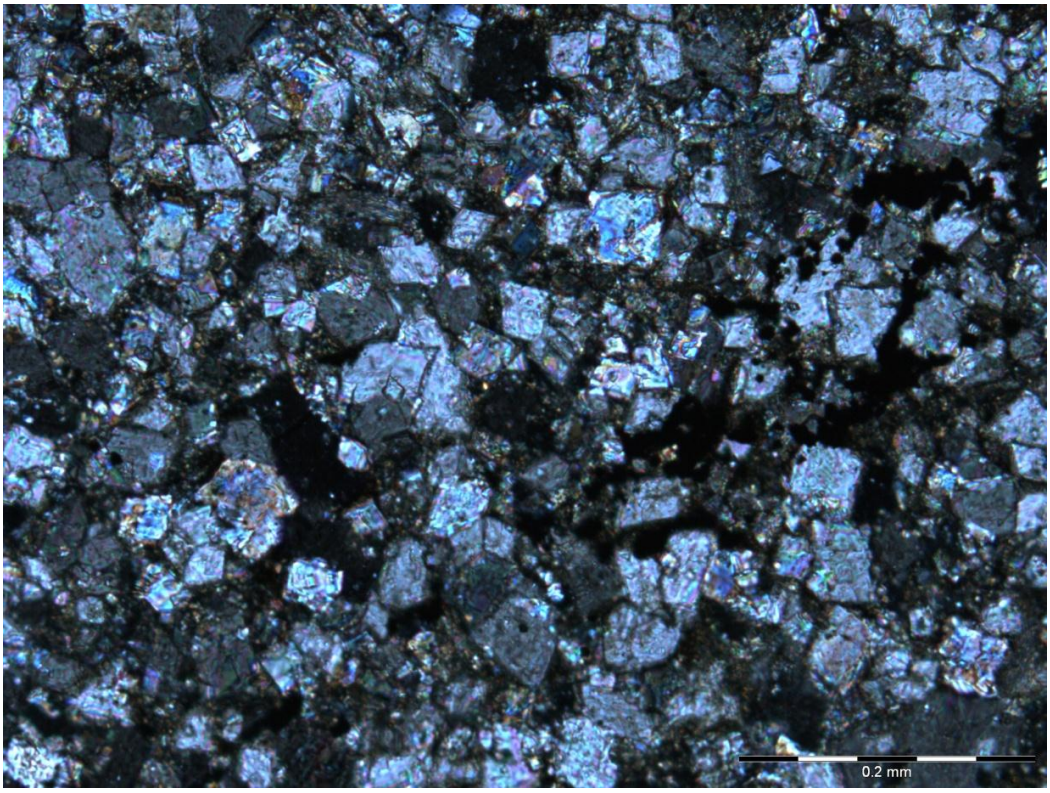

Photograph 42: Thin section photos for depth 4951' showing a punctate brachiopod with calcite cement infill in dolomite with pyrite.

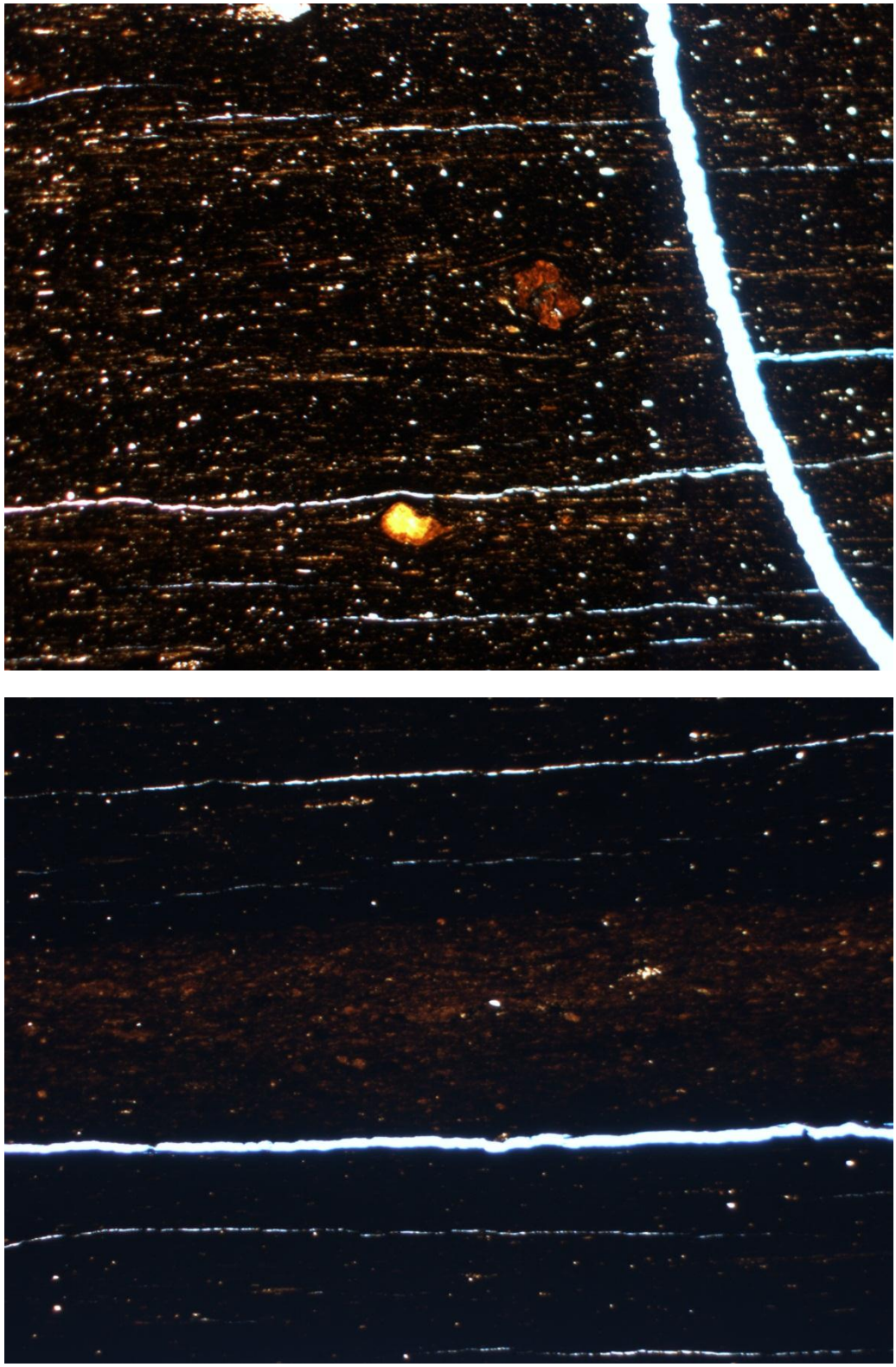

Photograph 43: Thin section photo for depth 4952’ showing phosphate nodules and phosphatic layering within the black shale. Silt and silica replacement of bioclasts decreases with depth.

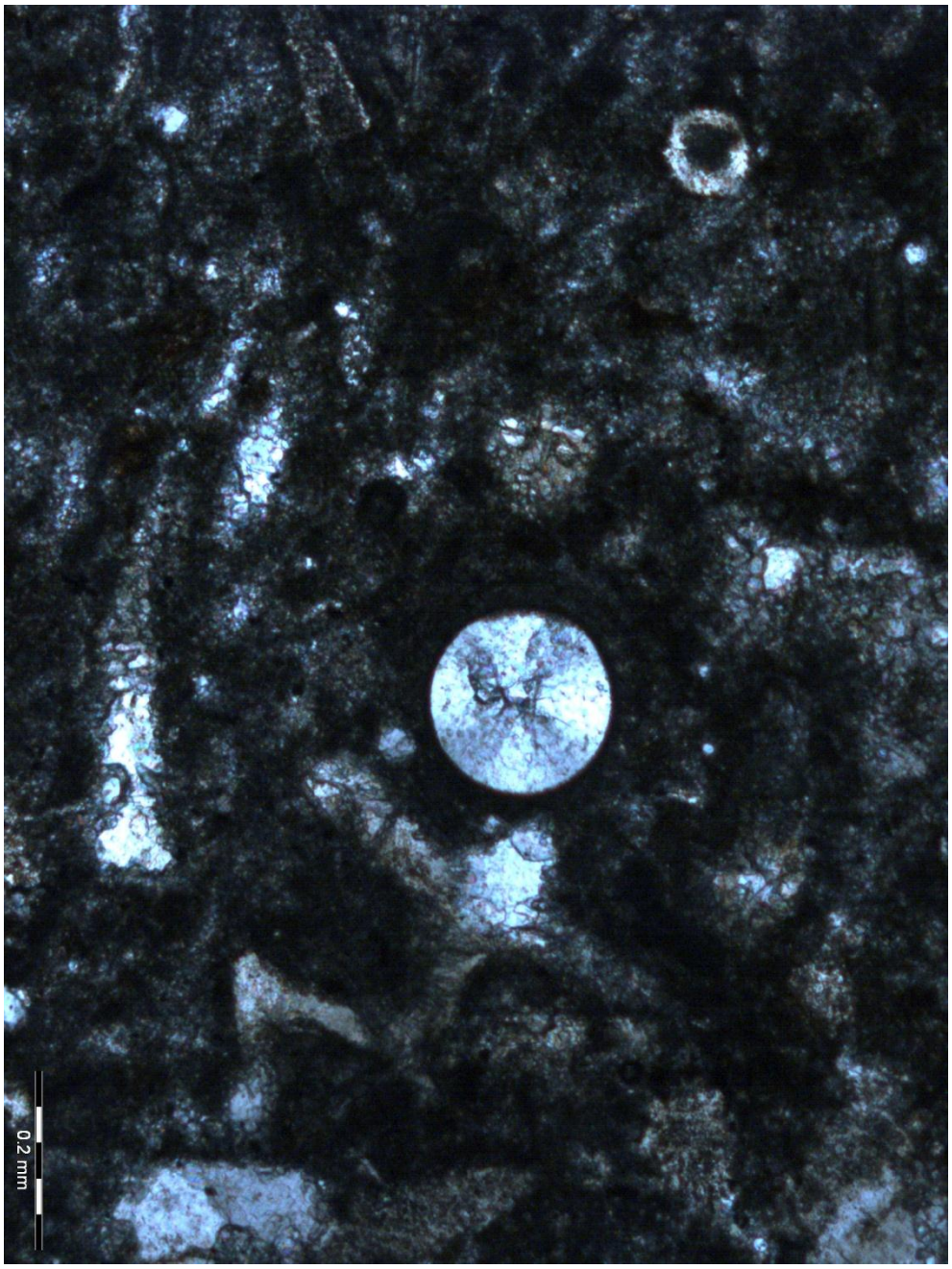

Photograph 44a: Thin section photo for depth 4955' showing a microcrystalline siderite nodule.

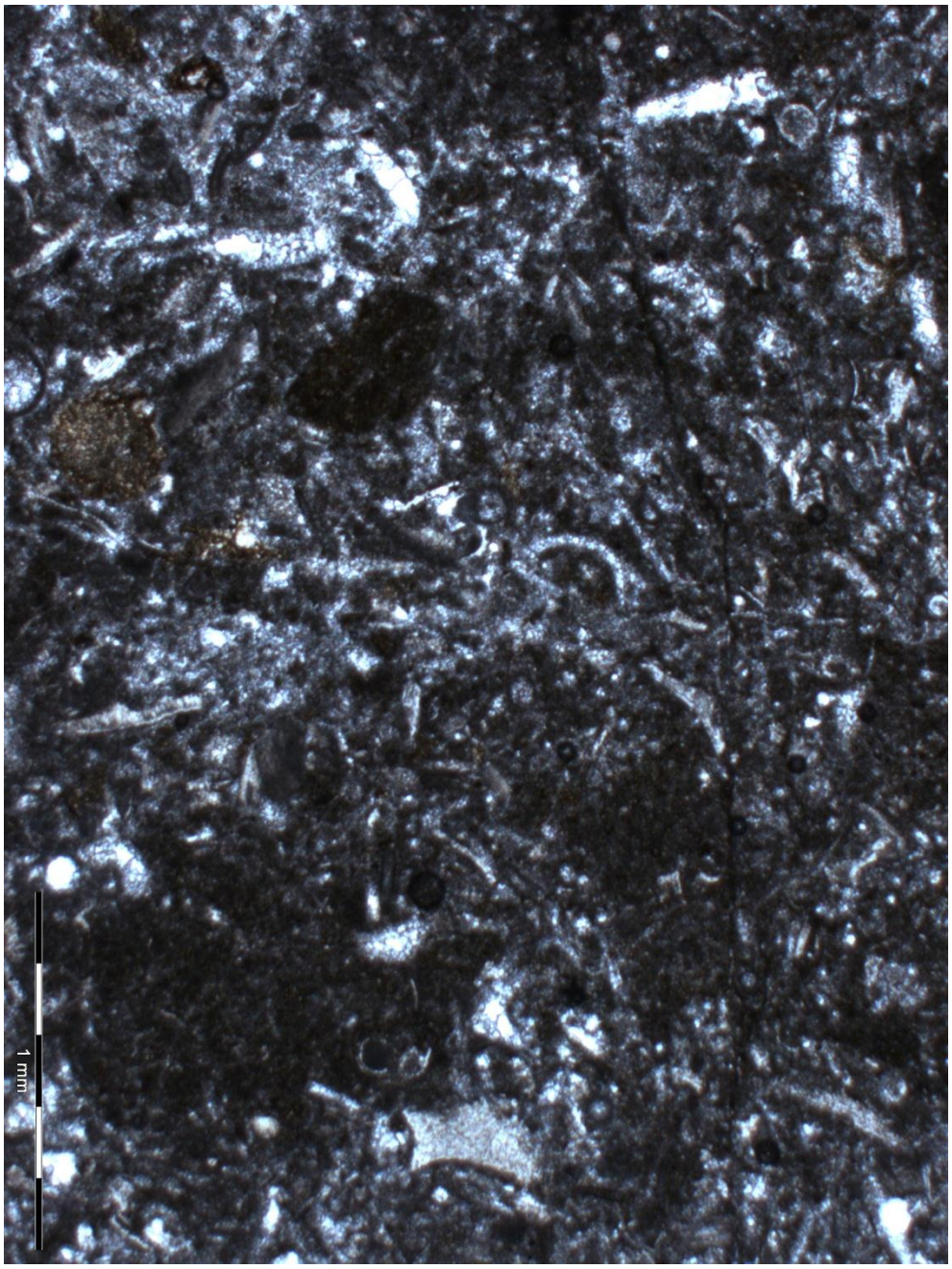

Photograph 44b: Thin section photo for depth 4955' showing texture of fossil hash with an open fracture approximately 18 µm wide.

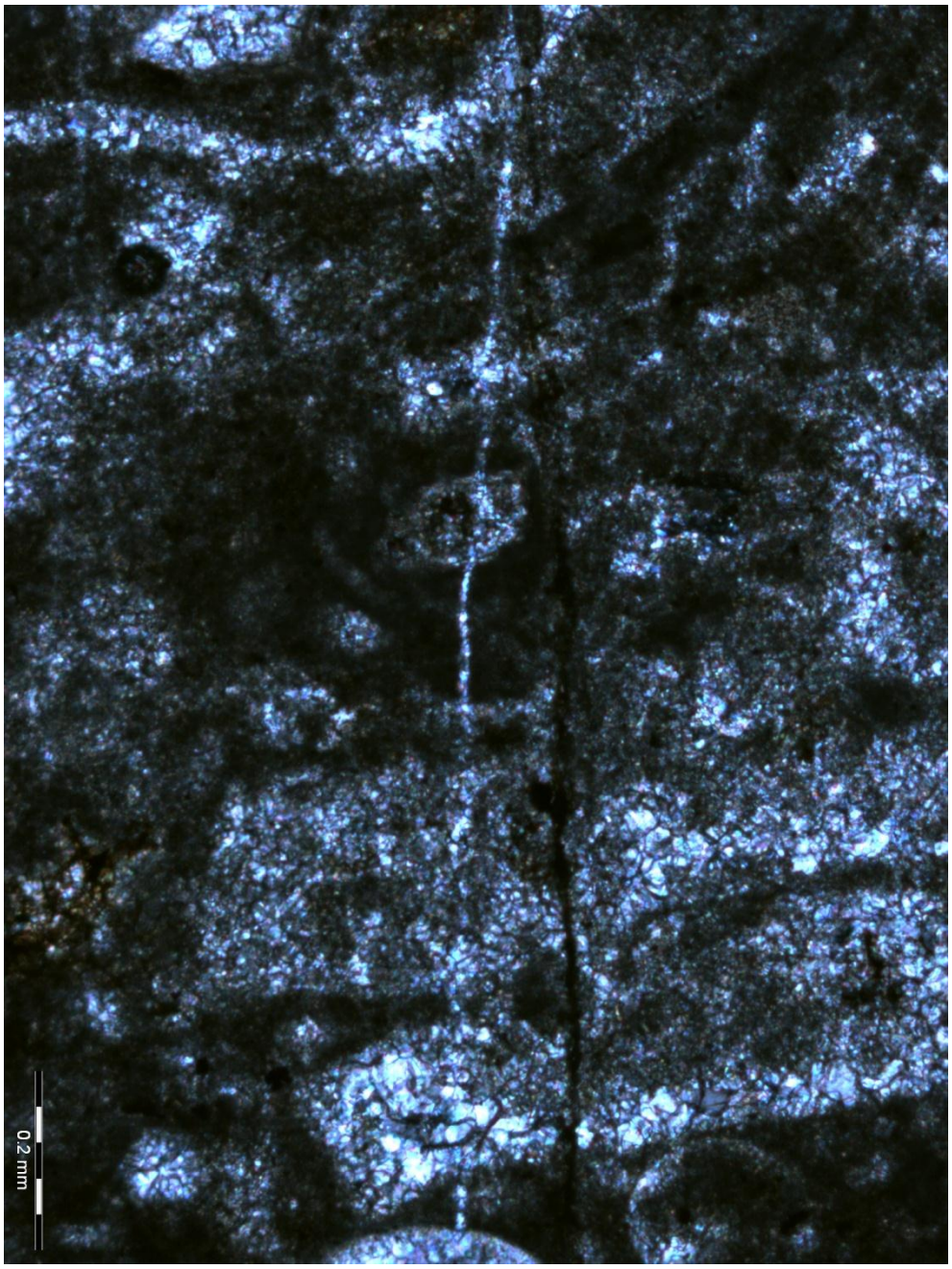

Photograph 45a: Thin section photo for depth 4966' showing healed and open fractures that are approximately 10 µm wide.

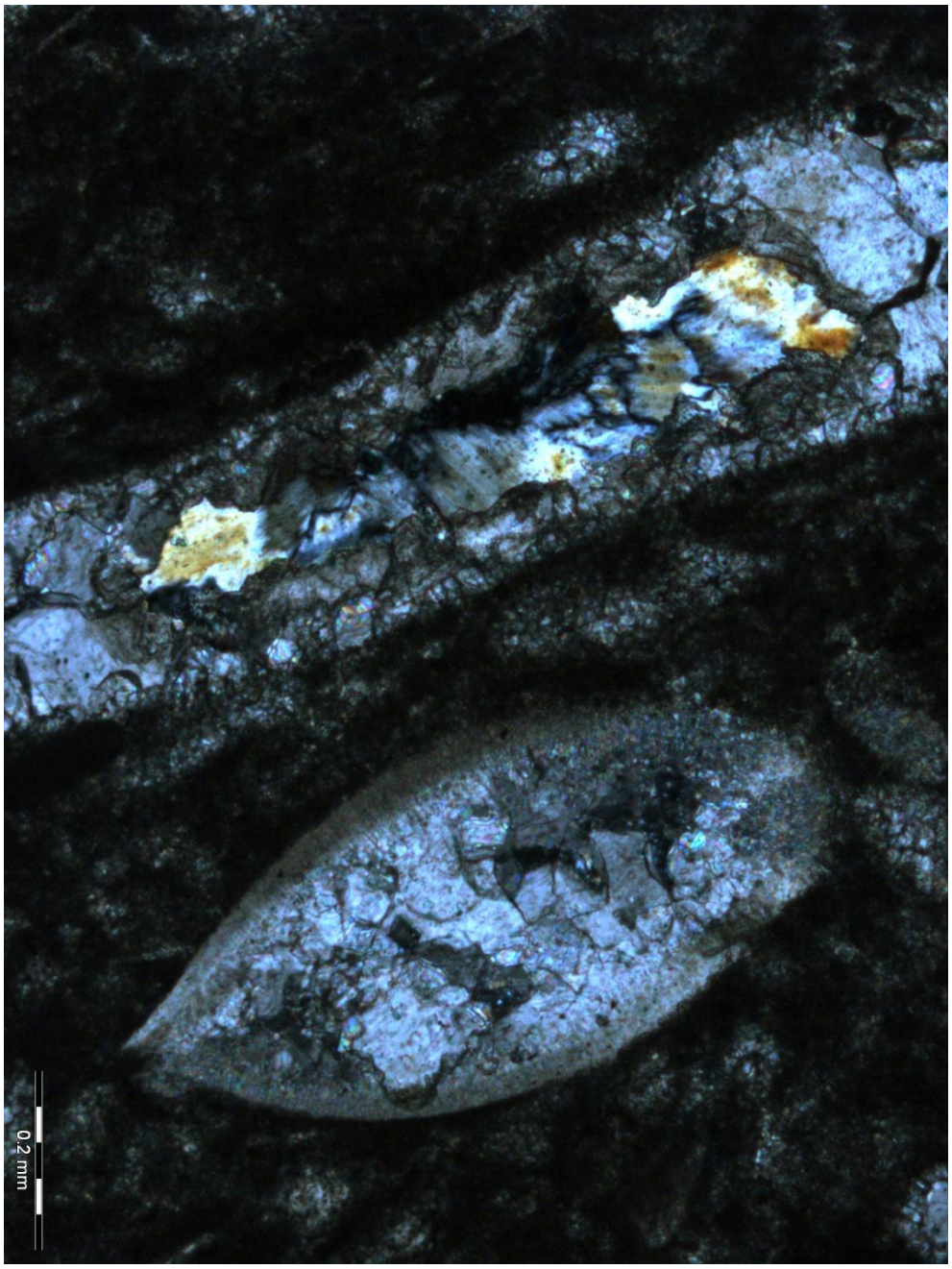

Photograph 45b: Thin section photo for depth 4966' showing calcite and silica replacement of bioclasts in a micrite host.

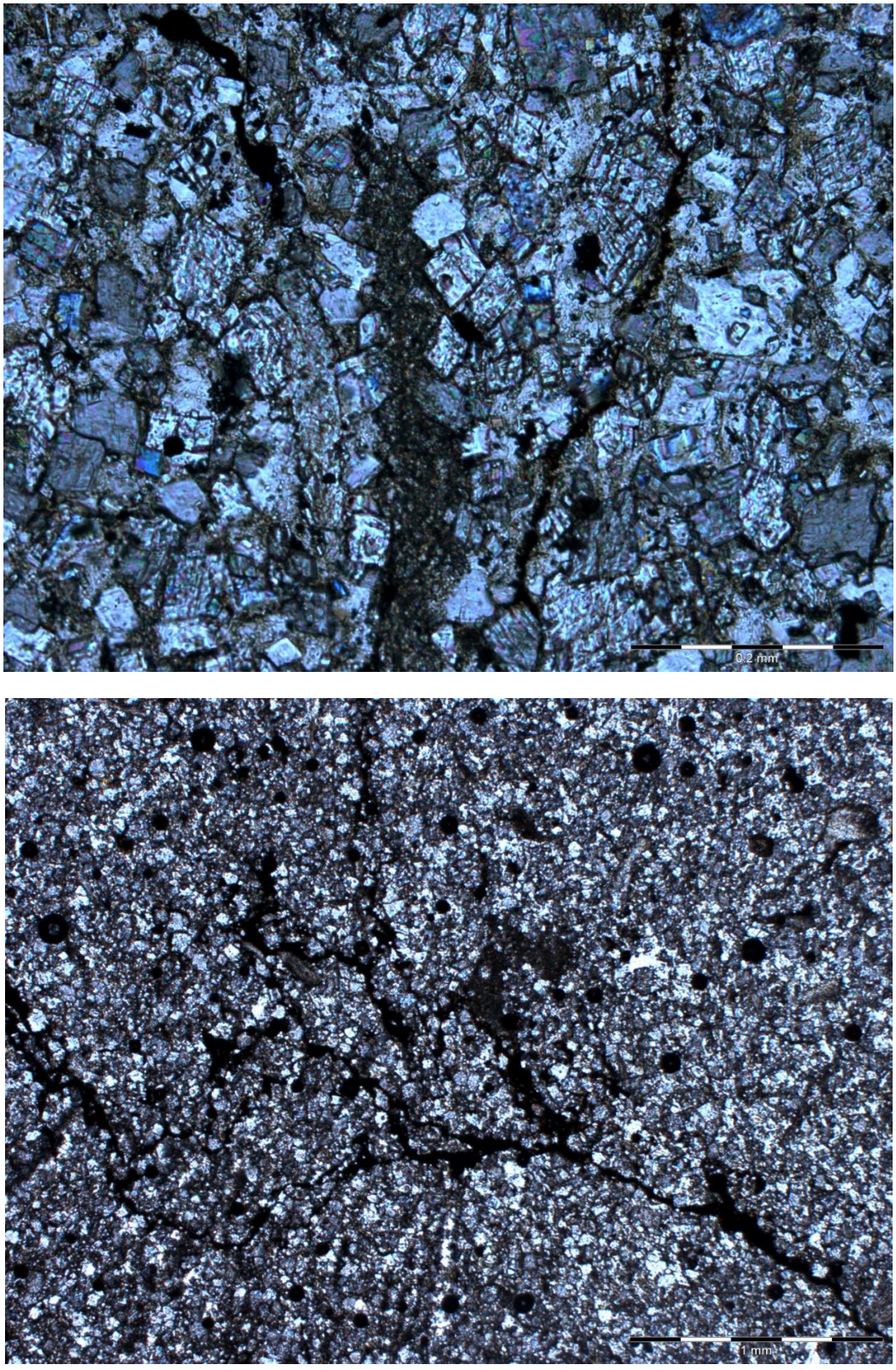

Photograph 46: Thin section photos for depths 4970-4971' showing fractured dolomitic microspar with pyrite and fractures averaging 9.5 µm.

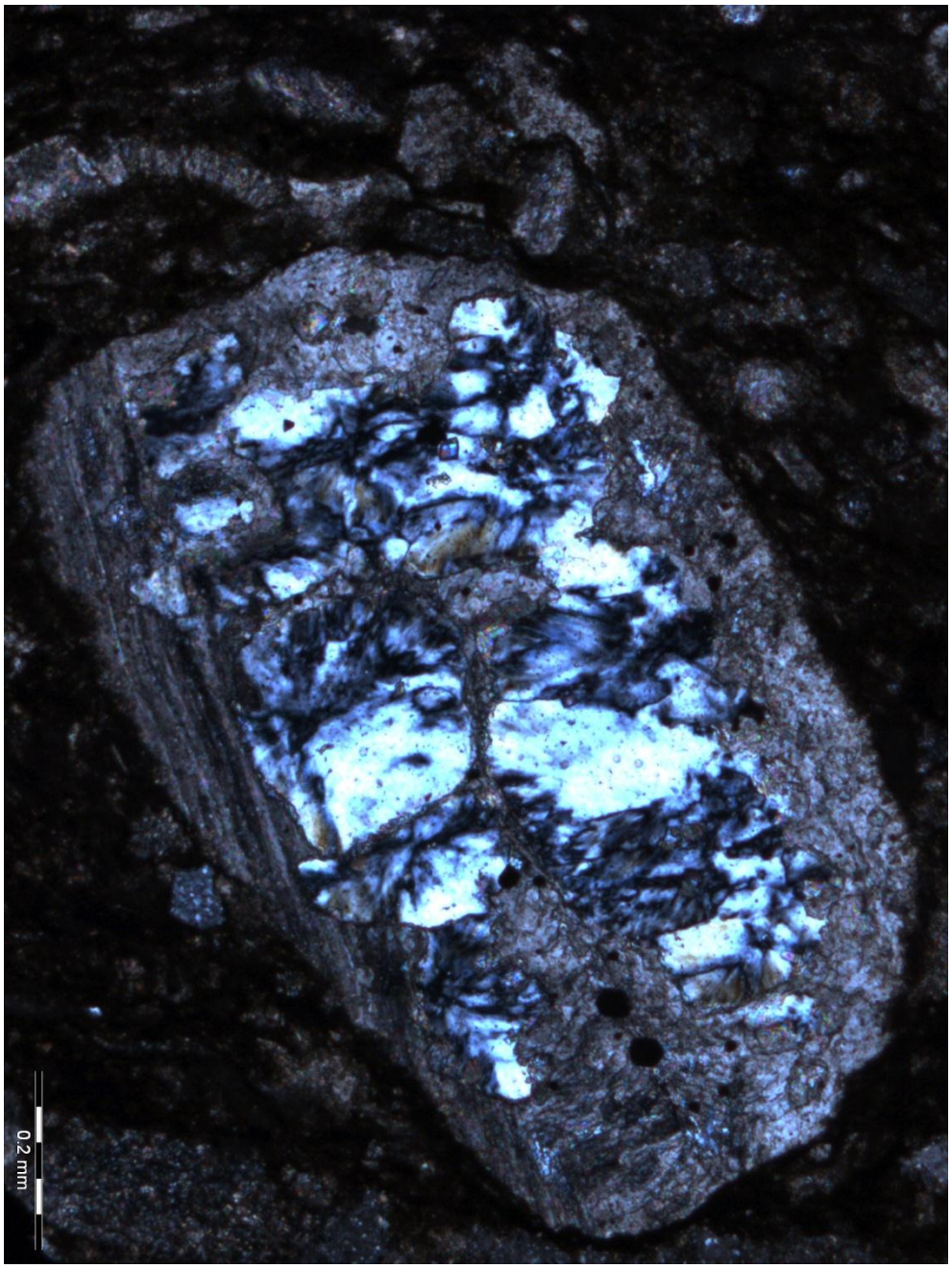

Photograph 47a: Thin section photo for depths 4973-4974' showing silica replacement of bioclasts in micrite host.

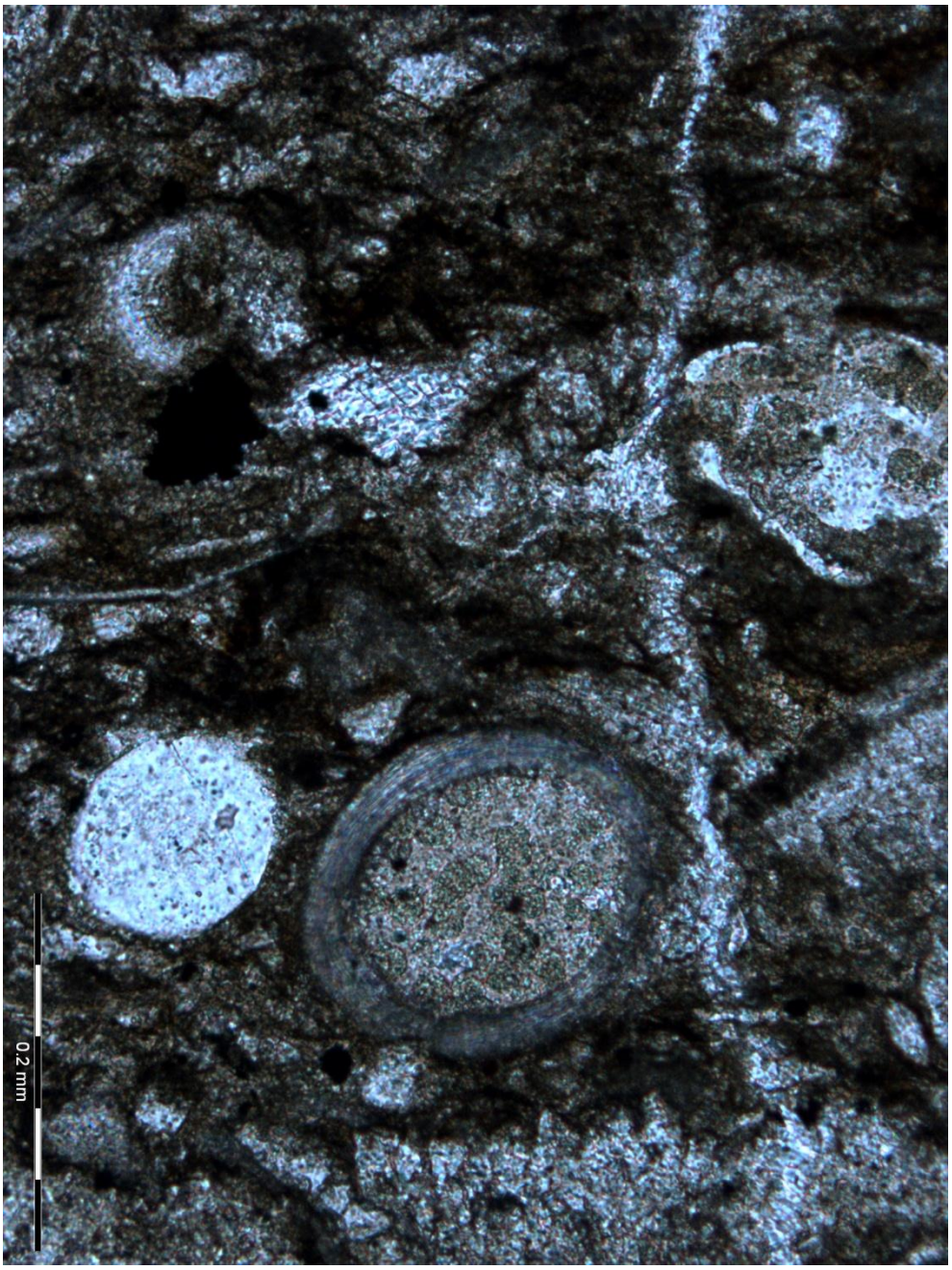

Photograph 47b: Thin section photo for depths 4973-74' showing wackestone-packstone with healed fracture that is approximately 16 µm wide.

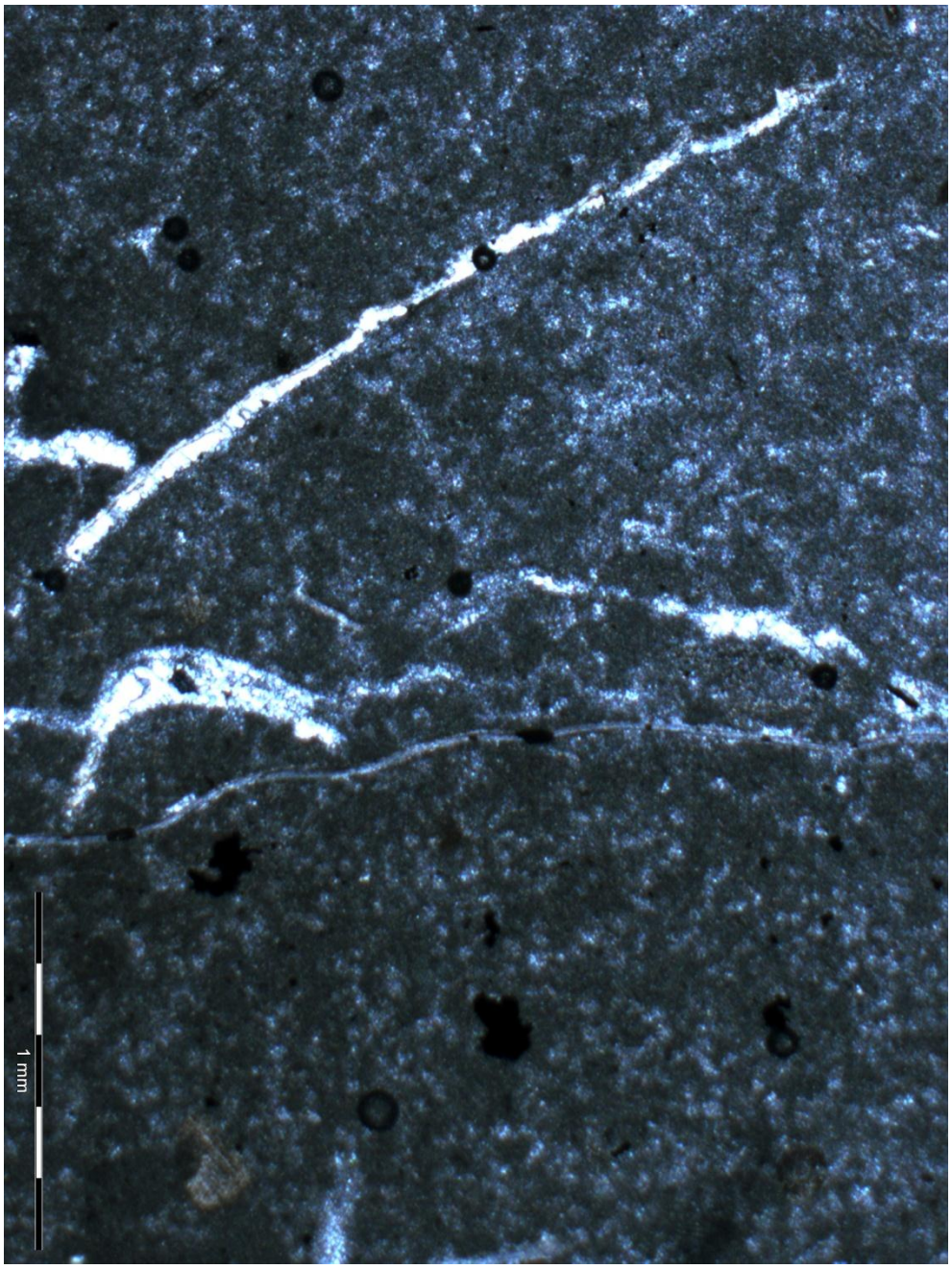

Photograph 48a: Thin section photo for depth 4999' showing bioclasts replaced with calcite cement in a micrite matrix.

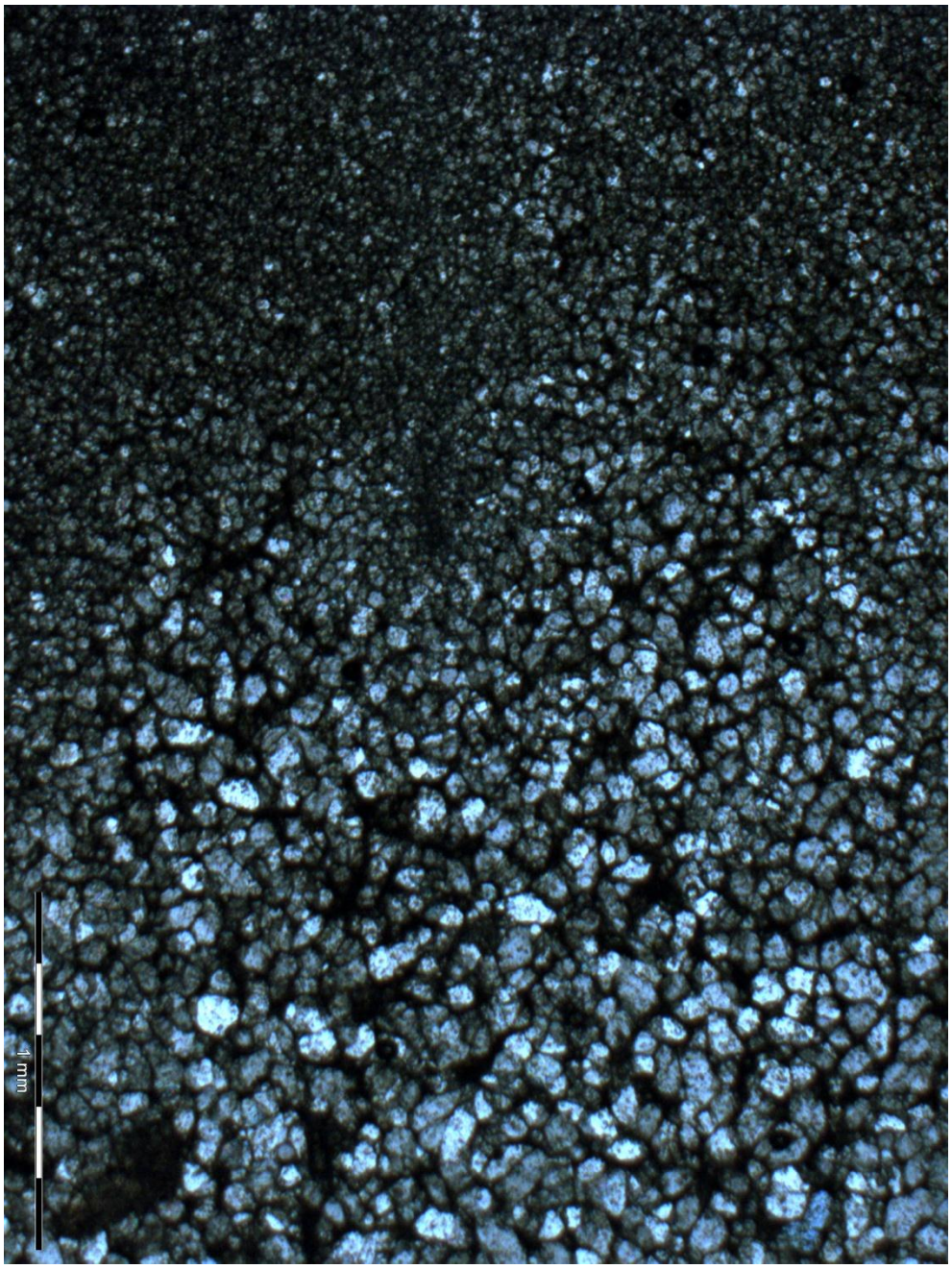

Photograph 48b: Thin section photo for depth 4999' showing an apparent transition from coarse crystalline microspar to micrite.

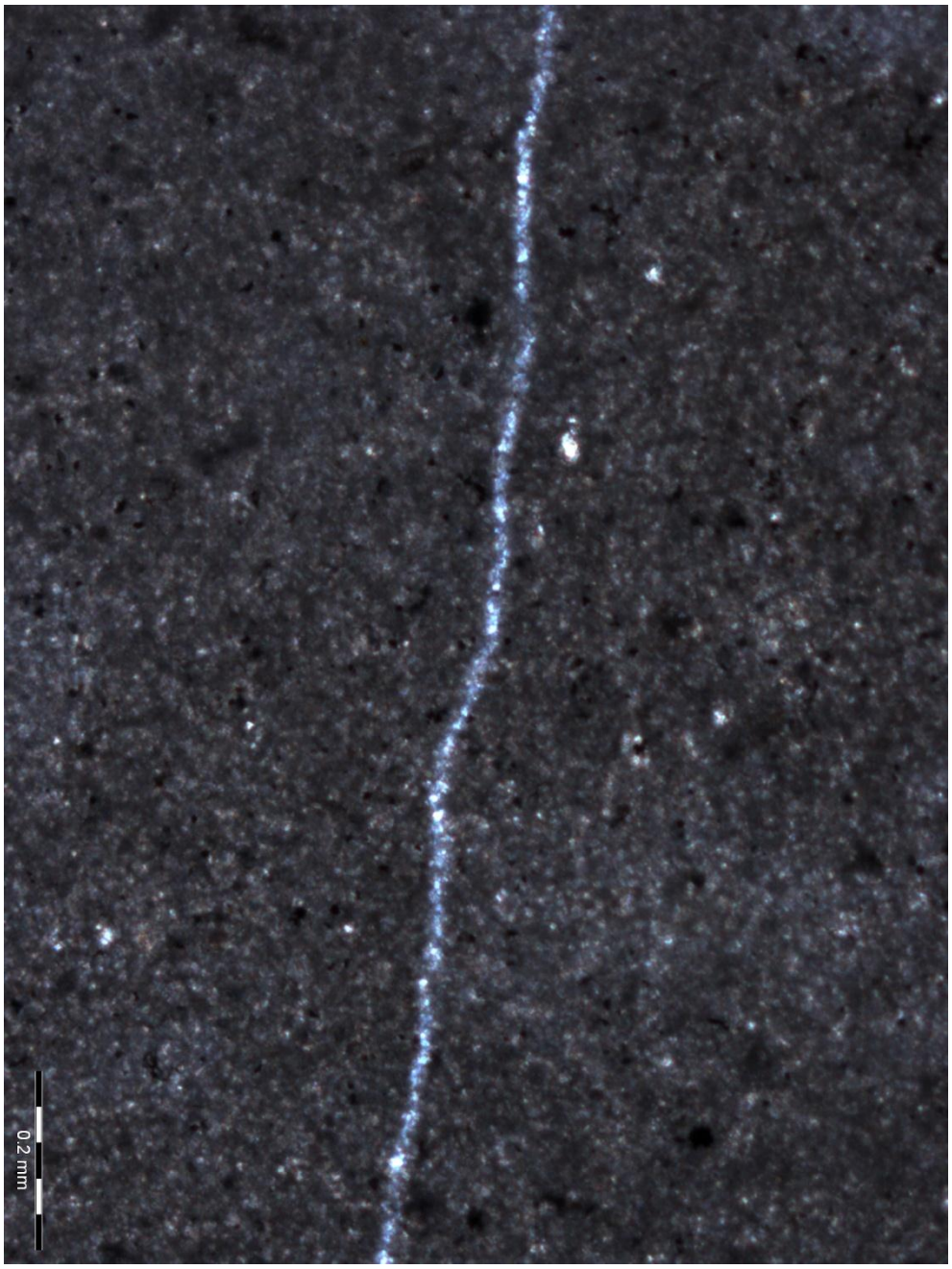

Photograph 49a: Thin section photo for depths 5004.4-5005.5' showing micrite with abundant pyrite and a healed fracture approximately 9.5 µm wide.

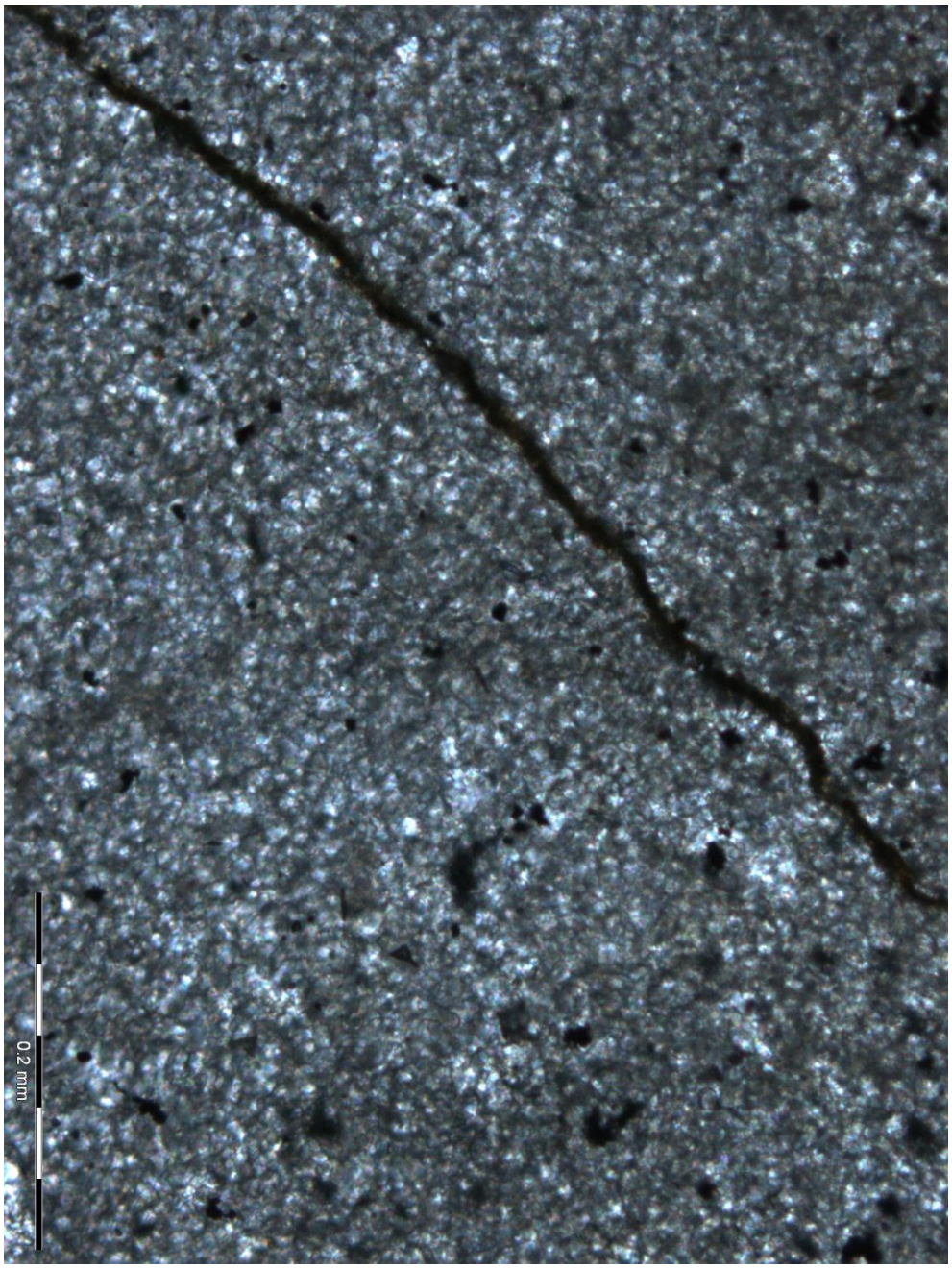

Photograph 49b: Thin section photo for depths 5004.4-5005.5' showing micrite with abundant pyrite and an open fracture approximately 9.5 µm wide.

APPPENDIX II

PRESENTATION OF DATA

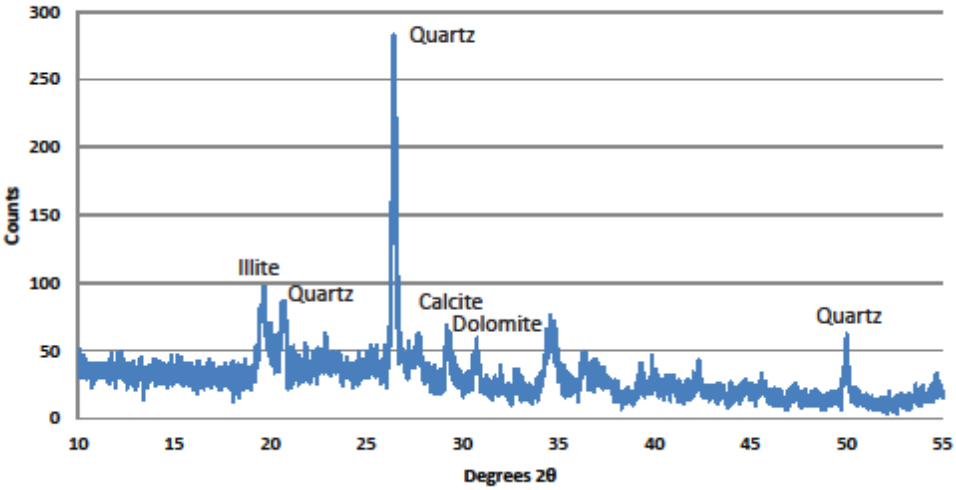

Figure 29: X-ray Diffraction measurements 4877'.

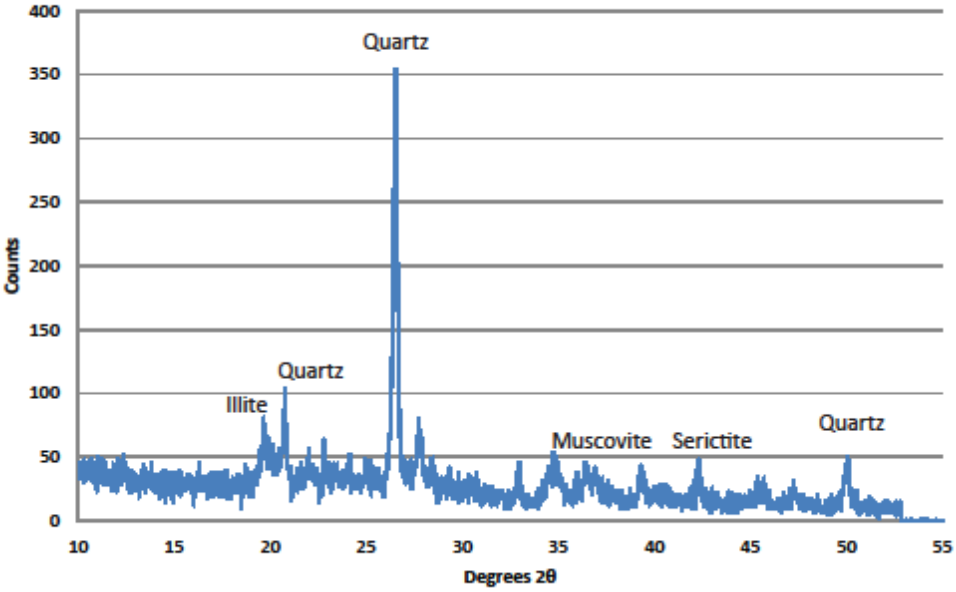

Figure 30: X-ray Diffraction measurements of 4947.5'

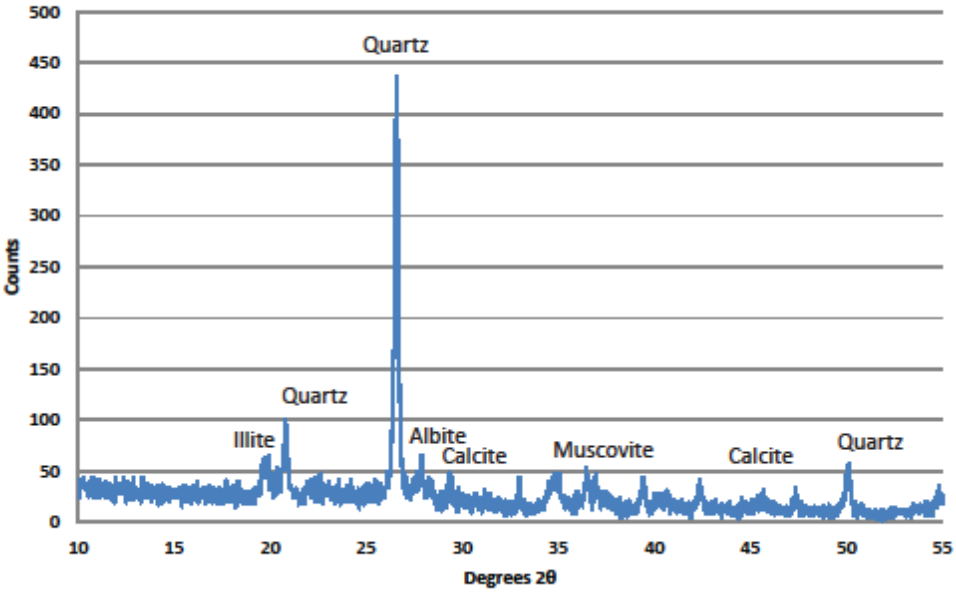

Figure 31: X-ray Diffraction measurements of 4952'.

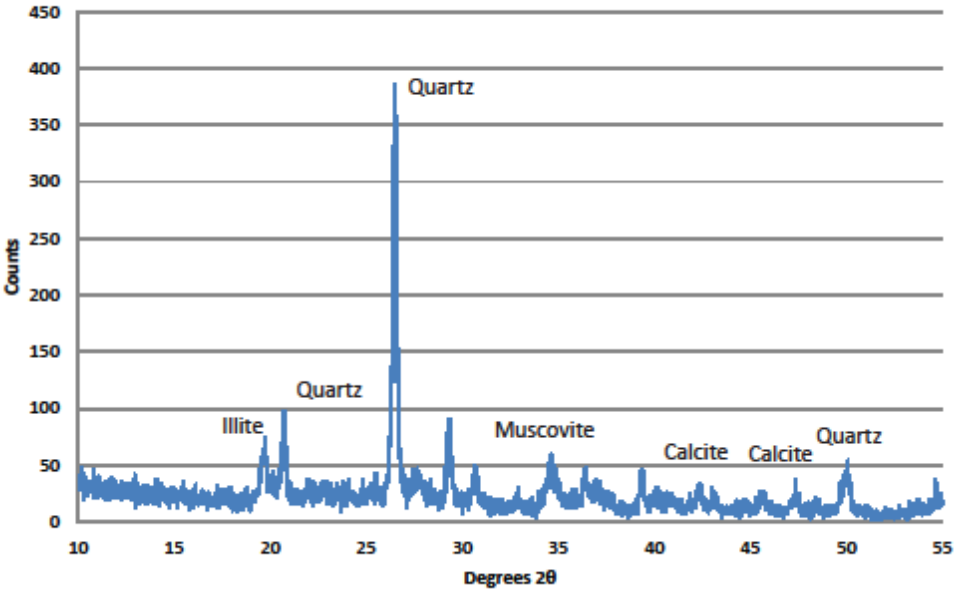

Figure 32: X-ray Diffraction measurements of 4953'.

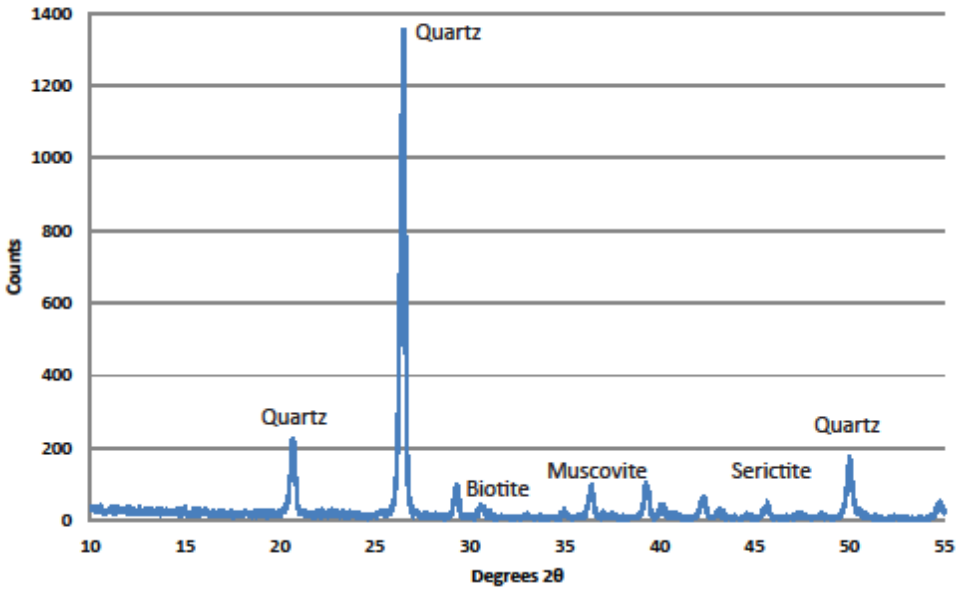

Figure 33: X-ray Diffraction measurements of 4973'.

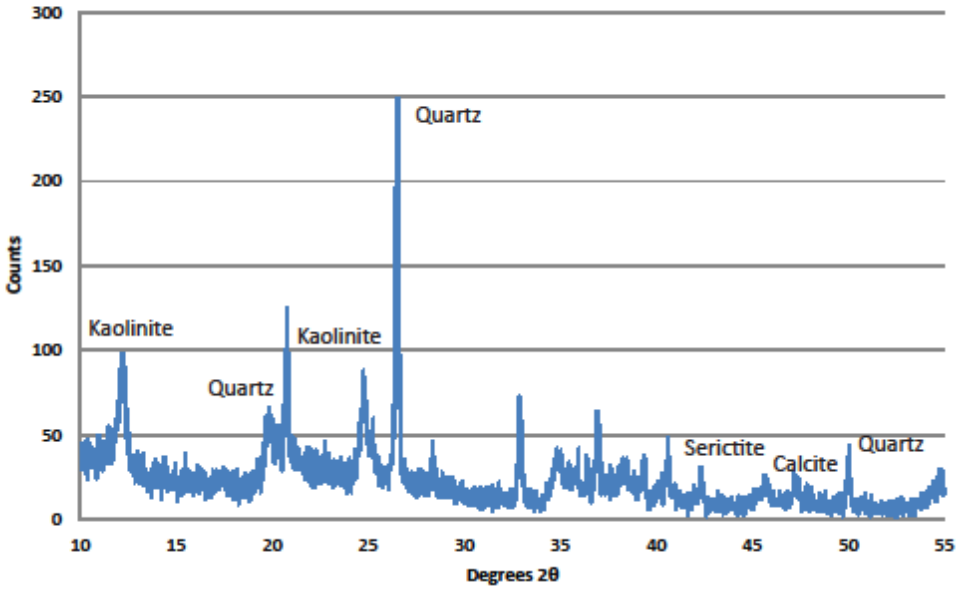

Figure 34: X-ray Diffraction measurements of 5023'.

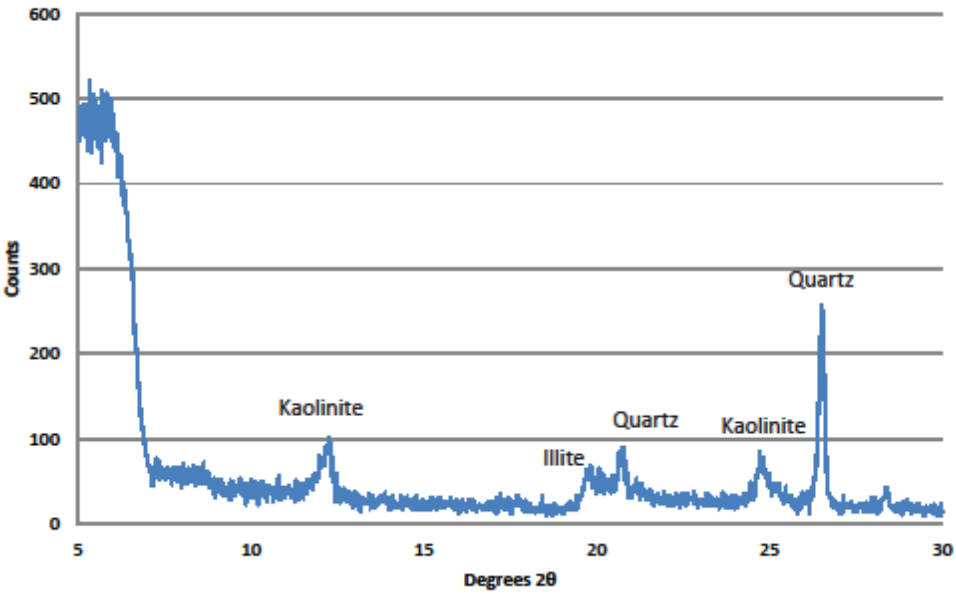

Figure 35: X-ray Diffraction clay measurements of 5023'.

Sample Depth	P1	P2	P1/P2	Grain Volume (cc)	Diameter (inch)	Diameter (cm)	Length (inch)	Length (cm)	Volume (cc)	PSIG	Flow Rate	Porosity (%)	Permeability (md)
4954	94.6	16.2	5.839506173	13.782	1.00656667	2.556679	1.0663	2.708402	13.9045	20.32	1.6	0.88101	0.2
4961-4963	94.6	16.2	5.839506173	13.782	1.00385	2.549779	1.0684	2.713736	13.85679	20.31	1.3	0.539735	0.1
4955	94.6	15.9	5.949685535	12.921	1.0039	2.549906	1.0016	2.544064	12.99171	20.32	1.1	0.54427	0.1
5004.4-5005.6	94.6	16	5.9125	13.213	1.00666667	2.556933	1.0257	2.605278	13.37774	20.3	1.05	1.231449	0.1

Coefficients Table

A	B	C	D
-0.019	0.1	-7.015	55.12

Figure 36: Porosity and Permeability measurements for select limestones of the Thirteen Finger Limestone.

Reading No.	730	740	745	755	765	775	780	791	801	Average	Certified
Ag	67.3	78.6	77.8	79.12	75.8	66.63	66.07	55.53	74.33	71.24222	27
Al	34923.41	36650.69	32952.36	34875.07	34376.33	36435.25	33105.53	34832.56	36701.83	34983.67	88700
As	< LOD	< LOD	< LOD	< LOD	< LOD	< LOD	< LOD	< LOD	< LOD	< LOD	48.8
Au	< LOD	< LOD	< LOD	< LOD	< LOD	< LOD	< LOD	< LOD	< LOD	< LOD	0.18
Ba	817.97	871	861.84	832.36	826.59	795.34	787.14	780.95	813.24	820.7144	993
Ca	2097.25	1773.86	1775.99	1819.05	1779.61	1842.1	1888.86	1919.4	1795.25	1854.597	1950
Cd	< LOD	< LOD	< LOD	< LOD	< LOD	< LOD	< LOD	< LOD	< LOD	< LOD	12.1
Co	< LOD	< LOD	< LOD	< LOD	< LOD	< LOD	< LOD	< LOD	< LOD	< LOD	2.2
Cr	59.52	67.91	61.28	72.43	85.81	75.08	59.5	63.21	59.68	67.15778	44
Cu	166.76	167.32	170.05	155.49	155.48	164.85	172.44	162.88	176.59	165.7622	216
Fe	29226.56	29240.97	28888.73	29185.24	29072.87	29153.12	29279.52	29250.1	29275.12	29174.69	27840
K	28176.96	28517.46	28191.95	28003.25	28229.64	28399.6	28439.93	28191.51	28120.7	28252.33	33800
Mg	< LOD	< LOD	< LOD	< LOD	< LOD	< LOD	< LOD	< LOD	< LOD	< LOD	5330
Mn	507.86	533.76	565.15	485.98	534.08	494.67	511.46	508.9	486.56	514.2689	462
Mo	< LOD	< LOD	< LOD	< LOD	< LOD	< LOD	< LOD	< LOD	< LOD	< LOD	11
Ni	< LOD	< LOD	< LOD	< LOD	< LOD	< LOD	< LOD	< LOD	< LOD	< LOD	12
P	2558.82	2625.46	2285.08	2532.53	2804.73	2405.52	2455.29	2648.91	3118.58	2603.88	427
Pb	5232.19	5257.41	5183.92	5249.33	5229.11	5164.96	5254.08	5214.88	5314.48	5233.373	5770
S	16672.05	17024.75	16096.03	15978.18	16840.63	16270.66	16231.57	16639.07	16235.36	16443.14	12630
Sb	146.72	157.05	149.84	155.28	146.35	150.2	141.81	145.81	147.89	148.9944	160
Sr	181.53	183.21	183.65	179.76	182.54	180	181.49	179.31	181.97	181.4956	217
Th	< LOD	< LOD	< LOD	< LOD	< LOD	< LOD	< LOD	< LOD	< LOD	< LOD	12
Ti	5568.43	5622.52	5583.38	5448.01	5627.16	5539.38	5571.13	5580.24	5500.42	5560.074	6990
U	262.14	276.54	251.1	251.44	267.82	266.53	253.58	262.32	273.25	262.7467	4
V	522.06	522.76	529.68	509.16	530.71	519.14	529.95	528.47	556.5	527.6033	268
W	131.58	103.26	124.85	94.68	122.87	120.59	89.98	100.97	107.75	110.7256	24
Zn	1963.63	2002.28	2014.18	2139.8	1955.19	2038.76	2024.36	1976.86	2144.22	2028.809	2570
Zr	160.97	162.92	162.74	161.31	163.15	164.78	164.44	162.05	162.65	162.7789	176

Figure 37: X-ray Fluorescence measurements of NIST 2780 compared to certified measurements.

Reading No.	722	732	742	747	757	767	777	782	793	803	Average	Certified
Al	33269.58	35016.7	38036.03	31030.95	33579.2	29013.37	34550.08	31913.79	34777.48	33854.79	33504.2	72508.3
As	29.84	31.26	31.03	31.45	30.16	27.95	31.46	29.25	31.58	28.88	30.286	12
Ba	71.67	79.75	98.97	92	113.8	88.24	106.81	99.42	123.73	97.11	97.15	570
Ca	18912.69	18312.15	18827.77	18725.69	18679.25	16626.96	18570.78	18597.32	18788.39	18462.85	18450.39	18725
Cl	1274.75	1408.5	1382.33	1321.84	1446.2	1111.05	1289.45	1355.64	1320.28	1395.19	1330.523	51
Co	< LOD	< LOD	< LOD	< LOD	< LOD	< LOD	< LOD	< LOD	< LOD	< LOD	< LOD	11
Cr	133.68	136.58	156.44	137.17	151.25	111.3	169.2	133.99	139.49	159.63	142.873	68
Cu	21.04	24.05	22.82	19.53	22.45	20.14	23.13	25.78	26.88	26.04	23.186	29
Fe	45422.56	43964.15	44995.4	44296.85	44954.11	39305.21	44054.76	43987.66	44625.12	44875.8	44048.16	35880
K	20898.83	20417.24	20668.74	20261.77	20656.69	18322.03	20240.88	20355.25	20516.34	20519.75	20285.75	22994.1
Mg	< LOD	< LOD	< LOD	< LOD	< LOD	< LOD	< LOD	< LOD	< LOD	< LOD	< LOD	16402.58
Mn	479.64	464.18	473.54	490.24	480.78	417.95	509.21	428.56	474.04	470.9	468.904	410
Mo	< LOD	< LOD	< LOD	< LOD	< LOD	< LOD	< LOD	< LOD	< LOD	< LOD	< LOD	1.4
Nb	14.74	14.36	15.04	14.14	14.79	9.45	14.02	14.96	14	14.17	13.967	11
Ni	< LOD	< LOD	< LOD	< LOD	< LOD	< LOD	< LOD	< LOD	< LOD	< LOD	< LOD	27
P	4005.31	3811.97	3992.35	3929.57	3710.71	3475.48	3976.67	3815.24	4055.88	4235.53	3900.871	916.4834
Pb	28.73	27.48	28.52	28.56	30.62	25.69	26.12	29.96	27.85	30.66	28.419	31
Pd	6.75	8.41	8.01	8.74	10.69	4.44	8.41	8.18	11.27	9.04	8.394	0.001
S	917.98	989.18	861.35	666.42	805.2	604.04	648.64	758.22	791.14	760.37	780.254	630
Sb	29.27	26.17	26.84	36	34.81	20.73	34.31	23.48	31.54	38.1	30.125	2.5
Si	172749.2	174278	177665	165018.5	172088.3	152275.9	171930.2	168291.5	172214.5	173075.6	169958.7	293570.1
Sn	< LOD	< LOD	< LOD	< LOD	< LOD	< LOD	18.02	< LOD	< LOD	< LOD	18.02	3.7
Sr	138.52	135.18	137.6	137.32	138.6	123.84	137.07	136.83	137.32	137.79	136.007	170
Th	< LOD	< LOD	< LOD	< LOD	< LOD	< LOD	< LOD	< LOD	< LOD	< LOD	< LOD	9.7
Ti	3432.9	3338.03	3444.4	3344.81	3405.19	2980.72	3357	3329.86	3374.97	3418.95	3342.683	3775.85
U	161.77	158.88	165.77	162.2	150.75	141.26	169.66	155.94	155.36	168.03	158.962	3
V	379.05	352.61	361.66	367.83	379.45	298.51	371.88	397.46	367.91	374.11	365.047	130
W	48.15	65.86	46.6	43.96	63.04	< LOD	51.5	62.64	56.33	53.28	54.59556	1.4
Zn	102.25	91.51	97.46	93.36	95.04	81.92	96.18	91.78	100.25	94.49	94.424	100
Zr	149.5	149.68	150.99	151.28	151.71	137.47	149.08	147.63	147.57	149.81	148.472	160

Figure 38: X-ray Fluorescence measurements of USGS SCo-1 compared to certified measurements.

Rebecca K. Bounds #1 Well, Sec. 17, T.18S., R.42W., Greeley Co., Kansas

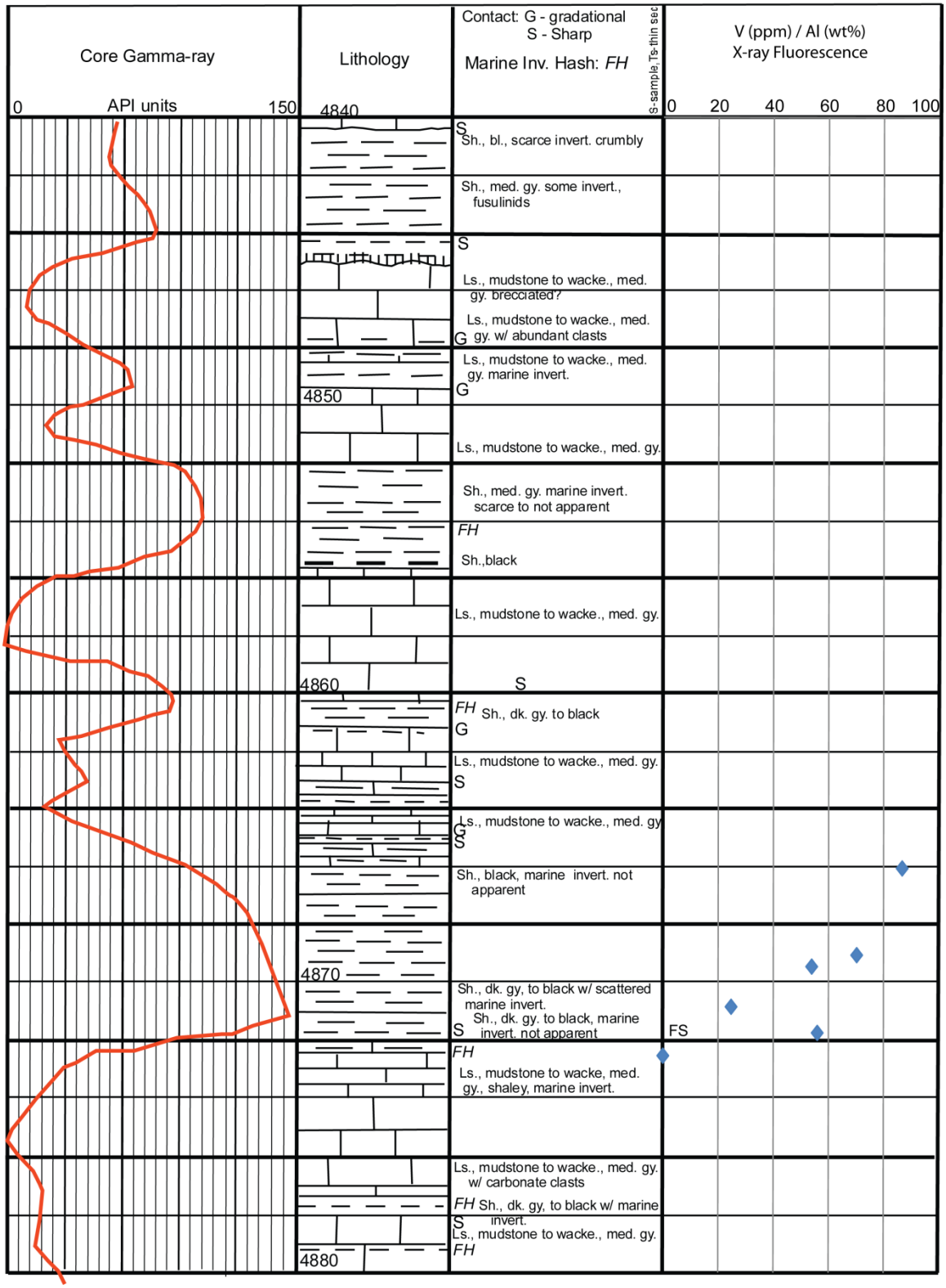

Figure 39: V/Al ratio plotted against the lithologic column for core depths 4840' to 4880'.

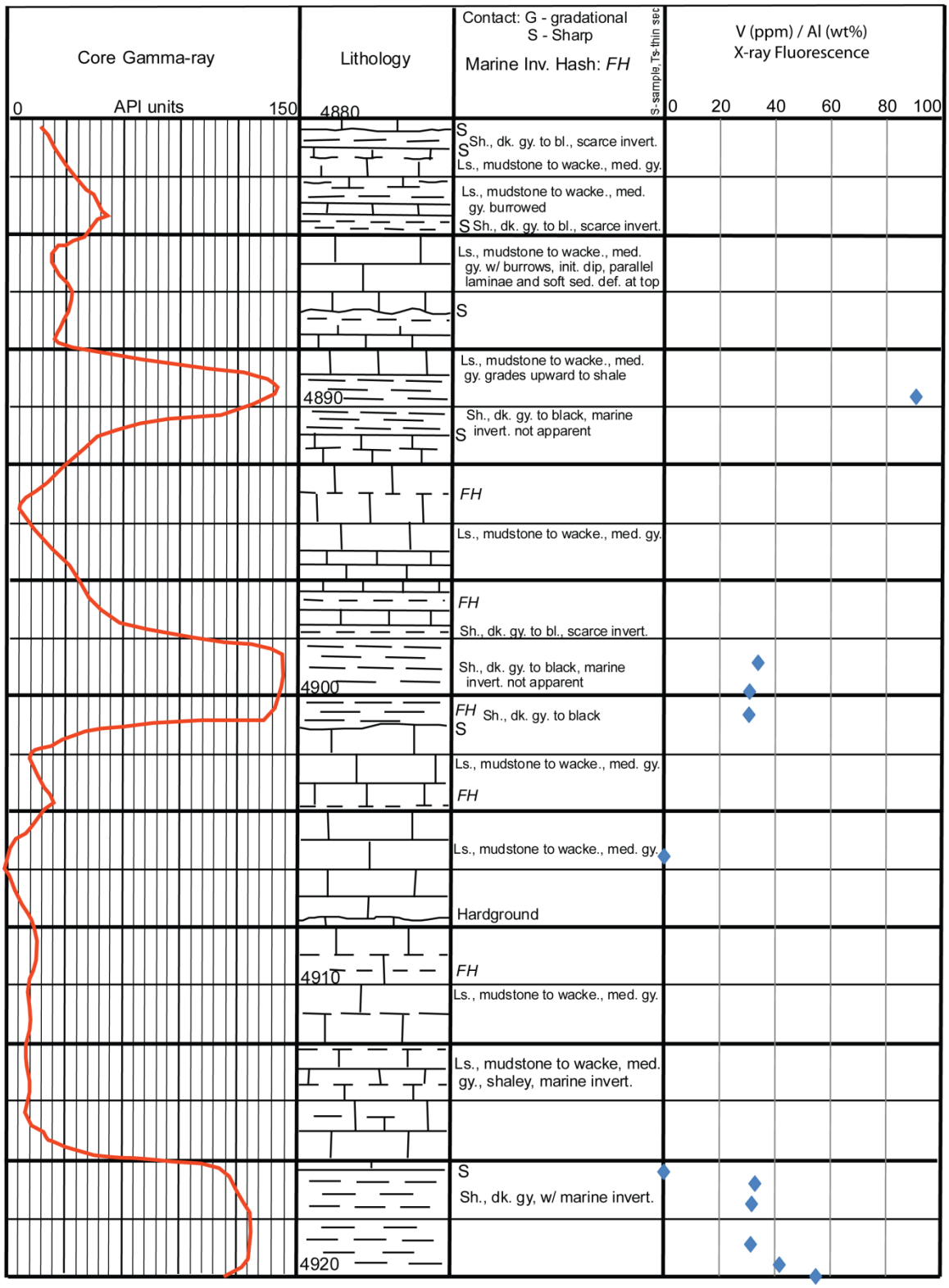

Figure 40: V/Al ratio plotted against the lithologic column for core depths 4880’ to 4920’.

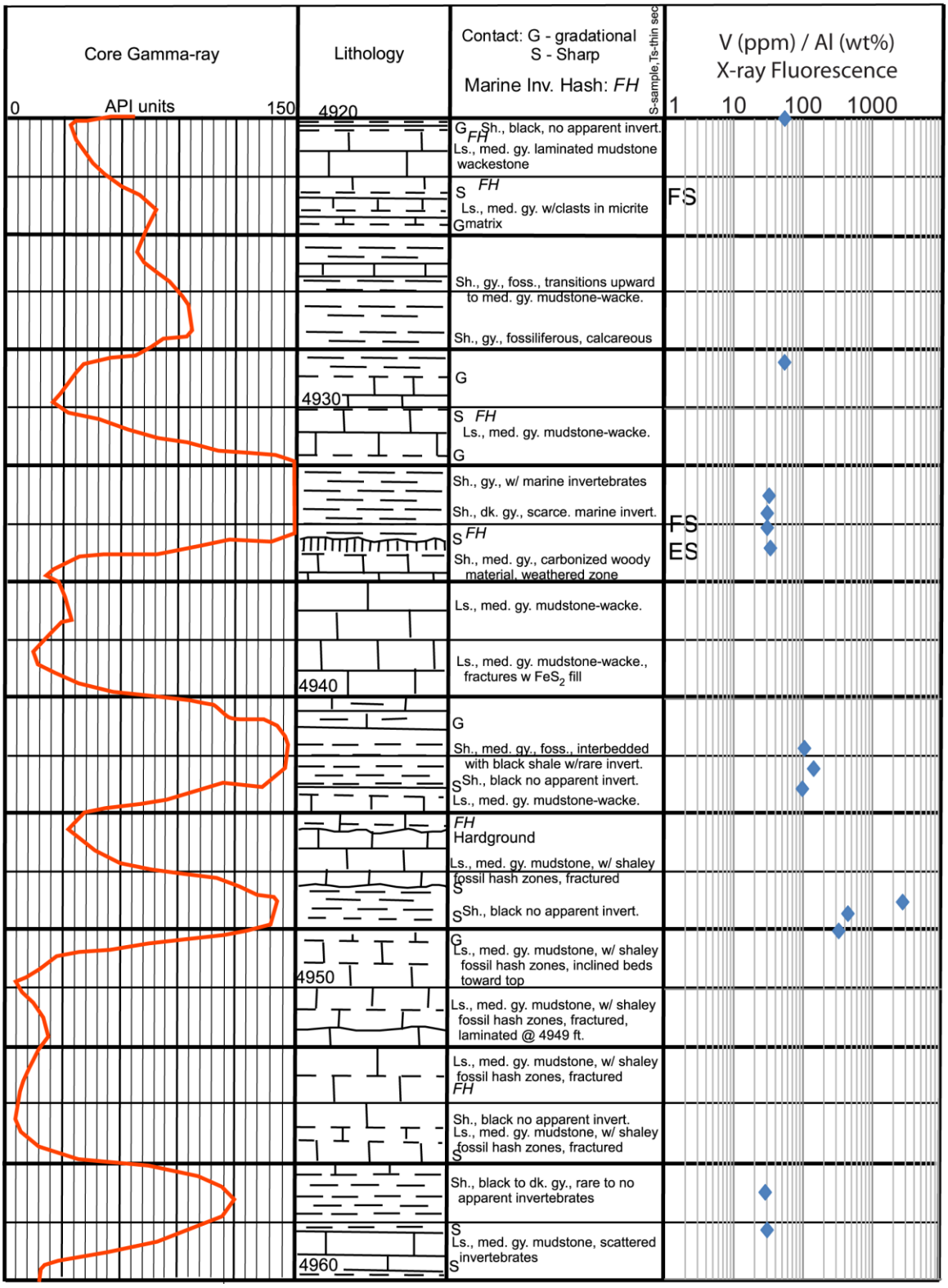

Figure 41: V/Al ratio plotted against the lithologic column for core depths 4920' to 4960'.

Rebecca K. Bounds #1 Well, Sec. 17, T.18S., R.42W., Greeley Co., Kansas

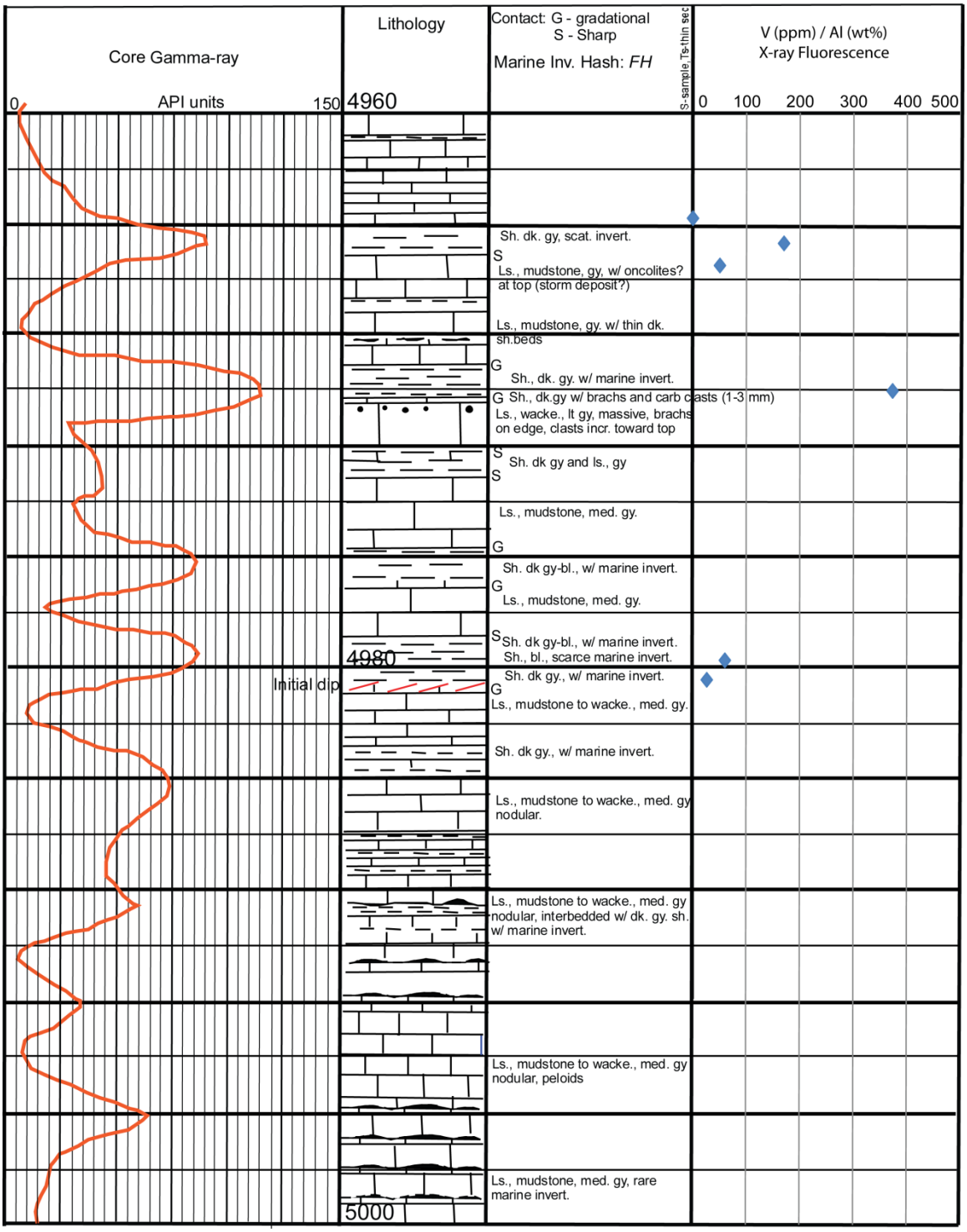

Figure 42: V/Al ratio plotted against the lithologic column for core depths 4960' to 5000'.

Rebecca K. Bounds #1 Well, Sec. 17, T.18S., R.42W., Greeley Co., Kansas

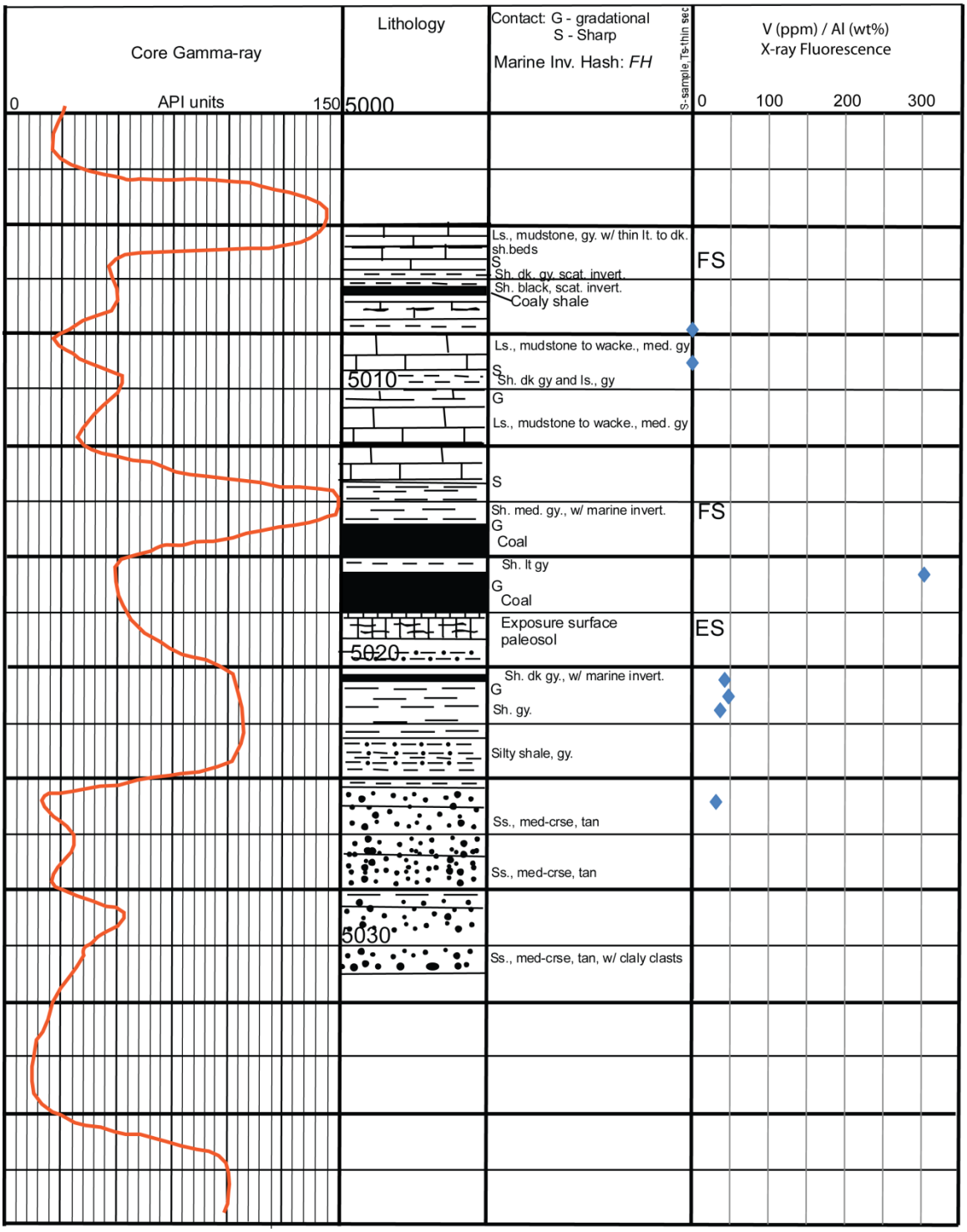

Figure 43: V/Al ratio plotted against the lithologic column for core depths 5000' to 5031'.

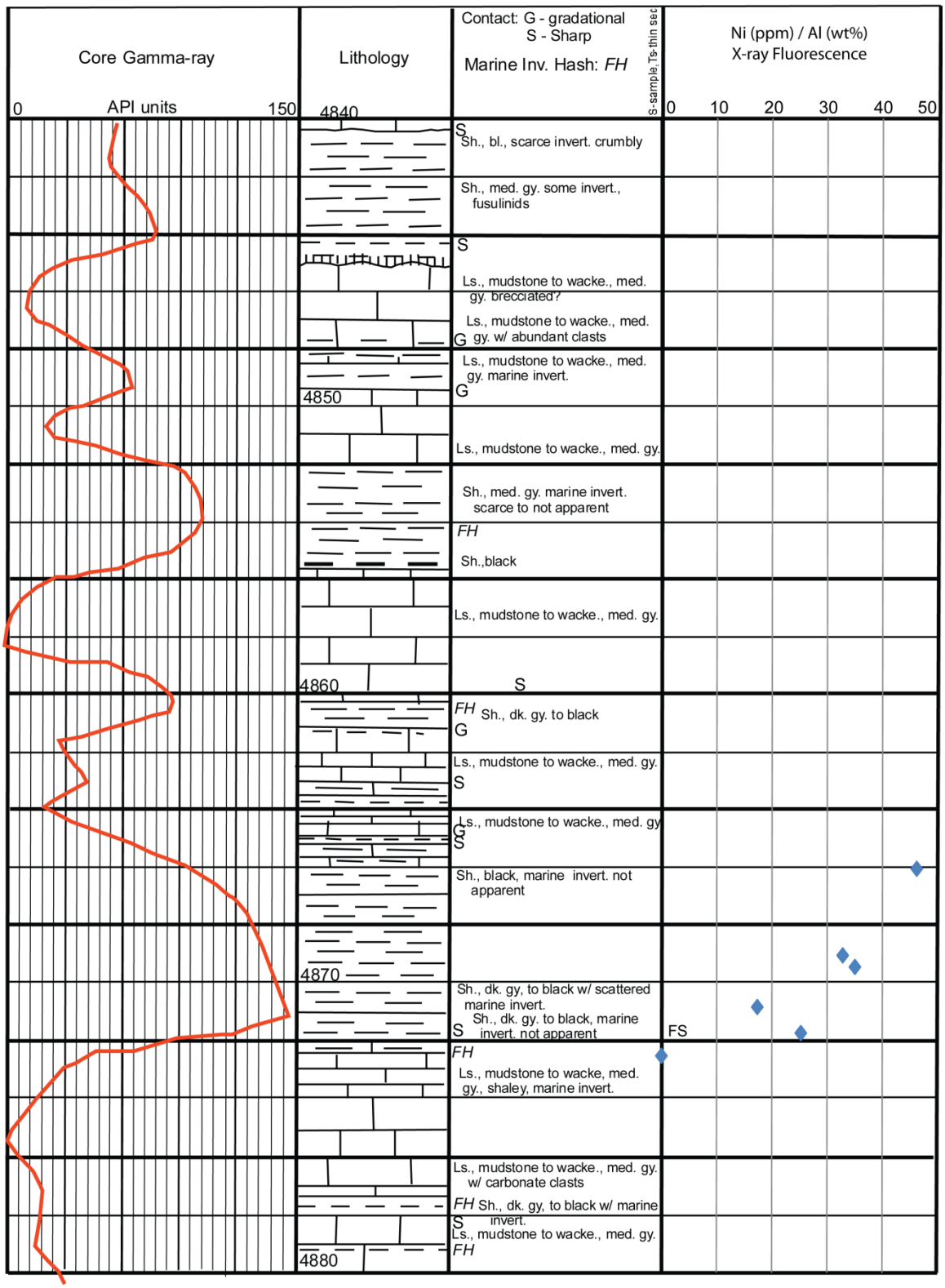

Figure 44: Ni/Al ratio plotted against the lithologic column for core depths 4840' to 4880'.

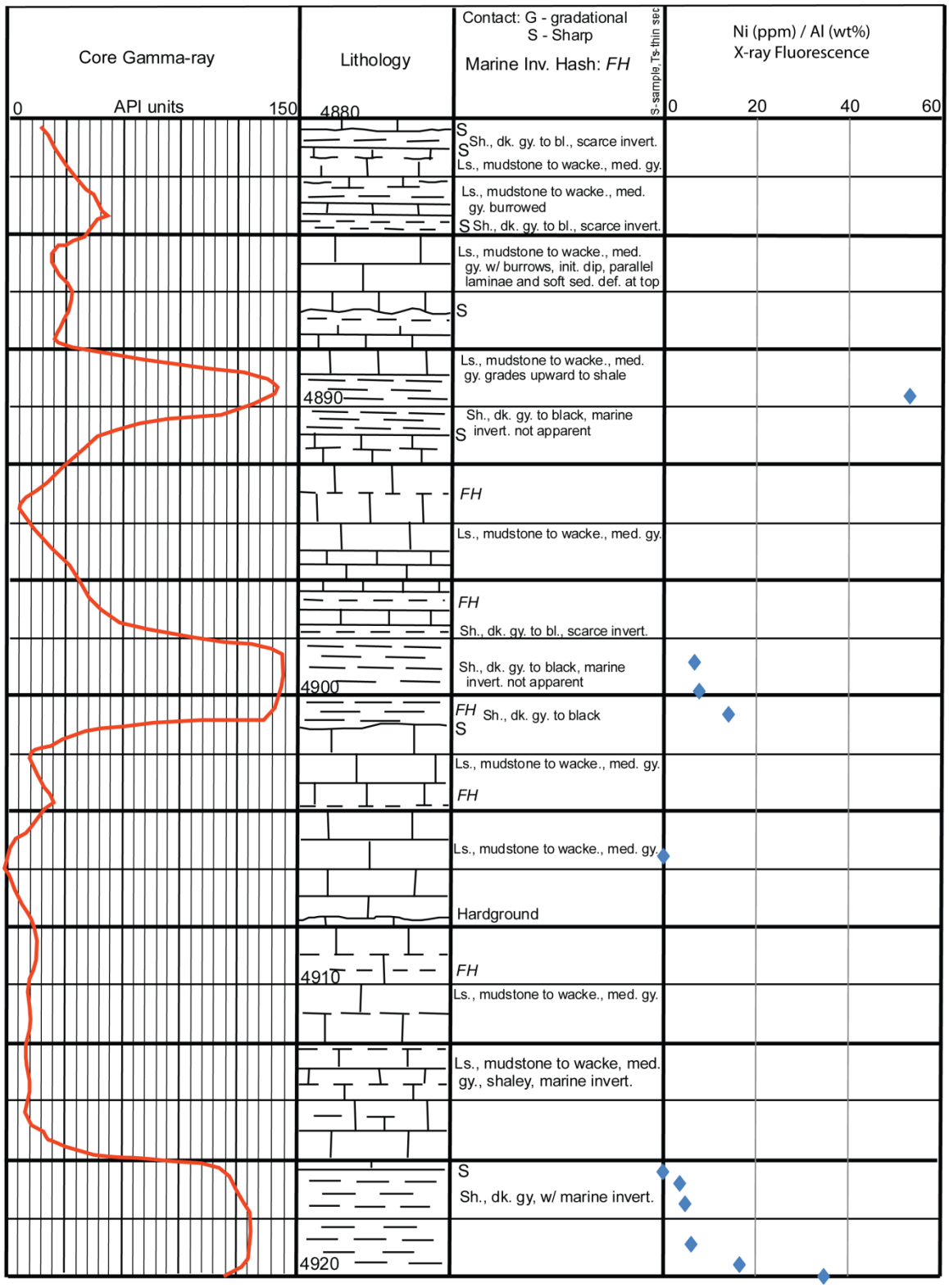

Figure 45: Ni/Al ratio plotted against the lithologic column for core depths 4880' to 4920'.

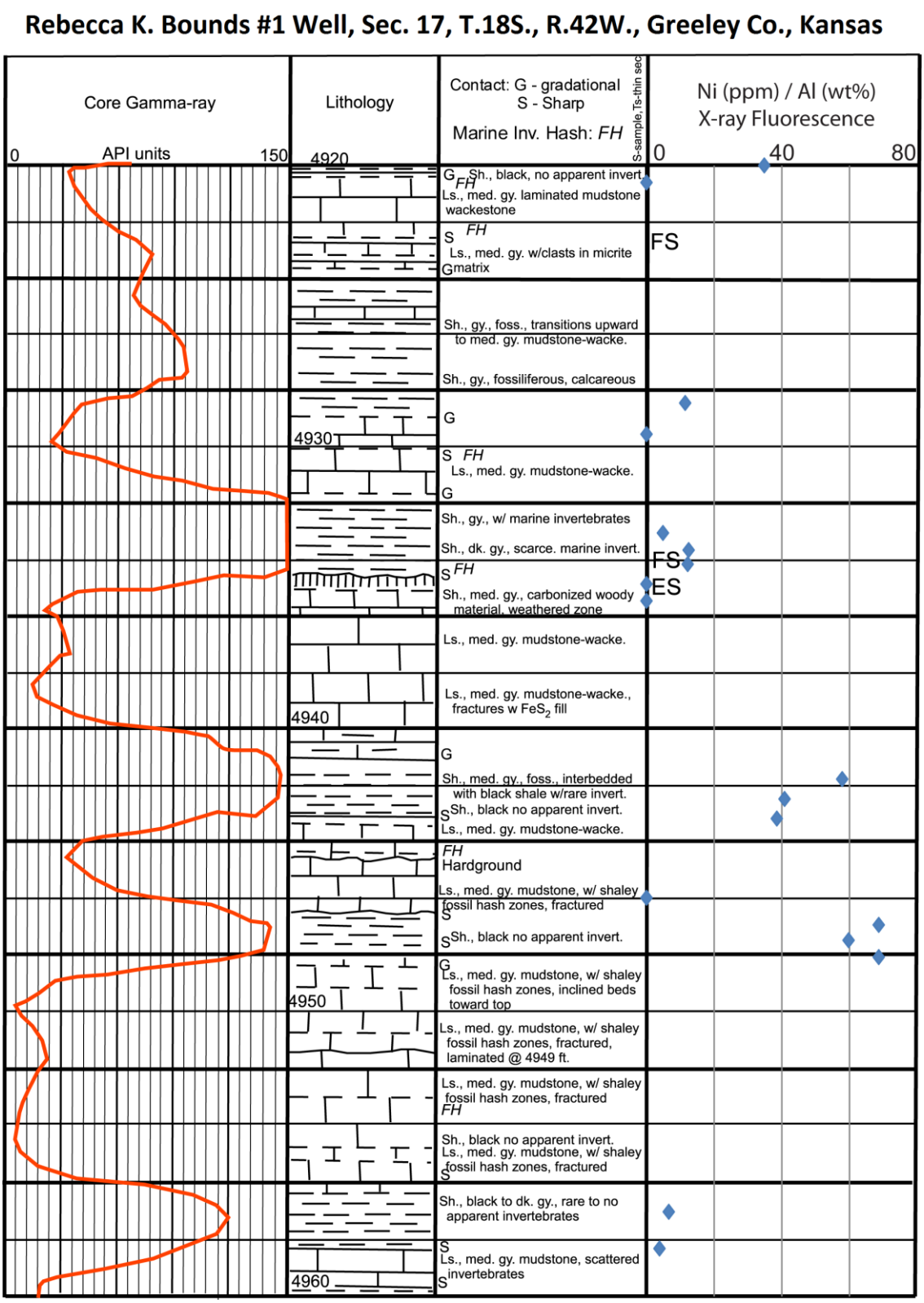

Figure 46: Ni/Al ratio plotted against the lithologic column for core depths 4920' to 4960'.

Rebecca K. Bounds #1 Well, Sec. 17, T.18S., R.42W., Greeley Co., Kansas

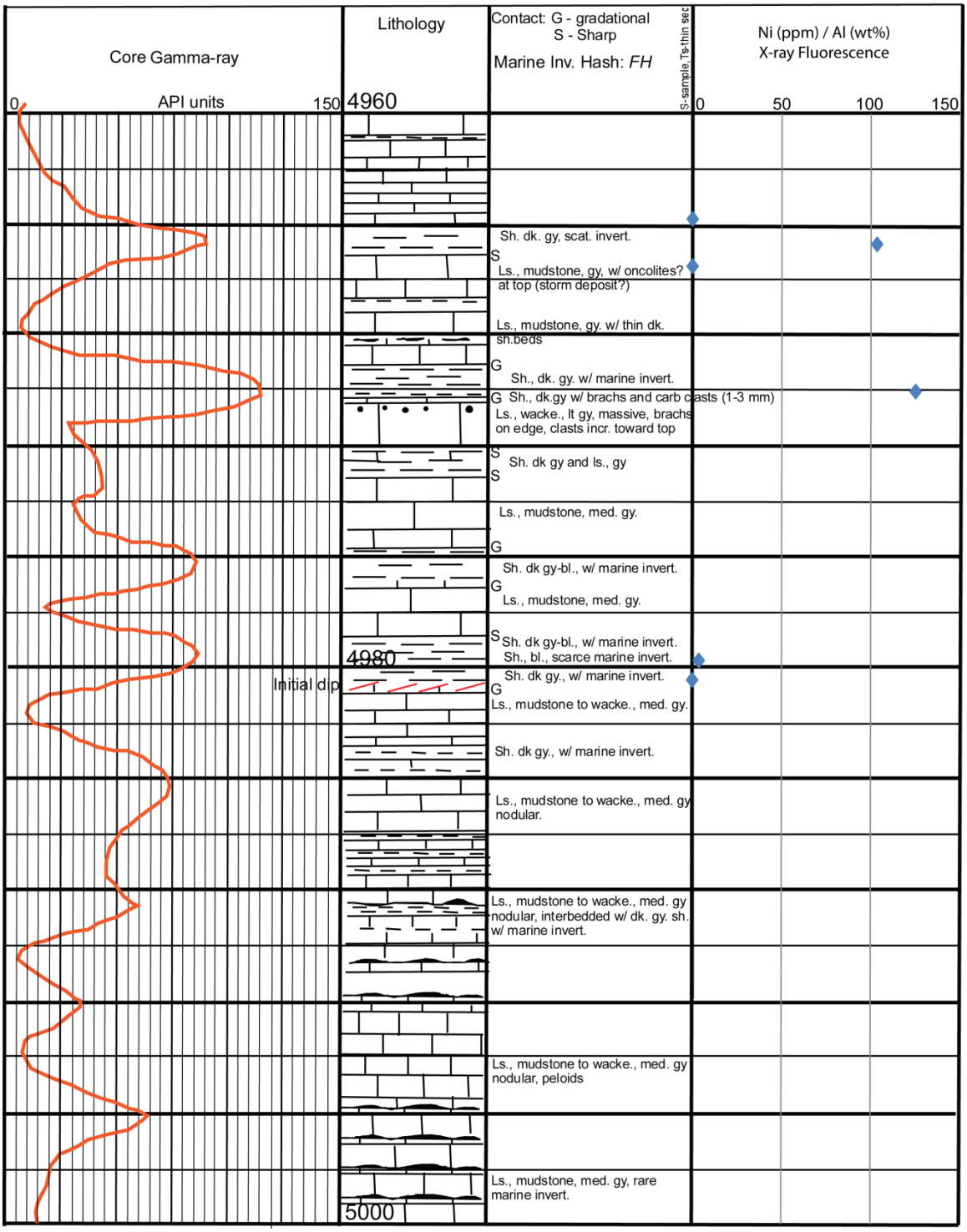

Figure 47: Ni/Al ratio plotted against the lithologic column for core depths 4960' to 5000'.

Rebecca K. Bounds #1 Well, Sec. 17, T.18S., R.42W., Greeley Co., Kansas

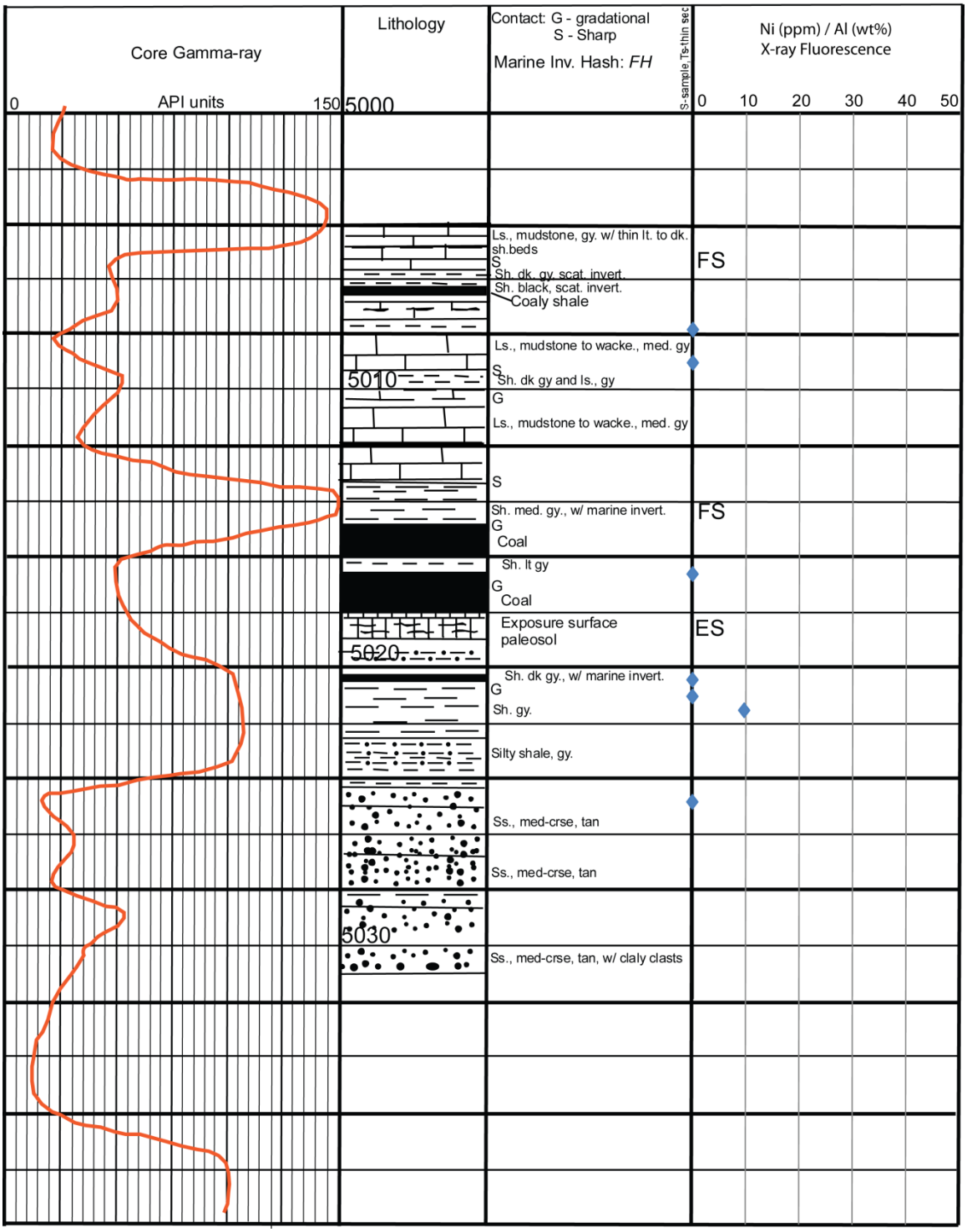

Figure 48: Ni/Al ratio plotted against the lithologic column for core depths 5000' to 5031'.

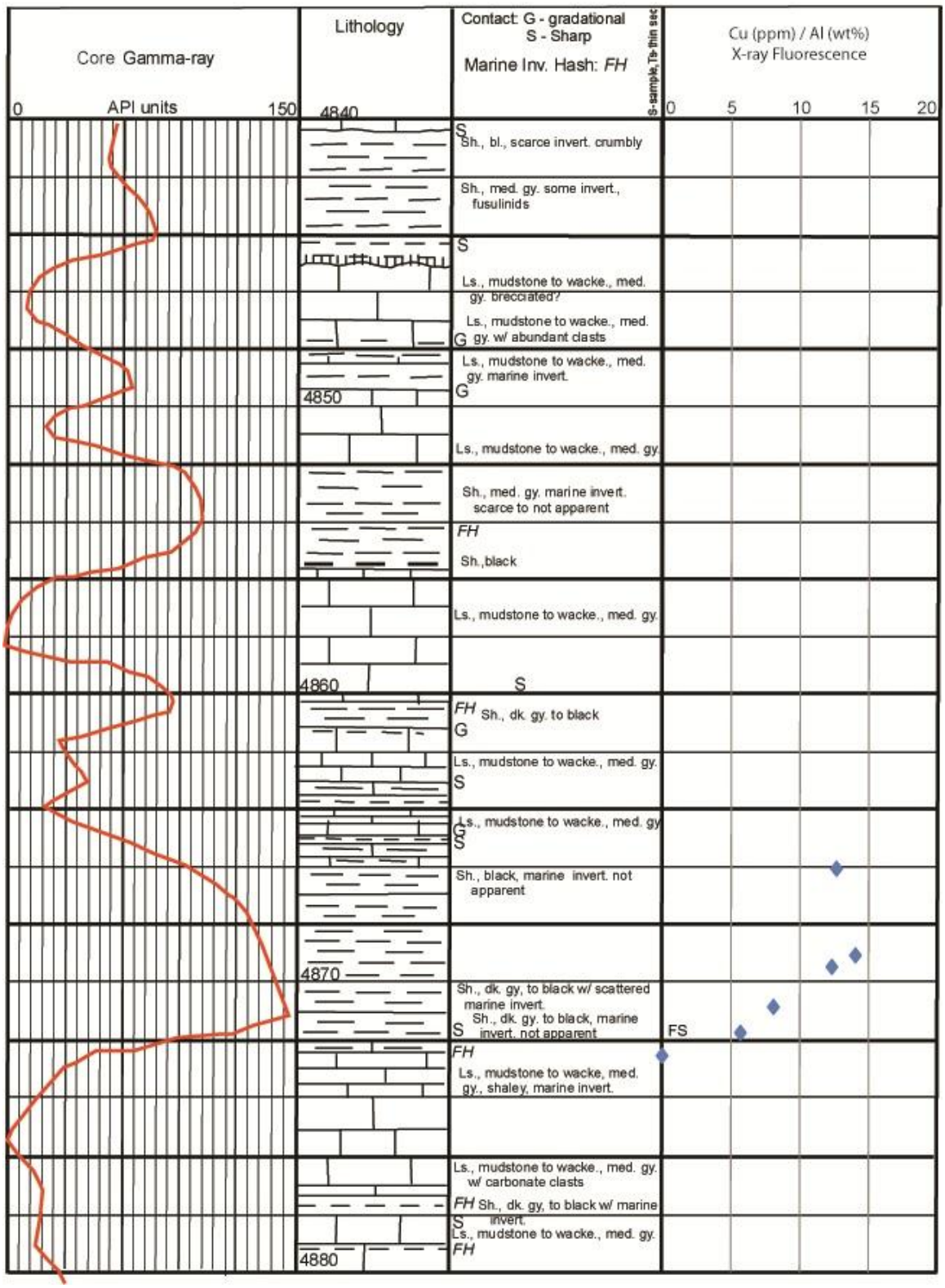

Figure 49: Cu/Al ratio plotted against the lithologic column for core depths 4840’ to 4880’.

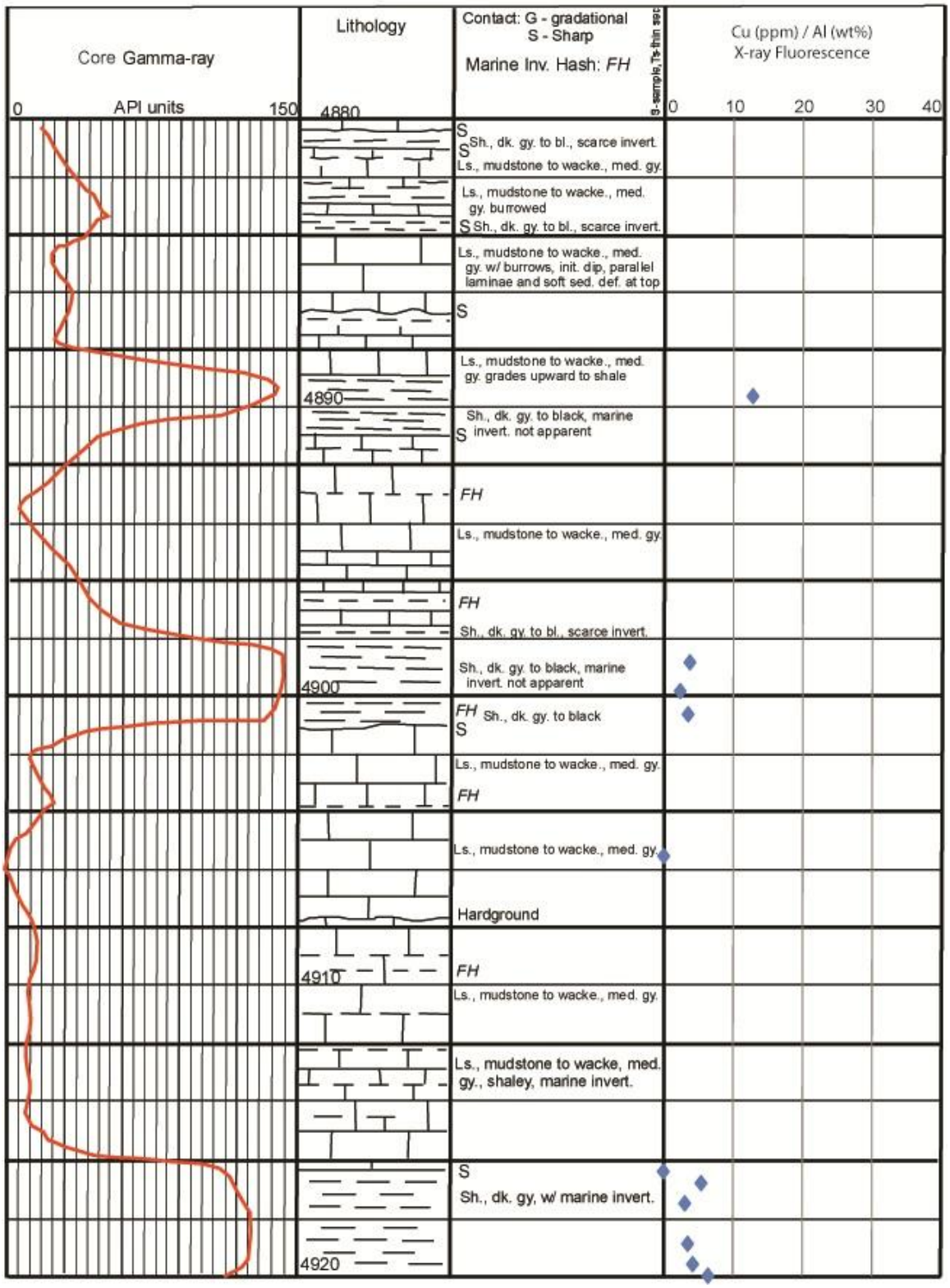

Figure 50: Cu/Al ratio plotted against the lithologic column for core depths 4880' to 4920'.

Rebecca K. Bounds #1 Well, Sec. 17, T.18S., R.42W., Greeley Co., Kansas

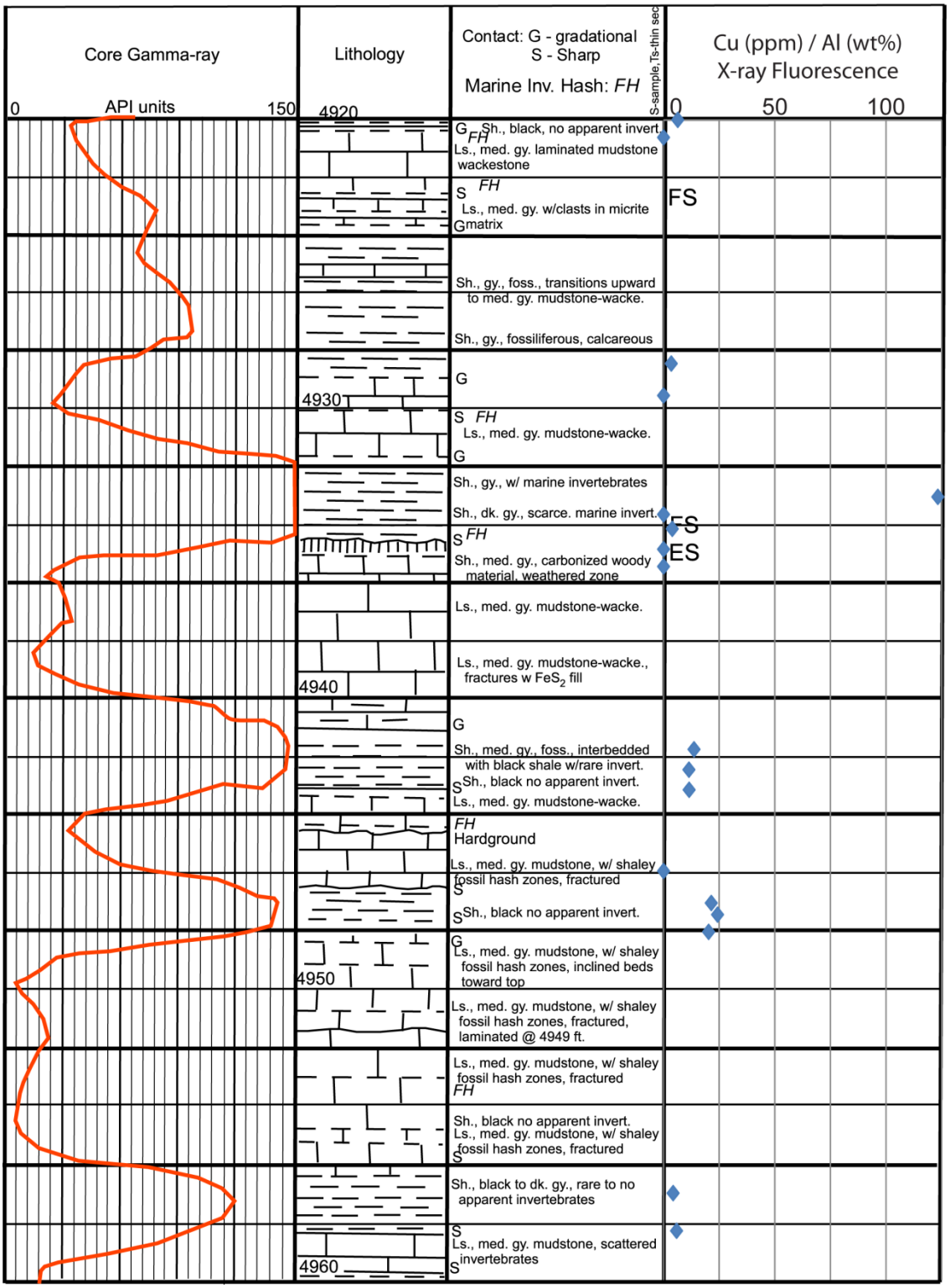

Figure 51: Cu/Al ratio plotted against the lithologic column for core depths 4920' to 4960'.

Rebecca K. Bounds #1 Well, Sec. 17, T.18S., R.42W., Greeley Co., Kansas

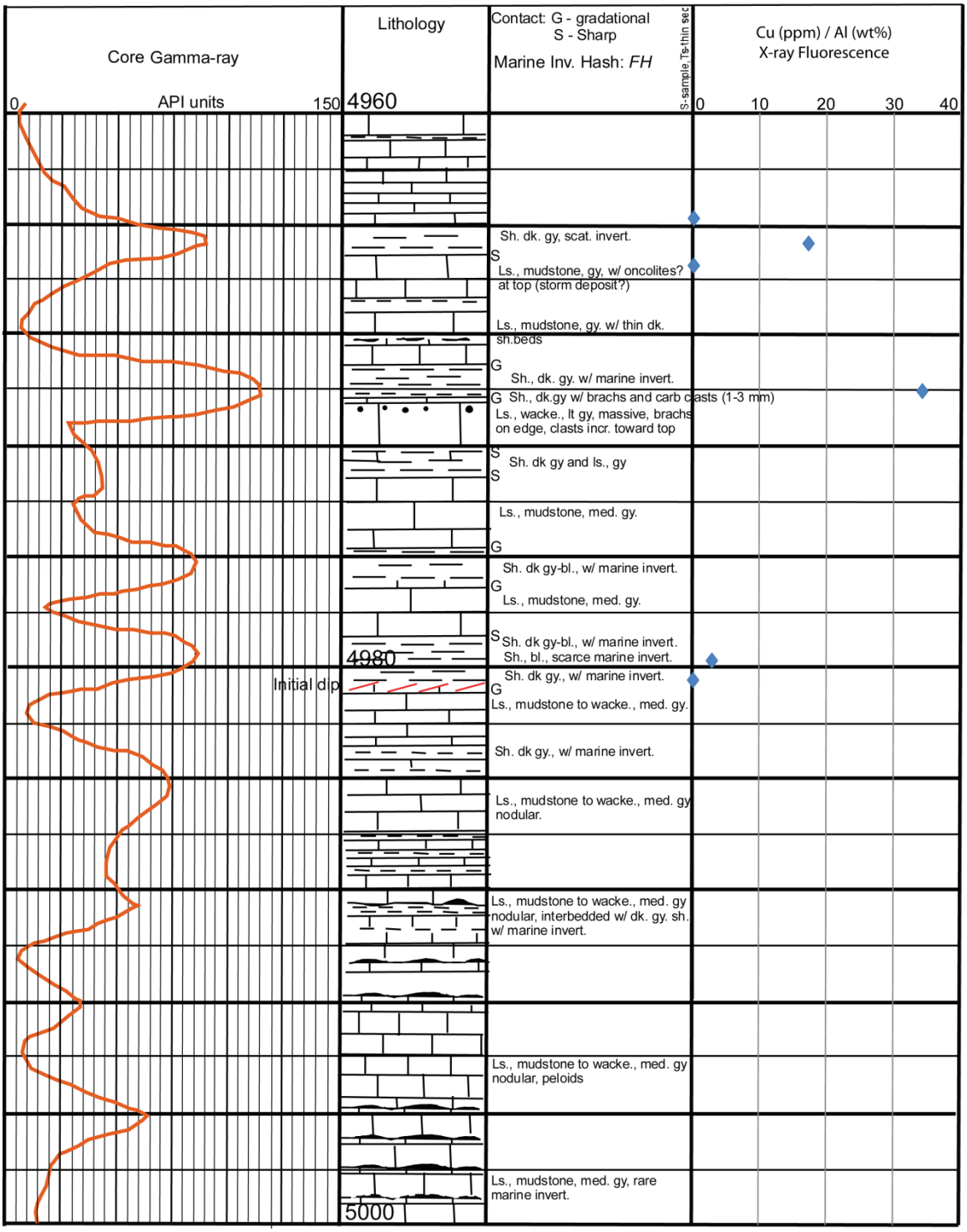

Figure 52: Cu/Al ratio plotted against the lithologic column for core depths 4960' to 5000'.

Rebecca K. Bounds #1 Well, Sec. 17, T.18S., R.42W., Greeley Co., Kansas

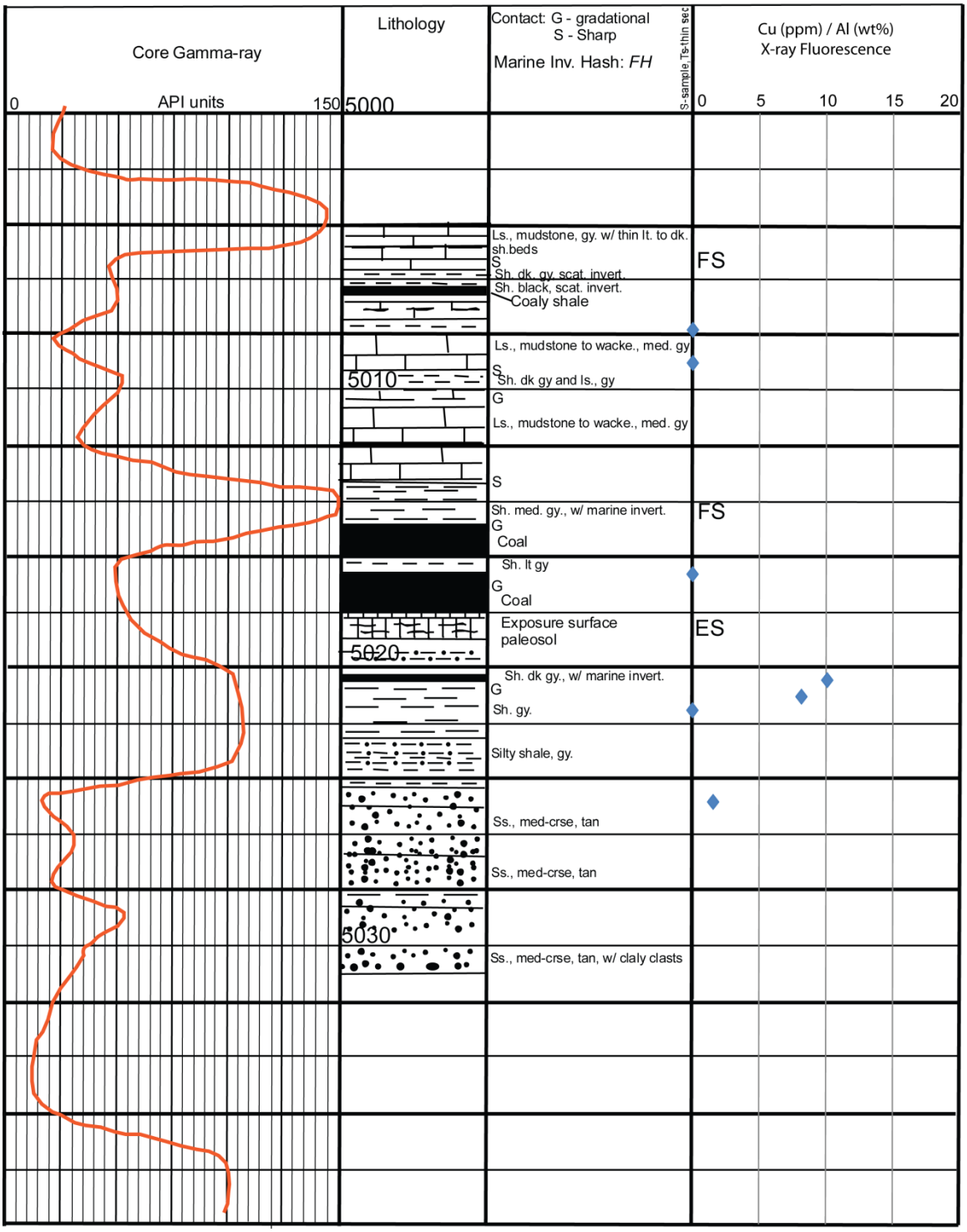

Figure 53: Cu/Al ratio plotted against the lithologic column for core depths 5000' to 5031'.

DEPTH	Ba	Sn	Cd	Pd	Ag	Mo	Nb	Zr
4828.5	343.11	< LOD	< LOD	< LOD	82.65	< LOD	7.16	106.02
4844	229.73	< LOD	< LOD	< LOD	38.71	< LOD	8.34	110.61
4871	278.64	< LOD	< LOD	< LOD	58.57	6.98	5.24	100.81
4874	304.9	< LOD	< LOD	< LOD	101.32	< LOD	18.63	74.16
4874.4	266.64	< LOD	< LOD	< LOD	72.95	< LOD	6.49	91.61
4875.8	252.78	24.26	< LOD	< LOD	61.58	< LOD	13.18	143.55
4876.7	264.18	< LOD	< LOD	< LOD	46.65	5.8	11.53	101.51
4877.5	217.66	< LOD	< LOD	< LOD	117.45	3.67	3.66	13.47
4894.6	276.41	< LOD	< LOD	< LOD	75.06	9.86	8.67	94.64
4903.8	421.24	< LOD	< LOD	< LOD	80.96	< LOD	18.6	159.99
4904.8	314.82	< LOD	< LOD	< LOD	62.97	< LOD	15.66	113.95
4905.6	300.43	< LOD	< LOD	< LOD	57.77	< LOD	9.41	116.99
4910.5	222.96	28.08	< LOD	< LOD	113.41	3.05	3.57	4.81
4921.4	190.98	< LOD	< LOD	< LOD	97.46	< LOD	3.37	7.47
4921.8	314.94	< LOD	< LOD	< LOD	78.82	< LOD	16.72	134.15
4922.5	332.9	< LOD	< LOD	< LOD	74.78	< LOD	14.9	123.68
4923.9	334.24	< LOD	< LOD	< LOD	74	< LOD	14.4	115.51
4924.6	287.7	< LOD	< LOD	< LOD	55.84	< LOD	16.91	101.56
4925	269.44	< LOD	< LOD	< LOD	83.91	< LOD	19.89	80.94
4925.6	196.07	< LOD	< LOD	< LOD	110.08	15.04	5.23	11.48
4933.4	298.61	< LOD	< LOD	< LOD	76.94	< LOD	13.52	104.81
4934.5	173	< LOD	< LOD	< LOD	95.23	< LOD	2.61	8.15
4938	340.93	< LOD	< LOD	< LOD	88.76	< LOD	16.89	111.28
4938.6	411.02	< LOD	< LOD	< LOD	89.48	< LOD	8.86	113.31
4939.1	346.8	< LOD	< LOD	< LOD	86.5	< LOD	8.78	148.67
4939.8	262.9	< LOD	< LOD	< LOD	63.01	< LOD	9.38	92.02
4940.4	243.92	< LOD	< LOD	< LOD	111.84	2.88	3.64	16.85
4946.7	222.77	< LOD	12.48	< LOD	62.26	22.99	18.67	81.29
4947.4	210.9	< LOD	12.45	< LOD	47.42	58.47	6.99	71.97
4948.1	249.89	< LOD	< LOD	< LOD	74.5	14.32	8.67	84.13
4950.9	188.69	< LOD	< LOD	< LOD	111.27	< LOD	2.62	6.81
4952	< LOD	< LOD	138.6	< LOD	53.36	275.55	6.82	67.62
4952.4	213.33	< LOD	88.08	< LOD	61.31	257.54	6	76.59
4953	242.74	< LOD	66.15	< LOD	62.93	87.95	5.46	80.07
4962	291.84	< LOD	< LOD	< LOD	54.24	< LOD	11.71	108.1
4963.3	318.82	< LOD	< LOD	< LOD	61.9	< LOD	12.23	124.32
4968.8	261.87	< LOD	< LOD	< LOD	126.45	< LOD	2.8	8.37
4969.7	198.53	< LOD	48.92	< LOD	41.55	63.67	4.88	88.59
4970.5	222.91	< LOD	< LOD	< LOD	92.8	< LOD	3.32	33.52
4975	209.5	< LOD	147.1	< LOD	52.87	108.32	5.41	87.22
4984.7	298.57	< LOD	< LOD	< LOD	49.32	< LOD	11.14	121
4985.4	208.17	< LOD	< LOD	< LOD	104.18	< LOD	6.05	20.66
5007.8	187.53	< LOD	< LOD	< LOD	108.89	20.42	4.15	6.73
5009	248.42	< LOD	< LOD	< LOD	133	30.68	5.33	8.43
5016.6	< LOD	< LOD	22	4.57	< LOD	2.76	6.21	19.88
5020.4	72.98	< LOD	< LOD	< LOD	26.77	< LOD	11.53	50.35
5021	124.58	< LOD	< LOD	< LOD	39.24	< LOD	12.96	52.11
5021.5	352.02	< LOD	< LOD	< LOD	128.6	< LOD	16.69	159.9
5024.8	248.31	< LOD	< LOD	< LOD	41.46	< LOD	21.92	276.19

Figure 54: X-ray Fluorescence measurements of the Rebecca K. Bounds #1 core. Values are in PPM.

DEPTH	Sr	U	Th	As	Au	Pb	Br	W
4828.5	123.23	189.13	< LOD	20.79	< LOD	7.08	< LOD	< LOD
4844	128.39	218.9	< LOD	20.86	< LOD	17.8	< LOD	< LOD
4871	86.48	184.59	< LOD	20.68	9.62	31.18	< LOD	< LOD
4874	219.19	224.18	< LOD	21.96	< LOD	19.42	< LOD	< LOD
4874.4	125.9	197.67	< LOD	21.51	< LOD	18.8	< LOD	< LOD
4875.8	62.87	292.39	< LOD	22.31	< LOD	26.12	< LOD	< LOD
4876.7	70.51	371.31	< LOD	26.42	< LOD	23.19	< LOD	< LOD
4877.5	205.59	15.19	< LOD	15.93	< LOD	10.89	< LOD	< LOD
4894.6	134.88	333.17	< LOD	16.55	27.21	44.71	< LOD	< LOD
4903.8	134.51	219.89	< LOD	18.56	< LOD	19.83	< LOD	< LOD
4904.8	112.31	241.87	< LOD	19.45	< LOD	13.45	< LOD	< LOD
4905.6	86.74	212.24	< LOD	20.77	< LOD	18.73	< LOD	< LOD
4910.5	349.15	< LOD	< LOD	14.43	< LOD	12.7	< LOD	< LOD
4921.4	428.66	< LOD	< LOD	15.09	< LOD	9.32	< LOD	< LOD
4921.8	98.83	245.19	< LOD	18.23	< LOD	14.9	< LOD	< LOD
4922.5	111.6	213.79	< LOD	17.44	< LOD	19.32	< LOD	< LOD
4923.9	116.46	205.93	< LOD	19.29	< LOD	18.9	< LOD	< LOD
4924.6	92.81	297.16	< LOD	18.8	< LOD	24.76	< LOD	< LOD
4925	127.02	255.83	< LOD	17.84	9.88	24.92	< LOD	< LOD
4925.6	365.87	< LOD	< LOD	19.43	< LOD	13.75	< LOD	< LOD
4933.4	104.66	274.58	< LOD	19.47	< LOD	6.59	< LOD	< LOD
4934.5	296.75	56.04	< LOD	15.29	< LOD	11.08	< LOD	< LOD
4938	242.32	178.41	< LOD	19.04	< LOD	18.09	< LOD	< LOD
4938.6	132.94	228.41	< LOD	27.9	< LOD	11.94	< LOD	< LOD
4939.1	140.7	227.47	< LOD	21.27	< LOD	14.69	< LOD	< LOD
4939.8	129.36	213.31	< LOD	16.79	< LOD	14.47	< LOD	< LOD
4940.4	342.13	25.35	< LOD	14.43	< LOD	14.07	< LOD	< LOD
4946.7	120.16	314.1	< LOD	21.66	< LOD	29.89	< LOD	< LOD
4947.4	59.45	263.23	< LOD	14.75	26.1	49.03	< LOD	< LOD
4948.1	94.86	228.97	< LOD	19.03	16.81	40.95	< LOD	< LOD
4950.9	300.37	< LOD	< LOD	14.74	< LOD	12.66	< LOD	< LOD
4952	75.54	372.4	< LOD	< LOD	35.08	40.18	< LOD	< LOD
4952.4	68.46	232.44	< LOD	15.89	34.83	44.78	< LOD	< LOD
4953	66.47	220.18	< LOD	17.1	32.8	45.36	< LOD	< LOD
4962	110.41	224.69	< LOD	21.01	< LOD	19.97	< LOD	< LOD
4963.3	117.38	260.75	< LOD	19.75	< LOD	21.06	< LOD	< LOD
4968.8	428.24	19.32	< LOD	16.5	< LOD	12	< LOD	< LOD
4969.7	100.38	299.89	< LOD	39.72	20.11	41.59	< LOD	< LOD
4970.5	276.91	28.58	< LOD	17.41	< LOD	8.12	< LOD	< LOD
4975	94.53	266.35	< LOD	15.36	35.54	51.84	< LOD	< LOD
4984.7	115.46	344.59	< LOD	17.92	< LOD	22.32	< LOD	< LOD
4985.4	233.41	58.88	< LOD	15.38	< LOD	10.66	< LOD	< LOD
5007.8	335.61	88.77	< LOD	17.05	< LOD	10.85	< LOD	< LOD
5009	418.63	< LOD	< LOD	17.78	< LOD	10.32	< LOD	< LOD
5016.6	30.91	25.77	< LOD	17.5	< LOD	8.86	< LOD	< LOD
5020.4	121.31	60.67	< LOD	23.91	< LOD	44.78	< LOD	< LOD
5021	152.94	45.69	< LOD	24.58	< LOD	63.04	< LOD	< LOD
5021.5	138.81	63.4	< LOD	39.4	< LOD	379.6	< LOD	< LOD
5024.8	210.01	121.01	< LOD	21.82	< LOD	22	< LOD	< LOD

Figure 55: X-ray Fluorescence measurements of the Rebecca K. Bounds #1 core. Values are in PPM.

DEPTH	Zn	Cu	Ir	Ni	Co	Fe	Mn	Cr
4828.5	20.77	30.15	< LOD	59.44	< LOD	31235.1	230.35	201.86
4844	43.95	39.31	< LOD	< LOD	< LOD	23373.82	128.86	147.7
4871	1388.9	64.64	< LOD	235.99	< LOD	33152.11	176.03	546.92
4874	202.01	58.89	< LOD	137.63	< LOD	35769.7	258.27	307.08
4874.4	553.38	55.44	< LOD	157.6	< LOD	30993	189.55	425
4875.8	73.28	65.06	< LOD	139.7	< LOD	30957.53	156.89	342.71
4876.7	146.95	38.48	< LOD	170.95	< LOD	30952.74	113.58	468.28
4877.5	< LOD	< LOD	< LOD	< LOD	< LOD	2336.36	344.84	< LOD
4894.6	274.13	62.81	< LOD	261.15	< LOD	32633.74	197.33	621.97
4903.8	77.25	27.98	< LOD	49.45	< LOD	37482.41	207.89	227.01
4904.8	51.09	18.61	< LOD	60.68	< LOD	30867.39	146.9	200.56
4905.6	65.5	26.77	< LOD	107.75	< LOD	31363.53	135.03	213.93
4910.5	< LOD	< LOD	< LOD	< LOD	< LOD	753.07	225.93	< LOD
4921.4	< LOD	< LOD	< LOD	< LOD	< LOD	4819.99	205.33	< LOD
4921.8	1451.74	42.32	< LOD	28.47	< LOD	27638.55	152.35	177.06
4922.5	15.37	23.3	< LOD	36.2	< LOD	26431.1	147.8	181.15
4923.9	56.52	26.41	< LOD	46.13	< LOD	27677.6	153.61	181.77
4924.6	158.57	30.96	< LOD	121.29	< LOD	25850.97	144.76	548.4
4925	718.56	38.38	< LOD	208.24	< LOD	33733.29	171.72	713.04
4925.6	< LOD	< LOD	< LOD	< LOD	< LOD	22935.94	278.11	< LOD
4933.4	101.15	24.15	< LOD	78.53	< LOD	30020.38	264.95	801.89
4934.5	< LOD	< LOD	< LOD	< LOD	< LOD	4232.88	816.02	< LOD
4938	17.11	832.33	< LOD	32.88	< LOD	41639.97	199.1	165.83
4938.6	21.91	< LOD	< LOD	97.9	< LOD	28719.13	145.42	259.98
4939.1	< LOD	25.53	< LOD	79.22	< LOD	26547.4	146.81	171.48
4939.8	< LOD	< LOD	< LOD	< LOD	< LOD	12712.63	68.48	112.32
4940.4	< LOD	< LOD	< LOD	< LOD	< LOD	2517.54	373.37	< LOD
4946.7	1458.29	65.96	< LOD	278.86	< LOD	24043.01	175.74	547.94
4947.4	1037.79	66.32	< LOD	236.71	< LOD	25163.87	113.19	888.47
4948.1	673.99	64.87	< LOD	216.73	< LOD	29430.27	132.76	709.64
4950.9	< LOD	< LOD	< LOD	< LOD	< LOD	1069.75	378.6	< LOD
4952	2684.18	164.71	< LOD	528.2	< LOD	25261.13	< LOD	651.31
4952.4	2869.53	93.88	< LOD	230.95	< LOD	33149.14	126.49	572.44
4953	1750.59	89.86	< LOD	304.39	< LOD	34762.61	128.46	770.53
4962	19.64	30.68	< LOD	46.33	< LOD	27280.53	207.09	184.15
4963.3	31.23	46.22	< LOD	30.03	< LOD	27617.03	208.07	223.41
4968.8	< LOD	< LOD	< LOD	< LOD	< LOD	2409.79	258.89	< LOD
4969.7	2387.95	87.82	< LOD	525.24	< LOD	34860.01	153.07	386.22
4970.5	< LOD	< LOD	< LOD	< LOD	< LOD	12769.87	489.61	< LOD
4975	7617.96	148.07	< LOD	540.49	< LOD	31624.16	164.6	750.75
4984.7	47.84	24.61	< LOD	30.19	< LOD	23785.6	116.7	271.19
4985.4	< LOD	< LOD	< LOD	< LOD	< LOD	8931.68	633.06	51.74
5007.8	< LOD	< LOD	< LOD	< LOD	< LOD	4827.84	803.45	52.99
5009	< LOD	< LOD	< LOD	< LOD	< LOD	9889.89	922.75	< LOD
5016.6	249.42	< LOD	< LOD	< LOD	< LOD	9374.86	< LOD	67.2
5020.4	< LOD	29.87	< LOD	< LOD	< LOD	71330.32	558.95	164.27
5021	< LOD	20.54	< LOD	< LOD	< LOD	73457.92	461.74	176.82
5021.5	21.29	< LOD	< LOD	66.02	< LOD	121581.7	988.87	373.83
5024.8	20.77	15.42	< LOD	< LOD	< LOD	29507.9	229.44	232.26

Figure 56: X-ray Fluorescence measurements of the Rebecca K. Bounds #1 core. Values are in PPM.

DEPTH	V	Ti	Ca	K	Sb	Al	P	Si
4828.5	177.4	2820.86	39418.45	24120.02	< LOD	61534.02	< LOD	228731.8
4844	171.72	3222.69	21257.08	28406.73	< LOD	74427.15	< LOD	224101
4871	442.77	2551.24	34322.16	21292.81	< LOD	51048.49	< LOD	198078.3
4874	294.78	2086.14	99727.65	14739.54	< LOD	41931.91	25037.77	170696.6
4874.4	242.7	2294.92	53469.54	18688.38	< LOD	44977.07	3679.68	206494.7
4875.8	198.93	4143.62	5095.49	29241.93	< LOD	80452.04	< LOD	235440.5
4876.7	379.08	3466.26	14395.6	28355.88	< LOD	67671.68	7146.02	207546.2
4877.5	< LOD	177.65	397899.2	1268.18	< LOD	4054.93	< LOD	19773.27
4894.6	445.88	2730.92	64673.63	18391.26	< LOD	49170.72	18171.33	164705
4903.8	251.79	3550.55	22198.16	25093.72	< LOD	74527.93	726.4	232275.3
4904.8	242.69	3613.83	10375.21	28821.56	< LOD	78894.41	881.07	218180.4
4905.6	234.85	3350.36	18290.15	28955.91	< LOD	76907.95	580.92	227291.1
4910.5	< LOD	< LOD	429373.3	< LOD	< LOD	< LOD	< LOD	4528.91
4921.4	< LOD	77.54	326320.8	289.94	< LOD	4227.21	< LOD	82199.59
4921.8	255.87	4144.49	10533.33	29591.15	< LOD	77930.94	1817.33	221973.2
4922.5	238.76	3693.22	17868.22	26923.59	< LOD	75381	< LOD	232727.8
4923.9	234.88	3467.24	21710.04	26638.35	< LOD	74978.88	< LOD	228365.3
4924.6	304.62	3430.85	11312.76	27031.45	< LOD	73050.25	3556.92	224517.3
4925	328.09	3019	28178.61	22627.37	< LOD	59781.12	1838.12	202357.8
4925.6	< LOD	310.35	327500.7	1871.63	< LOD	9897.95	< LOD	74512.22
4933.4	375.32	3029.4	27714.96	26201.61	< LOD	68744.44	1342.93	235268.5
4934.5	< LOD	121.64	296181.1	553.89	< LOD	4547.91	< LOD	111122.7
4938	220.47	2898.03	53848.5	22289.38	< LOD	67488.98	844.06	211128.2
4938.6	241.01	3133.57	21836.65	28156.02	< LOD	78591.54	< LOD	235217.8
4939.1	198.51	3053.91	41013.86	24375.13	< LOD	64979.09	< LOD	214646.5
4939.8	174	3402.97	45694.05	23800.74	< LOD	51108.94	1599.23	180398.9
4940.4	< LOD	278.42	352754	2274.5	< LOD	6547.53	< LOD	46624.43
4946.7	506.39	2369.07	41672.34	16576.94	< LOD	48208.39	15409.69	200977
4947.4	827.55	2230.9	6544.01	17759.96	< LOD	58015.72	1150.68	230368.8
4948.1	551.72	2483.59	29859.63	19076.36	< LOD	56244.83	4212.07	196500.1
4950.9	< LOD	87.33	399338	485.57	< LOD	< LOD	< LOD	19792.5
4952	< LOD	2378.73	14750.45	11635.75	< LOD	76866.84	8671.56	334635.3
4952.4	1722.54	1991.79	18495.05	14571.66	< LOD	38669.44	< LOD	221259.3
4953	1455.11	2153.78	18237.14	16381.39	< LOD	44333.36	736	195620.6
4962	202.5	3264.37	29304.35	27645.35	< LOD	70761.8	< LOD	209602
4963.3	239.25	3474.78	23964.33	28953.14	< LOD	78679.16	2167.41	225993.6
4968.8	< LOD	152.83	328275.5	873.53	< LOD	< LOD	< LOD	17114.43
4969.7	864.85	2247.39	33157.61	18983.16	< LOD	50783.21	1025.31	161525.8
4970.5	34.71	438.57	218379.8	2227.58	< LOD	6868.86	< LOD	90567.89
4975	1613.56	2247.23	30129.6	17459.46	< LOD	43209.76	4784.55	163054.3
4984.7	496.51	3697.85	12352.08	29769.34	< LOD	81967.34	977.99	226314.6
4985.4	52.27	486.12	298026.9	5133.3	< LOD	19587.93	< LOD	90388.56
5007.8	88.6	81.6	319807.4	775.34	< LOD	< LOD	< LOD	7301.52
5009	< LOD	143.56	405294.8	761.02	< LOD	4250.44	< LOD	10004.08
5016.6	259.85	414.36	5373.59	491.34	< LOD	8570.38	< LOD	17235.55
5020.4	126.65	1398.56	30720.5	4405.75	< LOD	29613.07	12337.29	65430.11
5021	120.03	1706.11	36730.75	4400.53	< LOD	25165.76	13218.69	59419.5
5021.5	250.51	3873.52	6616.42	10306.66	< LOD	68123.2	< LOD	99492.11
5024.8	311.58	6243.54	8651.52	9234.85	< LOD	98960.2	903.2	148398.2

Figure 57: X-ray Fluorescence measurements of the Rebecca K. Bounds #1 core. Values are in PPM.

DEPTH	Cl	S	Mg
4828.5	2417.74	3268.61	< LOD
4844	2856.93	3125.64	< LOD
4871	2190.92	17894.88	< LOD
4874	1341	12735.39	< LOD
4874.4	1811.6	13098.58	< LOD
4875.8	2462.04	9746.97	< LOD
4876.7	1709.6	14096.97	< LOD
4877.5	< LOD	2993.92	< LOD
4894.6	1954.44	22127.96	< LOD
4903.8	2216.5	27116.85	< LOD
4904.8	2767.23	13178.79	< LOD
4905.6	2206.09	8028.75	< LOD
4910.5	2515.92	848.65	< LOD
4921.4	5187.85	2927.25	< LOD
4921.8	2132.68	3485.73	< LOD
4922.5	2259.6	4240.46	< LOD
4923.9	1975.81	5284.47	< LOD
4924.6	2202.45	4801.85	< LOD
4925	3007.48	9447.7	< LOD
4925.6	< LOD	30184.03	< LOD
4933.4	2623.53	1584.31	< LOD
4934.5	< LOD	1177.57	< LOD
4938	2650.5	15431.18	< LOD
4938.6	2960.37	4504.38	< LOD
4939.1	2725.67	13838.57	< LOD
4939.8	5017.54	11273.99	< LOD
4940.4	911.02	2068.04	< LOD
4946.7	1854	20948.18	< LOD
4947.4	2361.04	15691.39	< LOD
4948.1	2647.33	20571.78	< LOD
4950.9	899.38	1990.05	< LOD
4952	433.91	33054.29	< LOD
4952.4	2288.19	32374.87	< LOD
4953	2588.6	26669.35	< LOD
4962	2153.66	11468.01	< LOD
4963.3	2166.69	12446.06	< LOD
4968.8	257516	1337.53	< LOD
4969.7	2282.44	37586.61	< LOD
4970.5	518.82	4962.84	35978.73
4975	2543.5	34802.05	< LOD
4984.7	2245.27	3993.13	< LOD
4985.4	< LOD	2480.57	< LOD
5007.8	286376.1	2267.03	< LOD
5009	10636.87	8515.98	< LOD
5016.6	5553.66	57828.66	< LOD
5020.4	2678.01	110951.5	< LOD
5021	2700.55	130990.4	< LOD
5021.5	5390.87	157121.9	< LOD
5024.8	2966.04	41747.7	< LOD

Figure 58: X-ray Fluorescence measurements of the Rebecca K. Bounds #1 core. Values are in PPM.

VITA

Michael Evan Bagley

Candidate for the Degree of

Master of Science

Thesis: LITHOFACIES, GEOCHEMICAL TRENDS, AND RESERVOIR POTENTAL, THIRTEEN FINGER LIMESTONE, HUGOTON EMBAYMENT, KANSAS

Major Field: Geology

Biographical:

Education:

Completed the requirements for the Master of Science in Geology at Oklahoma State University, Stillwater, Oklahoma in May, 2012.

Completed the requirements for the Bachelor of Science in Geology at Brigham Young University - Idaho, Rexburg, Idaho in December, 2007.

Experience:

Graduate Teaching Assistant, Department of Geology, Oklahoma State University, Stillwater, Oklahoma, August 2009 to May 2011; Faculty, Department of Geology, Brigham Young University – Idaho, Rexburg, Idaho, April 2008 – July 2009; Teaching Assistant, Department of Geology, Brigham Young University – Idaho, Rexburg, Idaho, January 2006 – December 2007.

Professional Memberships:

Geological Society of America, 2005 to Present
American Association of Petroleum Geologists, 2006 to Present
Society for Sedimentary Geology, 2007 to Present

Name: Michael Evan Bagley Date of Degree: May, 2012

Institution: Oklahoma State University Location: Stillwater, Oklahoma

Title of Study: LITHOFACIES, GEOCHEMICAL TRENDS, AND RESERVOIR POTENTAL, THIRTEEN FINGER LIMESTONE, HUGOTON EMBAYMENT, KANSAS

Pages in Study: 157 Candidate for the Degree of Master of Science

Major Field: Geology

Scope and Method of Study: The Rebecca K. Bounds #1 core from Greeley County, KS was described and sampled for various analyses including conodont biostratigraphy, total organic carbon (TOC), x-ray diffraction and x-ray fluorescence to determine reservoir depositional setting, reservoir potential and establish the chronostratigraphic and lithostratigraphic boundaries of the Atokan Stage in western Kansas.

Findings and Conclusions: The base of the Thirteen Finger Limestone (Atokan/Morrowan boundary) is placed at a prominent exposure surface at 5017.5 feet. Immediately above this surface is a thin coal followed by marine shale and limestone. The top of the Thirteen Finger Limestone (Atokan/Desmoinesian boundary) is chosen as the exposure surface at 4939.7 feet. The 83 feet of Atokan strata contains limestones (70%) separated by fossiliferous dark gray shale (10%) or black shales (20%) with few macroinvertebrates. Seven prominent flooding surfaces and two hardgrounds help define Atokan high-frequency cycles that consist of dark shale (initial flooding) that transitions upward to shallower-water limestone. The dark gray-black uranium-rich shales are higher TOC (up to 9.7% in noncarbonaceous shale), have higher transition metal content and few normal marine invertebrates. The conodonts recovered from the Thirteen Finger Limestone are upper Atokan, but the size of core prevented sampling of the entire interval and confident determination of chronostratigraphy. Atokan limestones are dominantly dense wackestones and packstones with average matrix porosity and permeability values of 0.8% and 0.1 md, respectively. However, these limestones contain numerous open- and healed-vertical fractures that may provide the pore network necessary to produce oil and gas.

ADVISER'S APPROVAL: Dr. Jim Puckette